UPPSALA
UNIVERSITET

UPTEC W 19 016
Examensarbete 30 hp
Mars 2019

# Groundwater Flow and Transport Modelling of PFASs in Åkersberga

Worada Boonraksasat

# ABSTRACT

**Groundwater Flow and Transport Modelling of PFASs in Åkersberga**
*Worada Boonraksasat*

Per- and polyfluoroalkyl substances (PFASs) are a group of man-made organic chemicals that have been commercially used since the 1950s in many consumer products, including impregnated textiles, impregnated paper, nonstick products (e.g., Teflon), cleaning agents, and in firefighting foams. However, PFASs have in recent years received increasing public attention due to their persistence, bioaccumulative potential, and potentially toxic effects on humans and animals. Firefighting training sites have been identified as one of the most important sources for the spread of PFASs in the environment, due to the use of PFAS-containing firefighting foam of type AFFFs (aqueous film forming foams). This has resulted in contamination of both drinking water and groundwater in several municipalities in Sweden.

At the former fire station in Åkersberga, AFFFs were handled and used during the fire-training exercises. WSP Environmental Sweden has performed a preliminary investigation on site and elevated levels of PFASs in both soil and groundwater were observed. Since the property is located next to a railroad track, there is a concern that PFASs will spread through the railroad track towards the nearby Åkers canal. The aim of this master's thesis has therefore been to map the transport of PFASs in groundwater from this former fire station. A groundwater flow model was first constructed in the software program Visual MODFLOW. The groundwater model was then used as a basis for the construction of a transport model with MODPATH and MT3DMS. The transport of four PFAS homologues was modeled; perfluorooctane sulfonic acid (PFOS), perfluorooctanoic acid (PFOA), 6:2 Fluorotelomer sulfonate (6:2 FTS), and perfluoropentanoic acid (PFPeA).

The result of the groundwater modelling showed that groundwater from the property flows towards the southwest and then further towards Åkers canal. The approximated velocity of a water molecule varied between 270 m/year and 400 m/year. The transport modelling showed that all four PFAS homologues traveled towards Åkers canal via the railroad track and that the short-chain PFAS homologues (6:2 FTS and PFPeA) traveled longer and faster than the long-chain PFAS homologues (PFOS and PFOA). The approximated velocity of the contaminant plume for the concentration $4.5 \cdot 10^{-5}$ mg/L was 0.6 m/year for PFOS, 3 m/year for PFOA, 8 m/year for 6:2 FTS, and 16 m/year for PFPeA.

**Keyword**: Groundwater modelling, contaminant transport, Visual MODFLOW, MODPATH, MT3DMS, PFASs, AFFFs

*Department of Earth Sciences, Program for Air, Water, and Landscape Sciences; Hydrology. Uppsala University. Villavägen 16, SE-752 36 UPPSALA.*

# REFERAT

**Spridningsmodellering av PFAS i Åkersberga**
*Worada Boonraksasat*

Per- och polyfluorerade alkylsubstanser (PFAS) är en grupp av konstgjorda organiska kemikalier som sedan 1950-talet har kommersiellt använts i många konsumentprodukter, inklusive impregnerade textilier, impregnerat papper, nonstick-produkter (t.ex. Teflon), rengöringsmedel och brandsläckningsskum. PFAS har dock under senare år fått ökad allmän uppmärksamhet på grund av deras persistens, bioackumuleringspotential och potentiella toxiska effekter på människor och djur. Brandövningsplatser har identifierats som en av de största källorna för spridningen av PFAS i miljön, på grund av användningen av PFAS-innehållande brandsläckningsskum av typen AFFF (aqueous film forming foams). Detta har resulterat i förorening av både dricksvatten och grundvatten i flera kommuner i Sverige.

På den tidigare brandstationen i Åkersberga har hantering och användning av AFFF ägt rum under släckningsövningarna. WSP Environmental Sverige har utfört förundersökning på plats och förhöjda halter PFAS i både jord och grundvatten observerades. Då fastigheten gränsar mot en banvall, finns det en oro att PFAS ska sprida via banvallen mot den närliggande Åkers kanalen. Syftet med detta examensarbete har därför varit att kartlägga transporten av PFAS i grundvatten från denna tidigare brandstation. En grundvattenflödesmodell konstruerades först i programvaran Visual MODFLOW. Grundvattenmodellen användes sedan som grund för konstruktionen av en transportmodell med MODPATH och MT3DMS. Transporten av fyra PFAS-homologer modellerades; perfluoroktansulfonat (PFOS), perfluorooktansyra (PFOA), 6:2 fluortelomersulfonat (6: 2 FTS) och perfluorpentansyra (PFPeA).

Resultatet av grundvattenmodelleringen visade att grundvatten från fastigheten strömmar mot sydväst och sedan vidare mot Åkers kanal. Den approximerade hastigheten hos en vattenmolekyl varierade mellan 270 m/år och 400 m/år. Transportmodelleringen visade att alla fyra PFAS-homologerna spred mot Åkers kanal via banvallen och att de kortkedjiga PFAS-homologerna (6:2 FTS och PFPeA) spred längre och snabbare än de långkedjiga PFAS-homologerna (PFOS och PFOA). Ungefärlig hastighet av föroreningsplymen för koncentration $4.5 \cdot 10^{-5}$ mg/L var 0,6 m/år för PFOS, 3 m/år för PFOA, 8 m/år för 6: 2 FTS och 16 m/år för PFPeA.

**Nyckelord**: Grundvattenmodellering, föroreningstransport, Visual MODFLOW, MODPATH, MT3DMS, PFAS, AFFF

*Institution för geovetenskaper, luft-, vatten- och landskapslära; Hydrologi. Uppsala Universitet. Villavägen 16, 752 36 UPPSALA.*

## PREFACE

This thesis is a 30 credits degree project of Master Programme in Environmental and Water Engineering at Uppsala University, Sweden. The project was done in corporation with WSP Environmental Sweden, where Leo Regazzoni was supervisor from WSP. Thank you Leo for making this degree project possible and for all the support you gave me throughout the project. Many thanks also to Martin Larsson from WSP. Your guidance and continuous help through the whole modelling process were greatly appreciated.

Furthermore, I would like to express my gratitude to Fritjof Fagerlund who was my supervisor from Uppsala University. Your competence was important for this project. I would also like to extend my thankfulness to Tom who has encouraged and supported me throughout this period. Finally, I would like to thank my family for supporting me in different ways during these five years and a half. Thank you mom for being my source of motivation.


UPTEC W 19 016, ISSN 1401-5765
Digitally published at the Department of Earth Sciences, Uppsala University, Uppsala, 2019.

# POPULÄRVETENSKAPLIG SAMMANFATTNING

**Spridningsmodellering av PFAS i Åkersberga**
*Worada Boonraksasat*

Per- och polyfluorerade alkylsubstanser (PFAS) är en grupp av konstgjorda kemikalier som sedan 1950-talet har använts i många konsumentprodukter, inklusive impregnerade textilier, impregnerat papper, nonstick-produkter (t.ex. Teflon), rengöringsmedel och brandsläckningsskum. PFAS har dock under senare år fått ökad allmän uppmärksamhet på grund av deras persistens, bioackumuleringspotential och potentiella toxiska effekter på människor och djur. Detta innebär att vissa PFAS-homologer inte bryts ned i naturen, ansamlas i och är giftigt för levande organismer. Brandövningsplatser har identifierats som en av de största källorna för spridningen av PFAS i miljön, på grund av användningen av PFAS-innehållande brandsläckningsskum av typen AFFF (aqueous film forming foams). Från de förorenade jordmassorna på en brandövningsplats transporteras PFAS ofta via vatten som finns under markytan (grundvatten). PFAS kan sedan transporteras en lång väg med grundvattnet och förorenar exempelvis sjöar och dricksvattentäkter nedströms. Detta utgör en potentiell risk för bland annat vattenlevande organismer (såsom fiskar) och människor som får i sig PFAS via intag av förorenade fisk och/eller dricksvatten.

Hur PFAS sprider sig i grundvatten beror på hur genomsläpplig jorden är. Ju mer genomsläpplig jord desto större bli omfattningen av PFAS spridning. Även PFAS sorption till jord och sediment är en viktig parameter. Eftersom PFAS kan bindas till jordpartiklar i marken påverkas detta därför transportshastigheten. För att begränsa spridning av PFAS från en brandövningsplats krävs därför en god kännedom om områdets hydrogeologi, dvs. den delen av geologin som studerar grundvattnet. Grundvatten- och transportmodell är ett verktyg som kan användas för att göra detta. En grundvattenmodell kan användas för att beräkna och visualisera grundvattenflöde inom ett valt område. En transportmodell kan sedan konstrueras baserat på beräknade grundvattenflöden för att studera transport av en förorening.

På den tidigare brandstationen i Åkersberga har hantering och användning av AFFF ägt rum under släckningsövningarna. WSP Environmental Sverige har utfört förundersökning på plats och förhöjda halter PFAS i både jord och grundvatten observerades. Då fastigheten gränsar mot en banvall, finns det en oro att PFAS ska sprida via banvallen mot den närliggande Åkers kanalen. Syftet med detta examensarbete har därför varit att kartlägga transporten av PFAS i grundvatten från denna fastighet. En grundvattenflödesmodell konstruerades först i programvaran Visual MODFLOW. Grundvattenmodellen användes sedan som grund för konstruktionen av en transportmodell med MODPATH och MT3DMS. Transporten av fyra PFAS-homologer modellerades; perfluoroktansulfonat (PFOS), perfluorooktansyra (PFOA), 6:2 fluortelomersulfonat (6: 2 FTS) och perfluorpentansyra (PFPeA).

Med hjälp av data över områdets geologi, hydrogeologi och hydrologi kunde grundvattenmodellen sedan konstrueras. För att säkerställa att de beräknade grundvattennivån överensstämmer med verkligheten utfördes en kalibrering. Under kalibreringen justerades olika parametervärden tills de beräknade grundvattennivån överensstämde med den observerade grundvattennivån. Resultatet av grundvattenmodelleringen visade att grundvatten från fastigheten strömmar en kort bit mot sydväst, för att sedan via banvallen strömma vidare mot Åkers kanal, som är belägen till väster om fastigheten. Den approximerade hastigheten hos grundvattenflöde varierade mellan 270 m/år och 400 m/år.

En transportmodell konstruerades därefter baserat på resultat av grundvattenmodelleringen och observerade PFAS koncentrationer på fastigheten. Beräknade koncentrationer av de fyra PFAS-homologerna jämfördes sedan mot de observerade koncentrationerna. Resultatet av transportmodelleringen visade att alla fyra PFAS-homologerna spreds mot Åkers kanal via banvallen och att de PFAS-homologerna med kortare fluorerade kolkedjor (6:2 FTS och PFPeA) spreds längre och snabbare än de PFAS-homologerna med längre fluorerade kolkedjor (PFOS och PFOA). Ungefärlig hastighet av föroreningsplymen för koncentration $4.5 \cdot 10^{-5}$ mg/L var 0,6 m/år för PFOS, 3 m/år för PFOA, 8 m/år för 6: 2 FTS och 16 m/år för PFPeA.

## ABBREVIATIONS

| | |
|---|---|
| AFFFs | Aqueous film forming foams |
| bw | Body weight |
| dw | Dry weight |
| EFSA | European Food Safety Authority |
| $K$ value | Hydraulic conductivity |
| $K_d$ value | Distribution coefficient |
| m a.s.l. | Meters above sea level |
| m b.g.l. | Meters below ground level |
| PFASs | Per- and polyfluoroalkyl substances |
| PFOS | Perfluorooctane sulfonic acid |
| PFOA | Perfluorooctanoic acid |
| 6:2FTS | 6:2 Fluorotelomer sulfonate |
| LOD | Limit of detection |
| PFPeA | Perfluoropentanoic acid |
| SMHI | Swedish Meteorological and Hydrological Institute |
| SGI | Swedish Geotechnical Institute |
| SGU | Geological Survey of Sweden |
| TDI | Tolerable daily intake |
| U.S. EPA | United States Environmental Protection Agency |
| USGS | United States Geological Survey |

# TABLE OF CONTENTS

# 1. INTRODUCTION

Per- and polyfluoroalkyl substances (PFASs) are an umbrella term for a group of man-made organic chemicals that have been commercially used in many products since the 1950s (Naturvårdsverket, 2018). The increasing use of PFASs is due to their unique properties to resist heat, dirt, fat, and water. One of PFASs most important uses is therefore as film-forming chemicals in firefighting foams of type AFFFs (aqueous film forming foams), which in turn make the firefighting training sites listed as one of the most important sources for the spread of PFASs in the environment (SGI, 2018). From a training site, PFASs are often transported via groundwater to the environment and poses a potential risk for humans and animals, because of their persistence, bioaccumulative potential and potential toxic effects (Ahrens et al., 2015). Good knowledge of the hydrogeological conditions is therefore very important to limit and map this spreading. Groundwater flow and transport modelling is a tool that can be used to map the transport of PFASs in groundwater.

In Sweden, increased levels of PFASs have been found in both drinking water and groundwater in several municipalities, where historical use of firefighting foam containing PFASs from the nearby firefighting training sites have been identified as sources (Kemikalieinspektionen, 2013). Thereby, identification and investigation of all potential sites where PFASs firefighting foams have been used are necessary so that remediation can be taken place. As in this case, WSP has been commissioned to investigate a property where Åkersberga's fire station was previously located. Training with firefighting foam containing PFASs has been carried out at the former fire station and the preliminary investigation performed on site has consisted of both soil and groundwater sampling. The results have shown elevated levels of PFASs in both soil and groundwater and that the direction of groundwater flow within the property is to the southwest. Since the former fire station is located next to a railroad track in the southwest, there is a concern/hypothesis that PFASs will spread through the railroad track and then further towards the nearby Åkers canal.

## 1.1. AIM AND QUESTIONS

The aim of this project is to map the transport of PFASs in groundwater from the former fire station in Åkersberga. Literature study, fieldwork, and groundwater flow model over the study area combined with transport model will be constructed to answer the following questions:

- What are the important properties of PFASs that should be taken into consideration when constructing a transport model?
- What are the hydraulic conductivities of different geologic materials in the study area as determined by slug tests in the field and literature studies?
- What is the direction and velocity of groundwater flow in the study area?
- How do PFASs spread from the former fire station and what velocity does the contaminant plume have?

- Do PFASs spread to Åkers canal from the former fire station via the railroad track?

## 1.2. LIMITATIONS

There are 11 PFAS homologues that were analyzed in the laboratory but only four have been chosen for further transport modelling attempt, which are perfluorooctane sulfonic acid (PFOS), perfluorooctanoic acid (PFOA), 6:2 Fluorotelomer sulfonate (6:2 FTS), and perfluoropentanoic acid (PFPeA). PFOS and PFOA have been chosen because they are the two most well-studied PFAS homologues and according to Kemikalieinspektionen (2013) they are also the two common homologues that are found with high concentrations in surface and groundwater that are affected by AFFFs containing PFOS. This type of AFFF is the so-called "old generations of AFFFs". In the new generations of AFFFs, PFOS has been substituted with 6:2 FTS which also presented in the old generations AFFFs (Kemikalieinspektionen, 2013). Moreover, 6:2 FTS is also one of the three dominant PFAS homologues that was found during the preliminary investigation of the former fire station in groundwater (together with PFHxA and PFPeA). With these reasons 6:2 FTS has been chosen for further examination. Lastly, PFPeA has been chosen for further transport modelling because it is a degradation product of 6:2 FTS. Also, because it is the dominant PFAS homologue that was found in groundwater and classified as a short-chain PFASs.

# 2. THEORY

## 2.1. PFASs

PFASs are a group of man-made chemicals that can be found in, for example, impregnated textiles, impregnated paper, nonstick products (e.g., Teflon), cleaning agents, and in firefighting foams (Kemikalieinspektionen, 2018).

### 2.1.1. Chemical and Physical Properties

PFASs consist of a carbon chain in which at least one hydrogen atom, bond to the carbon chain, has been replaced with fluorine. The carbon-fluorine chain has a functional group attached to its one end, that gives the compound special properties. A *polyfluorinated substance* is a group of PFASs where more than one, but not all hydrogen atoms have been substituted with fluorine atoms. If all the hydrogen atoms have been substituted with fluorine atoms the group is called a *perfluorinated substance*. Fluorine substitution and the resulting carbon-fluorine bond affects the properties of PFASs and creates very strong, stable, and unique compounds. (Buck et al., 2012)

According to Buck et al. (2012) the unique compounds of PFASs characterize by:

- Hydrophobic (water repelling) or oleophobic (oil/fat repelling) “tail”, which contains a high proportion of fluorine.
- Hydrophilic (water attracting) “head”.
- Organic linking group “spacer” that joins the hydrophobic/oleophobic tail and hydrophilic head together, see Figure 1 for an example of PFOS.

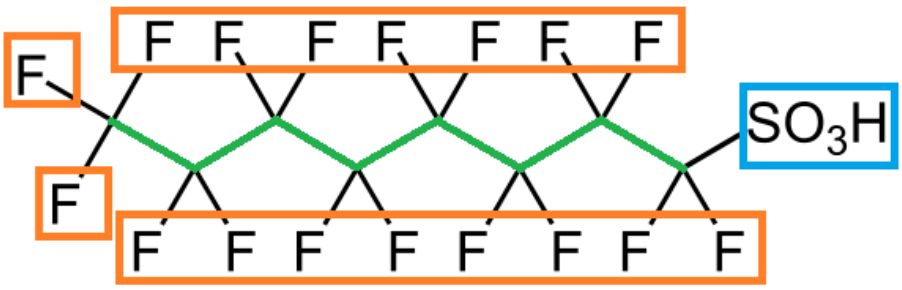


**Figure 1.** The chemical structure of PFOS. Hydrophobic/oleophobic tail in orange, hydrophilic head (functional group, here sulfonic acid) in blue, and the organic linking group spacer (carbon chain) in green.

The carbon-fluorine bond is one of the strongest chemical bonds known to man. PFASs are therefore extremely stable both chemically and thermally (Buck et al., 2012). This means that they do not degrade or are destroyed easily, neither by strong basic/acidic chemicals, heat, or reduction and oxidation (Kissa, 2001). Nevertheless, PFASs and their carbon-fluorine bond can

be destroyed in some conditions, such as under very high temperatures, up to 1,000 °C (Lutze et al., 2012).

Furthermore, PFASs can bind to particles in soil and sediment. There are, in particular, two different interactions that describe this sorption behavior. Hydrophobic interaction of the perfluorinated carbon ($CF_2$) tail with the soil organic carbon, and electrostatic interaction of functional group to the charged clay fraction of the soil (Higgins and Luthy, 2006). The sorption of PFASs has been observed to increase with the content of the organic carbon in the soil, and with decreasing pH (Higgins and Luthy, 2006). The other important factor affecting the sorption of PFASs is the $CF_2$ chain length. According to Higgins and Luthy (2006), the binding strength is proportional to the length of the $CF_2$ chain. In other words, the longer the $CF_2$ chain, the stronger is the binding/sorption to the soil. Furthermore, according to Gellrich et al. (2012) the distribution of PFASs between soil particles (solid phase) and water (liquid phase) is an important factor affecting the transport and fate of PFASs. To express the sorption behavior, the solid-liquid distribution coefficient ($K_d$) is used and it can be described by Equation (1):

$$K_d = \frac{C_s}{C_w} \tag{1}$$

where $C_s$ is the concentration of the adsorbed substance (ng/g dry weight (dw)) and $C_w$ is the concentration in water (ng/l).

### 2.1.2. Commercial Uses

The unique composition of PFASs has made them popular for many different uses in various industries, among them as firefighting foam of type AFFF. AFFFs have been used since the 1960s and were developed to extinguish hydrocarbon fuel fires. PFASs have been used as ingredients in AFFFs because of their ability to lower the surface tension (surfactant properties), and hence enable aqueous film formation to effectively spread over the lighter hydrocarbon fuels (Ahrens et al., 2015). No AFFFs based on non-fluorinated compounds/surfactants can provide as effective fire control as those with PFASs (Buck et al., 2012). The foam is used for emergency and training purposes at military bases, airports, oil rigs, and municipal fire departments. This has resulted in direct releases of PFASs to the environment (Filipovic et al., 2015). In the new generations of AFFFs, 6:2 FTS which is already an ingredient in old generations of AFFFs has been used to substitute PFOS (Kemikalieinspektionen, 2013). This is because the use of firefighting foams containing PFOS was banned in the EU in 2011, since PFOS was classified as PBT-compounds, meaning that it is extremely persistent, bioaccumulative and potentially toxic (Kemikalieinspektionen, 2013).

Furthermore, due to their properties to resist water, fat, and dirt PFASs have been applied in consumer products including impregnation- and waterproofing agents used for tents, shoes, sofas, carpets, all-weather clothing and such (U.S. EPA, 2018). According to

Kemikalieinspektionen (2018) textile and leather impregnation are two of the biggest uses for PFASs. Paper and food packages can also be treated with impregnation agents containing PFASs, especially those where oil/fat repellent properties are requested (Kemikalieinspektionen, 2018). Other uses of PFASs is as coatings. PFOA was, for instance, the main chemical used to provide nonstick coating surface for pans and other cookware, such as Teflon. The chemical is not present in significant amounts in the final products but the use during the process of making Teflon have historically resulted in huge emissions to the environment (Kemikalieinspektionen, 2018). In very low concentrations PFASs have also been used as ingredients in cleaning products, such as window cleaners, polishes, waxes, and car care products. Although the concentrations in the products are low, the emissions to the environment can be very significant.

### 2.1.3. Toxicity and Health Risks

Human is exposed to PFASs through contaminated drinking water and food, either directly or indirectly via food packaging. The exposure also occurs via air, mostly indoor air and dust, through the use of products containing PFASs (Naturvårdsverket, 2018).

Many PFASs degrade very slowly or not at all in the environment, and some degrade into very persistent chemicals that can bioaccumulate over time in living organisms (Kemikalieinspektionen, 2018). In particular, so-called long-chain PFASs are considered to be more harmful due to their high bioaccumulation potential (Ahrens et al., 2015). Unlike other bioaccumulative chemicals, PFASs do not accumulate in fatty tissue, instead they bind to proteins and accumulate in other human organs, such as the liver, kidneys, and in the blood (Kemikalieinspektionen, 2018).

Several studies have shown that both PFOS and PFOA can cause negative health effects in laboratory animals, such as reproductive and developmental, liver and kidney, and immunological effects (U.S. EPA, 2018). With regard to human health, in 2018, The European Food Safety Authority (EFSA) released the first of two assessments on PFOS and PFOA in food. The negative health effects observed from human epidemiological studies were: increased risk of cardiovascular disease, effects on hepatocytes, effects on the immune system, and decreased birth weight (EFSA, 2018). PFOA is also suspected of being carcinogenic to humans (Kemikalieinspektionen, 2018). Because of increased concerns due to the negative environmental and health effects caused by PFOS and PFOA, they have been substituted to the shorter chain alternatives with similar physical and chemical properties. However, very little are known regarding their fate, exposure, and adverse effects (U.S. EPA, 2018).

### 2.1.4. Guideline Values

In 2015, the Swedish Geotechnical Institute (SGI) released the preliminary guideline values for PFASs in soil and groundwater. A lot of data is required and for most PFAS homologues data is not sufficient, therefore SGI has chosen to only calculate guideline values for PFOS. For sensitive land use (e.g. housing), the generic guideline value is 3 µg/kg dw and is governed by the protection of soil environment. For less sensitive land use (e.g. industry), the generic

guideline value is 20 µg/kg dw and is governed by the protection of groundwater as a natural resource. For groundwater, the generic guideline value is $4.5 \cdot 10^{-5}$mg/l, governing by the protection of groundwater as a natural resource (Pettersson et al., 2015).

There are currently no guideline values for PFASs in food and drinking water. However, EFSA (2018) has recently released the preliminary tolerable daily intake (TDI) for PFOS and PFOA, for PFOS it is $1.9 \cdot 10^{-3}$ µg/kg body weight (bw) per day and for PFOA it is $0.9 \cdot 10^{-3}$ µg/kg bw per day. Furthermore, the Swedish National Food Agency recommends that drinking water should not contain higher than $9 \cdot 10^{-5}$ mg PFASs11/l (Livsmedelsverket, 2018). PFASs11 is the sum of 11 PFAS homologues that were included in the preliminary investigation of the former fire station and that are recommended for investigation in drinking water by Livsmedelsverket (2018), see Table 1.

**Table 1.** The 11 PFAS homologues that are included in the preliminary investigation and that are recommended for investigation in drinking water according to Livsmedelverket (2018). $CF_2$ chain length represents the number of perfluorinated carbon atoms for each PFAS homologue

| Number | PFAS-compound | $CF_2$ chain length |
|---|---|---|
| 1 | PFBS | 4 |
| 2 | PFHxS | 6 |
| 3 | PFOS | 8 |
| 4 | 6:2 FTS | 6 |
| 5 | PFBA | 3 |
| 6 | PFPeA | 4 |
| 7 | PFHxA | 5 |
| 8 | PFHpA | 6 |
| 9 | PFOA | 7 |
| 10 | PFNA | 8 |
| 11 | PFDA | 9 |

## 2.2. HYDRAULIC CONDUCTIVITY

Hydraulic conductivity is a parameter describing a material's capacity to transmit water (HydroSOLVE, 2016). The parameter, according to Butler (1997) is important in groundwater investigations especially when contamination is suspected.

### 2.2.1. Slug Test

Slug test is a controlled field experiment where the hydraulic conductivity of an aquifer is being estimated through a sudden change of water level in a well (HydroSOLVE, 2018). In practice, a slug test begins with an instantaneous change in water level in a well, either by increasing or decreasing it. The water pressure (or hydraulic head) in the well will also instantaneously change as a result. Subsequently, the water in the well will go back to its static level, by either moving out from or into the well (falling respective rising head). These hydraulic head changes over time are recorded (called response data) and can later be used to estimate the hydraulic conductivity through comparisons with theoretical models of test responses (Butler, 1997). How quick or slow the recovery of the groundwater level is, depends on the hydraulic properties of aquifers.

The mathematical solution by Hvorslev (1951) is one of the theoretical models used for the analysis of slug tests. It is suitable for slug tests performing in fully penetrating wells in confined aquifers. The method assumes the following (HydroSOLVE, 2018):

- The aquifer has infinite areal extent
- The aquifer is homogeneous, isotropic and of uniform thickness
- The water table is horizontal prior to the test
- Instantaneous injection/withdrawal of a volume of water results in an instantaneous change in water level
- Groundwater flow is horizontal toward or away from the well

Figure 2 shows an illustration of how a falling-head slug test works. Hvorslev's equation for fully penetrating well in confined aquifers is as follows:

$$ln\left(\frac{h_t}{h_0}\right) = -\frac{2KLt}{r^2 ln\left(\frac{L}{R}\right)} \quad (2)$$

Where $h_0$ is initial displacement at t=0 [m]

$h_t$ is displacement at time t [m]

$K$ is hydraulic conductivity $[m/s]$

$L$ is screen length [m]

$t$ is elapsed time since initiation of the test $[s]$

$r$ is radius of the well casing [m]

$R$ is radius of the well screen [m]

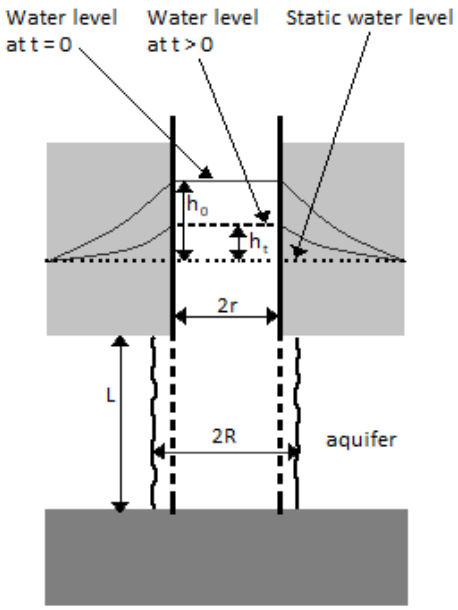


**Figure 2.** Illustration of a falling-head slug test. The figure is inspired by AquiferTest (2019). Note that $t = 0$ is the time at which the maximum displacement is obtained ($h_0 = h_t$ at $t = 0$).

The solution of Equation (2) in the format of a logarithm of a normalized head ($h_t/h_0$) versus time is a straight line (Butler, 1997). According to Butler (1997) the straight line should be fitted to the normalized head in the range of 0.15 to 0.25 in order to obtain the best results. The hydraulic conductivity can then be estimated through the help of this fitted straight line. By knowing that the natural logarithm of 0.37 ≈ - 1, the e-folding time at which $h_t/h_0$ = 0.37 can be obtained from the straight line and then used to simplified Equation (2) according to the Equation (3):

$$ln\left(\frac{h_t}{h_0}\right) = -\frac{2KLt}{r^2 ln\left(\frac{L}{R}\right)} \leftrightarrow ln(0.37) = -\frac{2KLt_{37}}{r^2 ln\left(\frac{L}{R}\right)} \leftrightarrow 1 = \frac{2KLt_{37}}{r^2 ln\left(\frac{L}{R}\right)} \quad (3)$$

where $t_{37}$ [s] is the time at which $h_t/h_0$ is equal to 0.37. Rewriting of Equation (3) results in Equation (4) of Hvorslev, which can be used to estimate hydraulic conductivity in fully penetrating well and confined aquifers (AquiferTest, 2019):

$$K = \frac{r^2 ln\left(\frac{L}{R}\right)}{2Lt_{37}} \quad (4)$$

According to Butler (1997) if the ratio of *L/R* is less than 8, then Equation (5) is used instead of Equation (4):

$$K = \frac{r^2 ln(200)}{2Lt_{37}} \quad (5)$$

### 2.2.2. SGU's Well Archive

Geological Survey of Sweden (SGU) provides details of the location and technical data for individual wells in Sweden, mainly those bored in rocks. They comprise the information that well drillers have been legally obligated to send to SGU since 1976 (SGU, 2018). Well data can, for example, include total depth, dimensions, water capacity, and groundwater level. The data can be downloaded from the web service, called GeoLagret.

The hydraulic conductivity of the bedrock can be calculated based on the estimated water capacity (*Q*) and well depth in the bedrock (*L* = total depth – casing depth) that obtain from SGU's well archive. In order to estimate the hydraulic conductivity in the bedrock, a new method recommended by SGU can be used. The method uses the connection between transmissivity (*T*) and estimated well capacity (*Q*). The hydraulic conductivity can finally be estimated by dividing the obtained *T* value with the well depth in bedrock, see Equation (6). (Ryd, 2017).

$$K = \frac{T}{L} = \frac{0.076 * Q^{1.026}}{L} \quad (6)$$

Where $T$ is transmissivity $[m^2/s]$

$Q$ is estimated water capacity $[m^3/s]$

$L$ is well depth in the bedrock [m]

The large-scale hydraulic conductivity (effective conductivity) according to Matheron (1967) can then be calculated using Equation (7).

$$K_{3D} = K_g exp\left(\frac{\sigma_{lnK^2}}{6}\right) \quad (7)$$

Where $K_{3D}$ is effective hydraulic conductivity [m/s]

$K_g$ is geometric mean value of hydraulic conductivity [m/s]

$\sigma_{lnK}$ is standard deviation of *ln(K)*

## 2.3. GROUNDWATER FLOW AND TRANSPORT PROCESS

There are two basic principles where all process-based models of groundwater flow are derived from Darcy's law and conservation of mass (Andersson et al., 2015).

### 2.3.1. Darcy's Law

One-dimensional groundwater flow through a saturated porous medium can be described with Darcy's law, Equation (8). This states that the water flow between two locations is directly proportional to the difference in water levels ($h$) and the cross-sectional area ($A$) but inversely proportional to the distance ($l$). The minus sign in Equation (8) indicates that the water flows in a negative direction, from higher to lower potential. (Knutsson and Morfeldt, 1993)

$$Q = -KA\frac{dh}{dl} \tag{8}$$

where $Q$ is quantity of water per unit of time $[\mathrm{m}^3/\mathrm{s}]$

$A$ is cross-sectional area perpendicular to the flow $[\mathrm{m}^2]$

$h$ is total potential in the y-axis [m]

$l$ is distance in x-axis between the two locations [m]

$\frac{dh}{dl}$ is hydraulic gradient $[-]$

According to Knutsson and Morfeldt (1993) the following assumptions are usually made when using Darcy's law: (i) the medium is porous, homogenous, and isotropic, (ii) the water flow, $Q$ is constant, and (iii) the specific discharge, $q$ (m/s) is defined as Equation (9):

$$q = \frac{Q}{A} = -K\frac{dh}{dl} \tag{9}$$

In three-dimensional, the specific discharge in Equation (9) is a vector with components $q_x$, $q_y$, and $q_z$. The three components can then be written as Equation (10) according to Andersson et al. (2015):

$$q_x = -K_x\left(\frac{\partial h}{\partial x}\right)$$
$$q_y = -K_y\left(\frac{\partial h}{\partial y}\right) \quad (10)$$
$$q_z = -K_z\left(\frac{\partial h}{\partial z}\right)$$

where $q_x, q_y, q_z$ are specific discharge in x, y, and z direction $[\mathrm{m/s}]$

$K_x, K_y, K_z$ are hydraulic conductivity in x, y, and z direction $[\mathrm{m/s}]$

$\frac{\partial h}{\partial x}, \frac{\partial h}{\partial y}, \frac{\partial h}{\partial z}$ are hydraulic gradient in x, y, and z direction $[-]$

### 2.3.2. Continuity Principle

The continuity principle is a consequence of the conservation of mass and it states that "what flows into a defined volume in a defined time, minus what flows out of that volume in that time, must accumulate in that volume" (Encyclopedia Britannica, 2018). The water balance within the defined volume can then be described as:

$$outflow - inflow = \Delta storage$$

This defined volume is further known as a representative elementary volume (REV). The REV is a cube of porous material, large enough to be representative of the properties of the porous medium and small enough so that the change of head within the volume is relatively small (Andersson et al., 2015). The three sides of the REV are of lengths Δx, Δy, and Δz. In Figure 3 the REV and $q_y$ which correspond to the in- and outflow respectively along the y-coordinate axis can be seen.

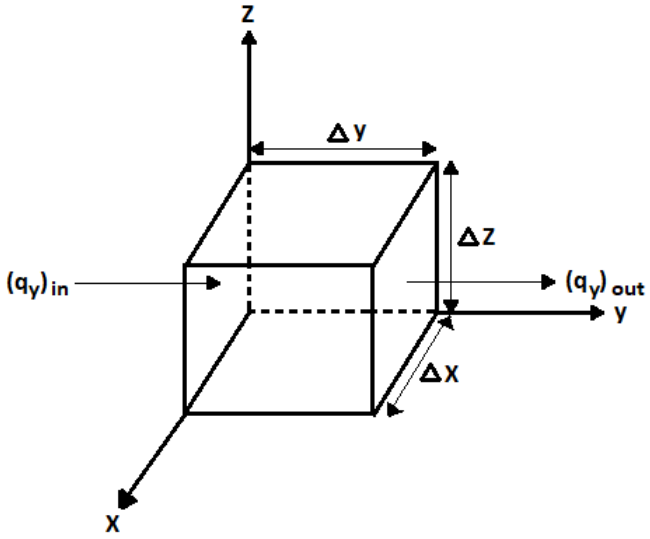


**Figure 3.** Representative elementary volume of lengths Δx, Δy, and Δz with the components of the flow $q_y$ along the y-axis. The figure is inspired by Andersson et al. (2015).

The final form of the water balance through the REV along x, y, and z-axis can then be written as Equation (11) according to Andersson et al. (2015):

$$\frac{\partial q_x}{\partial x} + \frac{\partial q_y}{\partial y} + \frac{\partial q_z}{\partial z} - w^* = -S_s \frac{\partial h}{\partial t} \tag{11}$$

where $w^*$is a volumetric flux per unit volume representing sources and/or sinks of water $[1/\mathrm{s}]$

$S_s$ is the specific storage $[1/\mathrm{m}]$

$\frac{\partial h}{\partial t}$ is changes in total potential over time $[-]$

### 2.3.3. Equation of Three-Dimensional Groundwater Flow

Finally, according to Andersson et al. (2015) the three-dimensional groundwater flow can be described by the partial differential equation in Equation (12), which obtained through the combination of Darcy's law, Equation (10), and continuity principle, Equation (11):

$$\frac{\partial}{\partial x}\left(K_x \frac{\partial h}{\partial x}\right) + \frac{\partial}{\partial y}\left(K_y \frac{\partial h}{\partial y}\right) + \frac{\partial}{\partial z}\left(K_z \frac{\partial h}{\partial z}\right) = S_s \frac{\partial h}{\partial t} - w^* \tag{12}$$

### 2.3.4. Contaminant Transport

Contaminant transport occurs with the water in the interstices of a porous medium, both in the unsaturated and saturated zone (Bear and Verruijt, 1987). How a contaminant moves through a porous medium is governed by how permeable the soil is, how well the contaminant dissolves in water, and how well the contaminant binds to particles in the soil (Kemikalieinspektionen, 2013). The processes that affect the transport of a contaminant in a porous medium are diffusion, advection, dispersion, and retardation (Fetter, 2001).

Diffusion is the process by which the concentration of a solute moves from areas of higher concentration to areas of lower concentration. Advection means that a solute is traveling at the same rate as the average linear velocity of the groundwater. Dispersion is a process where the solute is being diluted due to variations in the flow rate. And lastly, retardation is a process that slows down the solute movement, because of different chemical and physical processes (Fetter, 2001).

The process that has a significant effect on the transport of PFASs is retardation, due to sorption to the soil. The sorption for long-chain PFASs is as mentioned in 2.1.1. Chemical and Physical Properties generally higher than those with short-chain, because hydrophobicity increases with the number of perfluorinated carbon atoms (Kemikalieinspektionen, 2013). To determine the equilibrium between the concentration of a solute in water and on particles in the soil $K_d$ value is often used (Kemikalieinspektionen, 2013).

## 2.4. GROUNDWATER AND TRANSPORT MODEL

"A model is a simplified representation of the complex natural world" (Andersson et al., pp. 5, 2015). The model can be used to predict future/recreate past conditions, and to obtain a better understanding of a system (Andersson et al., 2015). For example, through a groundwater model the groundwater flow and contaminant transport can be computed and visualized (Brömssen et al., 2006). This example is the case where past conditions are recreated. The process to construct a groundwater model consists of two main parts: the conceptual model and the numerical model.

### 2.4.1. Conceptual Model

According to Brömssen et al. (2006), a conceptual model describing the study area's geology, hydrology and hydrogeology is the most important part when constructing a groundwater model. This is because the conceptual model provides a framework for designing the numerical groundwater model, which will later be used as a basis for calculations and/or estimation of the contaminant transport (Jonasson et al., 2007). To create a conceptual model a good understanding of the following is recommended (Brömssen et al., 2006):

- Geological conditions: soil types, soil layers, and bedrock elevations
- Hydrogeological conditions: groundwater levels, aquifer properties, and facilities that change the natural groundwater flows (such as pipes)
- Hydrological conditions: water balance for the study area (precipitation, evapotranspiration, and groundwater recharge), water levels and currents in the streams
- Contamination situation: information about contamination in soil and water

A compilation of collected data mentioned above provides support for the creation of a conceptual hydrogeological model. The conceptual model is three-dimensional and is represented in the form of map and plan profile, as well as the description in the text. Furthermore, the uncertainties contained in the conceptual model should also be described (Jonasson et al., 2007).

### 2.4.2. Numerical Model

Based on the conceptual model a numerical model is then built, using modelling software. The model is divided into layers according to the geological conditions, and the model domain is geographically defined based on the hydraulic conditions, such as lakes, streams, and water divides (Jonasson et al., 2007). Later, the boundary conditions are defined along the edges of the model domain, with the purpose to separate the model from the outside influence (Domenico and Schwartz, 1998). Finally, the groundwater flow is simulated by solving the groundwater flow equation, see Equation (12). There are two main numerical approaches to solve the groundwater flow Equation: finite-difference method and finite-elements method (Domenico & Schwartz, 1998). The output of a numerical model is calculated hydraulic head values at specific locations and times (Harbaugh, 2005). The steps included in the creation of the numerical model are summarized below (Brömssen et al., 2006):

- Demarcation of the model domain in plan and profile
- Defining the boundary conditions and aquifer characteristics
- Calibrations of the numerical flow model against field measurements, such as groundwater levels and flow, by successive alignment and adjustment of hydraulic conductivity and groundwater recharge
- Establishment of the final numerical flow model

Thereafter, depending on the aim of the modelling, different modules can be added to the numerical flow model to compute the contaminant transport with regards to diffusion, advection, dispersion, and retardation.

## MODFLOW

The software used for creating the numerical model in this project is called Visual MODFLOW Classic. MODFLOW is a three-dimensional finite-difference groundwater model that solves the groundwater-flow equation using linear and nonlinear numerical-solution method (Harbaugh, 2005). The software is developed by the U.S. Geological Survey (USGS) and released to the public domain in 1983.

The finite-difference method requires that the model domain is subdivided into a series of regular grid blocks, the process is called *discretization*. Figure 4 shows a spatial discretization of an aquifer system in three-dimension. A location within the system is described by rows, columns, and layers, using indices (i,j,k), see Figure 4. In each grid there is a block-centered node, which is the location where the head is calculated. Note that, the dimensions of each grid can be varied. For example, the area of interest can obtain smaller grid sizes.

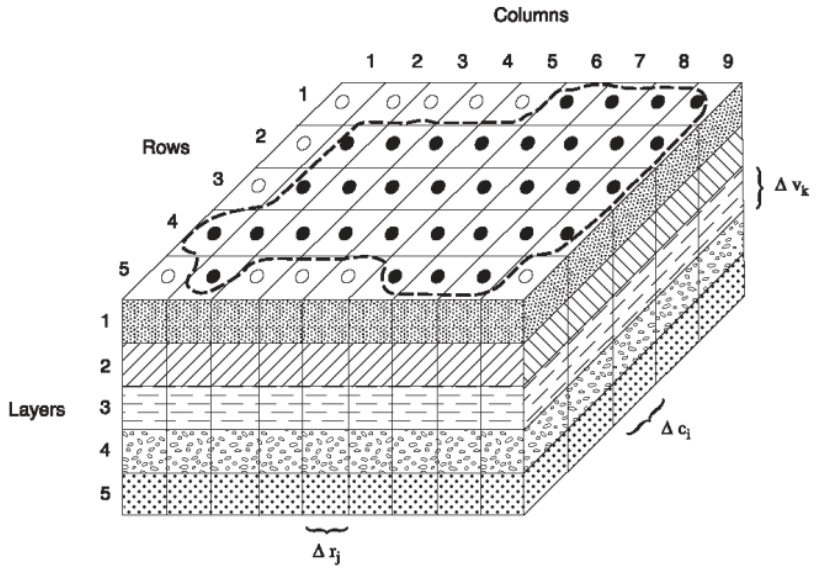


**Figure 4.** A discretized aquifer system in three-dimension. The dashed line marks the model domain. The dots represent nodes, where filled dots represent active cells and unfilled dots represent inactive cells. The location of the grid along row, column, and vertical direction is described with i, j, and k (Harbaugh, 2005).

Once the discretization is established, the aquifer characteristics (such as hydraulic conductivity and storage properties) can be assigned to each grid cell. The boundary conditions can also be defined. There are three types of boundary conditions that can be defined in MODFLOW:

1. Specified head boundary (Dirichlet conditions)
2. Specified flow boundary (Neumann conditions)
3. Head-dependent boundary (Cauchy conditions)

Firstly, the specified head boundary means that the head is set at a known value along the boundary, and it is independent of what is happening in the model. Note that, a specified head boundary can act as sources or sinks of water in the model. An example of a specified head boundary is the *constant head*, where heads are set to the same value along the boundary. The constant head can be used to define lakes and oceans. Secondly, the specified flow boundary defines the flow across the boundary and it is independent of what is happening in the model. An example is the *no flow* boundary, where the flow across the boundary is zero. It can be used to define the model boundary, where no water leaves or enter the grid cell. Lastly, the head-dependent boundary that defines the flow across the boundary as a response to the computed head at the node located on or near the boundary. An example of this boundary type is the *river* boundary, where the flow is changing according to the potential head. (Andersson et al., 2015)

**MODPATH**

MODPATH is a three-dimensional particle-tracking program, designed to work with the output of groundwater flow computed by MODFLOW (Pollock, 2012). MODPATH was developed to compute pathlines and travel time for the imaginary "particles" moving through the system, with a focus on the advective component of transport (Pollock, 1989). The pathline of each particle is computed by tracking the particle from one cell to the next until it reaches a boundary or another termination criterion has been satisfied (Pollock, 2012). Note that, both forward and backward particle tracking can be performed.

**MT3DMS**

MT3DMS is a modular three-dimensional multispecies transport model, where advection, dispersion/diffusion, and chemical reactions of contaminants in groundwater systems are taking into consideration. It was developed by Zheng and Wang (1999) for the US Army Corps of Engineers to work with the output of the groundwater flow computed by MODFLOW. The different transport processes are taking into consideration using various boundary conditions and external sources and sinks (Zheng and Wang, 1999).

# 3. METHOD

## 3.1. SITE DESCRIPTION

The contaminated site is a former fire station located in Åkersberga, a locality and the seat of Österåker municipality in Stockholm County, Sweden (Figure 5). To the southwest of the fire station there is a railroad track (Roslagsbanan) and to the southeast a green area. A car-repair garage, restaurants, and a petrol station can all be found to the north of the site (Woldegiorgis et al., 2017).

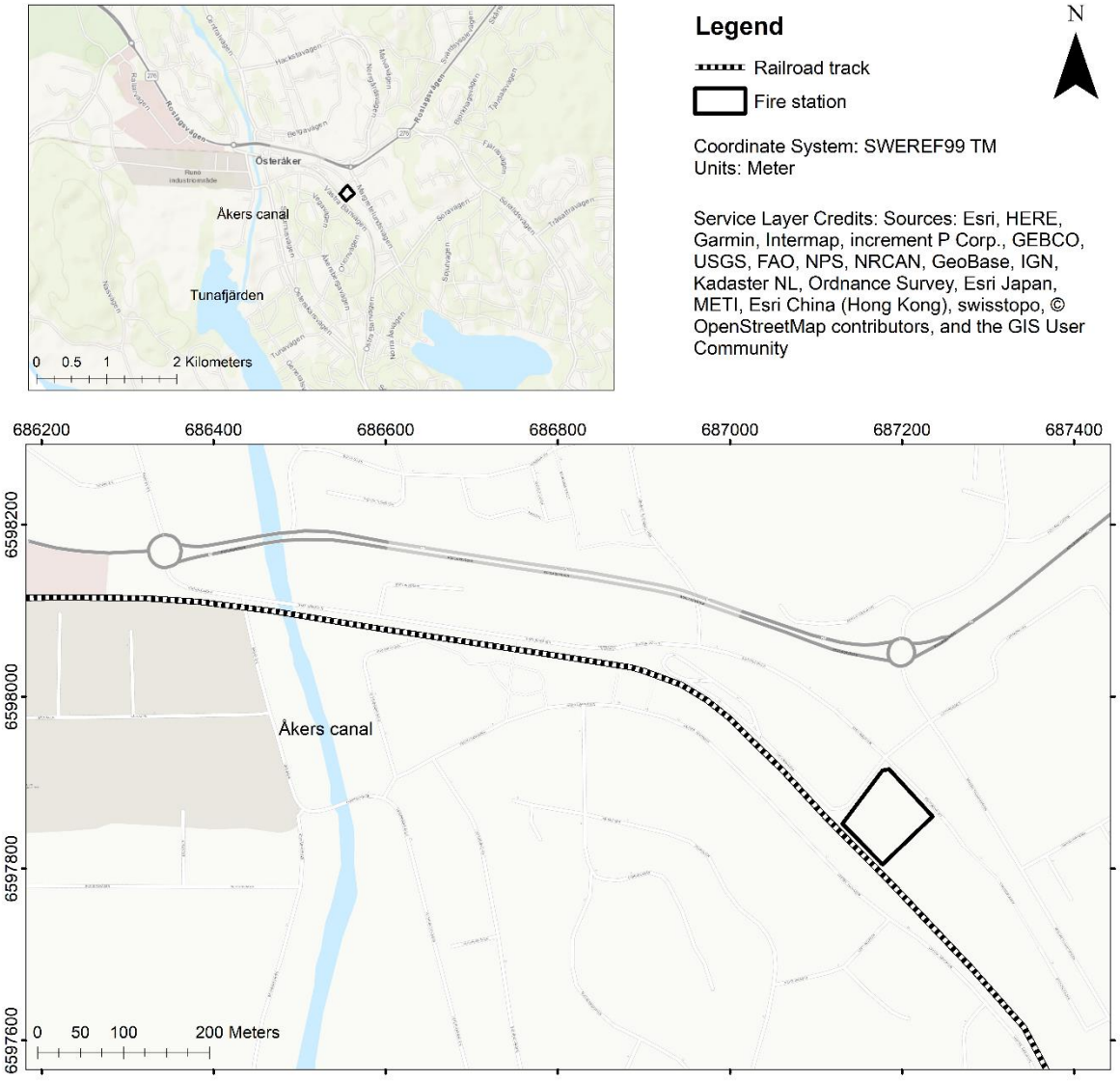


**Figure 5.** Location of the former fire station in Åkersberga, with the railroad track, Åkers canal, and Tunafjärden marked on the map.

The fire station was active between 1969 and 2017, where the firefighting foam of type AFFFs was handled and used for fire-training exercises. The firefighting trainings with AFFFs were

carried out until 1996–97, both inside and next to a small training building at the edge of the property located by the green area and the railroad track. Firefighting foam during training and leftover foam from the training exercises were also sprayed or flushed towards this green area. Approximately 1.5–2.5 kg of PFASs were used on the site. The future land use will be as a residential area, where several accommodations with patios at ground level will be built. It can therefore be said that the future land use is classified as sensitive land use as housing will be in the area (Woldegiorgis et al., 2017).

### 3.1.1. Geology

The following section summarizes the geology data known about the area: topography, soil types, soil layers, and type of bedrock.

#### Topography

Figure 6 represents a topographic map of the area. The former fire station is located in a low area, surrounded by higher areas in the northeast and southwest. It can also be noted that the fire station is located next to a smaller hill to the east. This is confirmed during the field investigation. Further to the west from the fire station, Åkers canal can be observed as a dark blue line stretching from north to south.

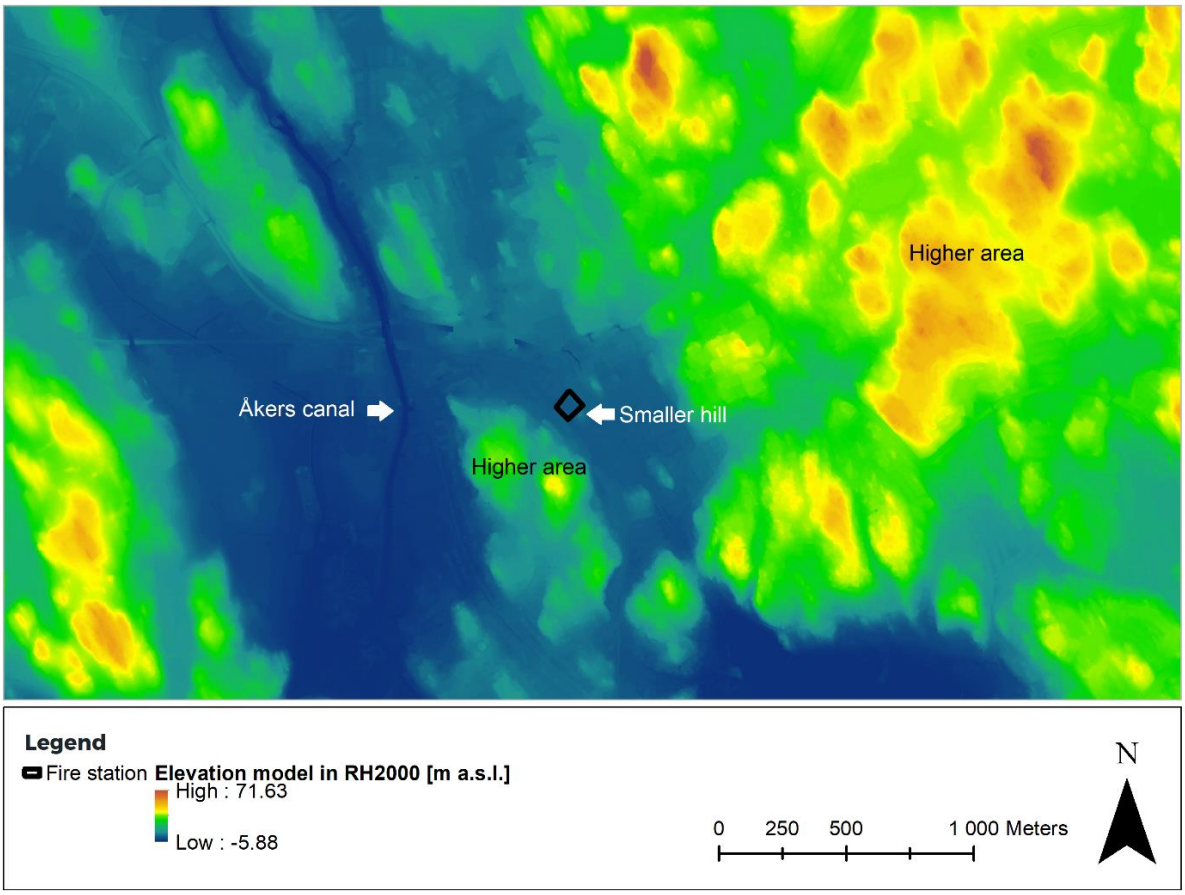


**Figure 6.** Elevation model over the former fire station and its surrounding in height system RH2000. GSD-Elevation data, grid 2+ ©Lantmäteriet.

## Soil

Figure 7 represents SGU's soil map of the area. Soil types under the former fire station consist of filling material, gyttja, and till on top of bedrock. The surrounding area consists of mainly glacial and postglacial clay, with bedrock appearing on the surface. The till deposited directly on the bedrock can also be found in most parts of the area.

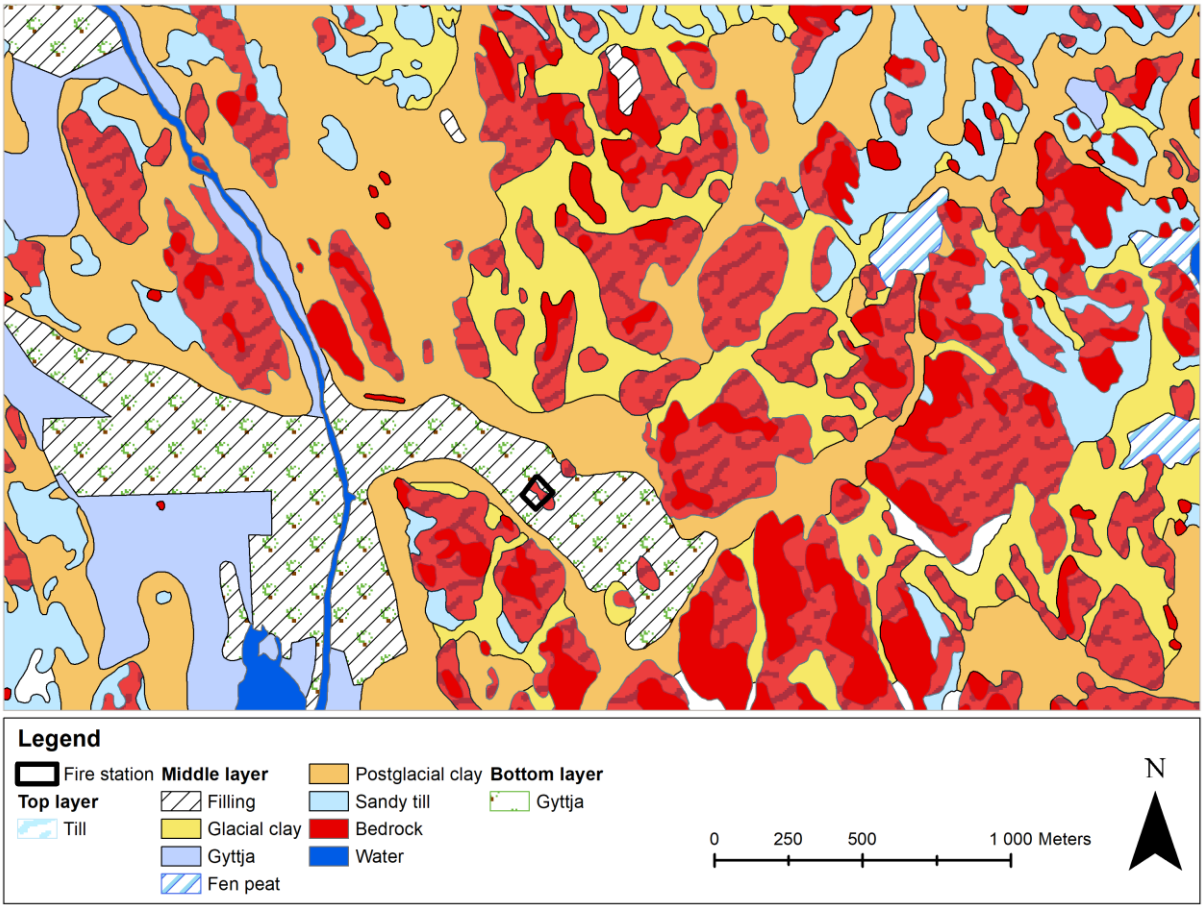


**Figure 7.** The map of soil types over the former fire station and its surroundings. Soil map 1:25000-1:100000 ©Geological Survey of Sweden.

The geotechnical survey performed by WSP has shown that existing filling material can be found in most sampling locations within the contaminated site, where its thickness varies from 0.1 to 1.8 meters. The filling material mainly consists of gravel and sand, and lies directly on top of a dry crust clay with thickness up to 2 meters. This is followed by a saturated clay, approximately 2 to 9 meters thick. The clay layer is followed by a thin layer of till on top of the bedrock. The thickness of till layer varies between 0.1 and 0.5 m, according to the ten probing points performed in the fire station area.

When it comes to the surrounding area, the numbers of investigations are limited. The available materials are geotechnical surveys conducted by WSP in conjunction with the expansion of Roslagsbanan (the railroad track southwest of the contaminated site). From the investigations, the existing railroad track has been estimated to be approximately 1 m thick and consists of

filling material called ballast. Under the filling material, 1 to 2 meters of dry cracked clay has been observed. The clay layer was then observed under the dry crack clay and its thickness varies along the railroad track, between 1 and 17 meters. The clay layer is followed by the till layer that lies on top of bedrock. The thickness of till layer varies between 1 to 2 meters. (Rigardt and Nilsson, 2015)

**Bedrock**

According to SGU's bedrock map obtained from kartgeneratorn, the area is located on a felsic intrusive igneous rock that mostly consists of granite, granodiorite, and monzonite. The texture of the igneous rock in the area is described as porphyry, which means that the rock consists of large-grained crystals. A smaller area consisting of ultramafic, mafic, and intermediate intrusive igneous rock (such as gabbro, diorite, and diabase) can also be observed in the southwest.

### 3.1.2. Hydrogeology

Several groundwater level measurements have been performed in the contaminated site. Overall, it can be said that the groundwater from the former fire station is flowing in the southwest direction. The top soil layer which consists of filling material can occasionally form an unconfined aquifer due to the impermeable clay layer below (Larsson et al., 2016). Its existence does in turn depend on the material that the filling consists of and according to Larsson et al. (2016) the unconfined aquifer is not considered to be coherent. The groundwater level measurements and the geological investigations further indicate that the till layer lying directly on top of the bedrock forms a confined aquifer in the area, meaning that the groundwater in the aquifer is under positive pressure and surrounded by impermeable layers. In this case, by a clay layer above and the bedrock below. The groundwater level measured in the till layer therefore represents an artesian pressure, meaning the level at which the water would rise to if the clay layer did not exist. For different types of aquifers, see Figure 8.

The clay layer between filling and till is considered to be relatively impermeable, due to its low hydraulic conductivity. This largely prevents the water in or above the clay layer from coming into the confined aquifer (Larsson et al, 2016). However, there are some exceptions caused by dry crust clay or shallow soil depth by a hill, where till has contact with the atmosphere (Figure 8). In these areas, recharge/outflow from a confined aquifer can occur. Finally, the intrusive igneous rock that was observed under the till can generally be said to hold a limited amount of water. According to Knutsson and Morfeldt (1993) water in this type of bedrock occurs in cracks and fractures.

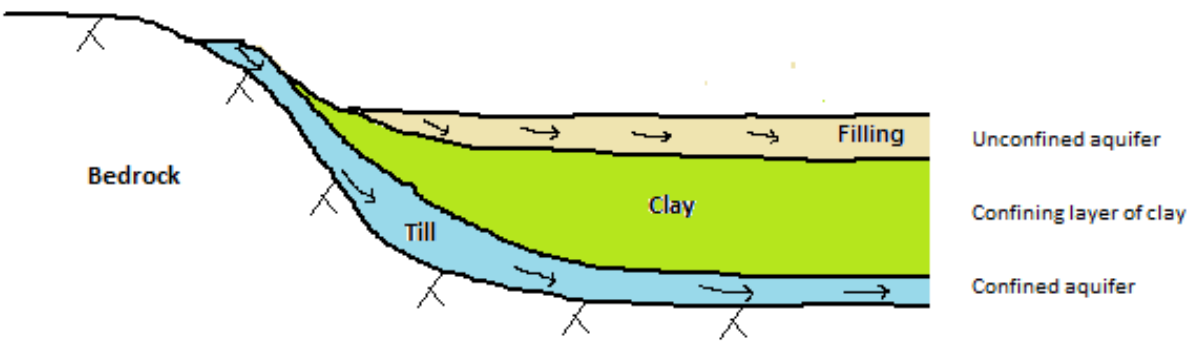


**Figure 8.** Schematic picture of soil and bedrock layers in the area, with different types of aquifers presented. The arrows describe the flow direction of groundwater in the soil.

### Aquifer Properties

The following properties of aquifers are needed for the groundwater flow and transport models: hydraulic conductivity ($K$), porosity (n), effective porosity ($n_e$), specific storage ($S_s$), and specific yield ($S_y$). Representative values of aquifer properties for each soil type that was found in the area can be seen in Table 2.

**Table 2.** Representative values of aquifer properties for each soil type

| **Soil type** | $\boldsymbol{K}$ $[\boldsymbol{m/s}]$ | $\boldsymbol{n}$ $[-]$ | $\boldsymbol{n_e}$ $[-]$ | $\boldsymbol{S_s}$ $[\boldsymbol{m^{-1}}]$ | $\boldsymbol{S_y}$ $[-]$ |
|---|---|---|---|---|---|
| Filling (fine gravel) | $10^{-5} - 10^{-3}$ (1) | 0.25 – 0.39 (4) | 0.05 – 0.2 (6) | $9.87 \cdot 10^{-5}$ (8) | 0.13 – 0.40 (4) |
| Filling (coarse gravel) | $10^{-4} - 10^{-2}$ (1) | 0.24 – 0.37 (4) | 0.05 – 0.2 (6) | $1.63 \cdot 10^{-6}$ (8) | 0.13 – 0.25 (4) |
| Clay | $10^{-11} - 10^{-8}$ (1)<br>$< 10^{-9}$ (2) | 0.5 (5) | 0.01 (7) | $9.81 \cdot 10^{-3}$ (8) | 0.02 (5) |
| Till | $10^{-10} - 10^{-5}$ (2) | 0.22 – 0.41 (4) | 0.01 – 0.1 (6) | $1.05 \cdot 10^{-5} - 9.82 \cdot 10^{-4}$ (8) | 0.01 – 0.34 (4) |
| Rock (granite) | $10^{-11} - 10^{-5}$ (3) | 0.001 (5) | $10^{-4} - 10^{-2}$ (6) | $1.63 \cdot 10^{-6}$ (8) | 0.0009 (5) |

(1) Fetter, 2001
(2) Larsson, 2008

(3) Brown et al., 1972 cited in Kuntsson and Morfeldt, 1993, p. 37
(4) Morris and Johnson, 1967
(5) Heath, 1983
(6) Carlsson and Gustafson, 1991 cited in Jonasson et al., 2007, p. 57
(7) Espeby and Gustafsson, 1997
(8) Younger, 1993

A site-based hydraulic conductivity of till and bedrock were estimated in this project. For the other soil types, the values of hydraulic conductivity were obtained from the literature (Table 2). To estimate the hydraulic conductivity of the till layer slug test could be performed, because there are observation wells drilled to the till layer in the area. The procedure of slug test and estimation of hydraulic conductivity in till will be described closely in 3.2.2. Slug Test.

To estimate the hydraulic conductivity in the bedrock an internal Excel model developed within WSP was used. First, data for wells located in the area of interest were downloaded from SGU's well archive (a data set of 113 wells were used). With information of estimated water capacity ($Q$) and well depth in the bedrock ($L$), the hydraulic conductivity in each well was calculated using Equation (6). The resulting hydraulic conductivities were then grouped in different populations representing depth in bedrock; (i) $L$ < 50 m, (ii) $L$ < 100 m, and (iii) $L$ < 210 m, which include all the 113 wells. Finally, the effective hydraulic conductivity ($K_{3D}$) was calculated using Equation (7) for each population. The results are represented in Table 3.

**Table 3.** Estimated effective hydraulic conductivity in bedrock for different population

| **Population** | $K_{3D,bedrock}$ [m/s] |
|---|---|
| $L$ < 50 m | $9.2 \cdot 10^{-7}$ |
| $L$ < 100 m | $7.8 \cdot 10^{-7}$ |
| $L$ < 210 m | $3.8 \cdot 10^{-7}$ |

### 3.1.3. Hydrology

### Water Balance

Groundwater recharge is a hydrological process where water from precipitation infiltrates and enters the groundwater aquifers (Eveborn et al., 2016). The starting point for determining the groundwater recharge is that the precipitation that does not evaporate is potentially available for groundwater recharge. With the information of precipitation ($P$) and evapotranspiration ($ET$), the potential groundwater recharge (also called effective precipitation, $P_e$) could therefore be calculated through: $P_e = P - ET$ (Eveborn et al., 2016). To estimate the effective precipitation in the area an internal Excel model developed within WSP was used.

Firstly, the average annual value of precipitation and evapotranspiration between the years of 1961 and 1990, called reference period, were obtained from Swedish Meteorological and Hydrological Institute (SMHI), see Table 4. The precipitation and the temperature are generally higher today compared to the reference period. This change was therefore taken into account by calculating the increase using the average annual precipitation and temperature data in Åkersberga, obtained from the SMHI's luftWebb. The results gave an increase in precipitation between 1991 and 2017 of 2.3% and 5.9% for evapotranspiration. The corresponding values for each parameter between 1991 and 2017 were then calculated and the results can be seen in Table 4.

**Table 4.** The average annual value of precipitation, evapotranspiration and effective precipitation for the periods 1961-1990 and 1991-2017

| **Parameter** | **1961 – 1990** | **1991 – 2017** |
|---|---|---|
| $P$ [mm/year] | 630 | 645 |
| $ET$ [mm/year] | 450 | 477 |
| $P_e$ [mm/year] | 180 | 168 |

## Surface Water

The former fire station belongs to a catchment area that drains off into the sea at Tunafjärden, where Åkers canal also has its outlet (Figure 9). Åkers canal is an 11.7-km long watercourse, whereof 3.7 km is man-made, that extends in the north-south direction to the west of the former fire station. The water level in Åkers canal is approximated to be around 0.13 m in RH2000 (Frost et al., 2018).

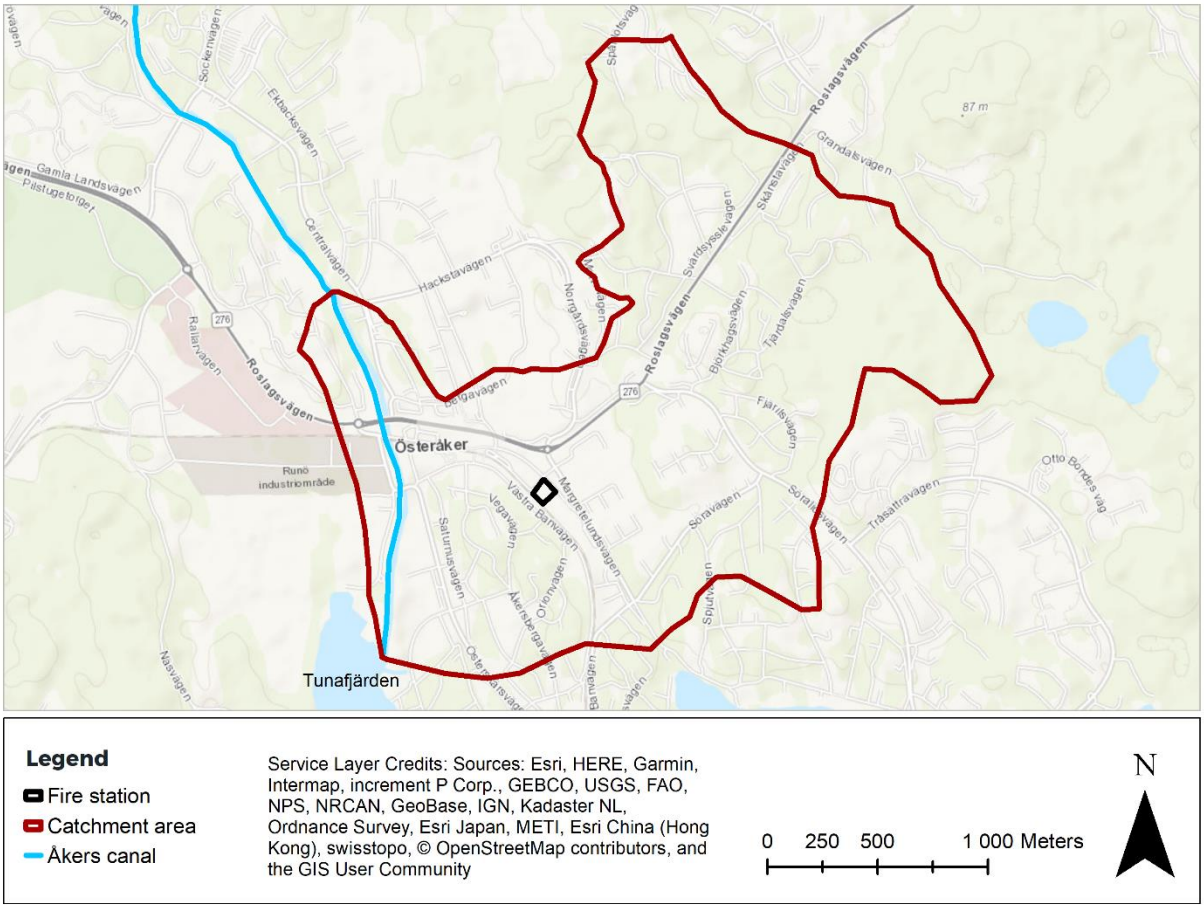


**Figure 9.** The former fire station, the catchment area that it belongs to, and Åkers canal ©SMHI.

### 3.1.4. Contamination

There have been some investigations performed on the site by WSP and SWECO during 2017 and 2018, where soil and groundwater samples in the contaminated area were collected for laboratory analysis with an aim to map the spreading of contaminants in the area. This section summarizes PFASs that were found during previous investigations.

#### Soil

The soil samples were collected at 27 sampling locations, whereof 24 are WSP's (17Wxx and 18Wxx) and 3 are SWECO's (18Sxx). In each sampling location, the soil samples were collected at different depths measured in meters below ground level (m b.g.l.). The sampling locations can be seen in Figure 10.

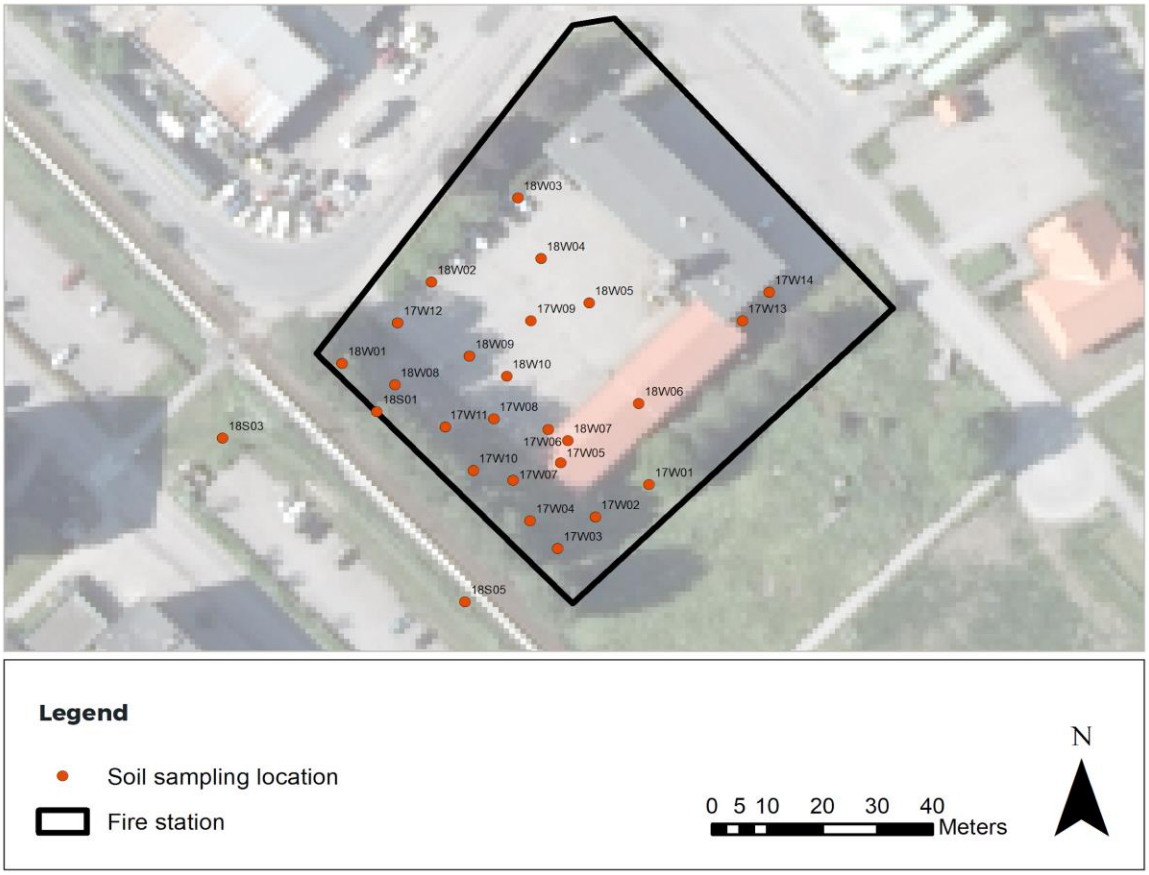


**Figure 10.** Soil sampling locations. Background map: GSD-Orthophoto, 1 m color © Lantmäteriet.

The samples were then analyzed, among other things, with regard to 11 different PFAS homologues. The laboratory results showed that PFASs in unsaturated soil could be detected in 26 of 27 sampling locations, where the concentrations of PFASs11 vary from 1.1 to 730 µg/kg dw. The only sampling location where no PFASs could be observed in the laboratory was 17W14. It can also be noted from the laboratory results that PFOS is the dominant homologue of the 11 analyzed PFASs in the soil (Figure 11).

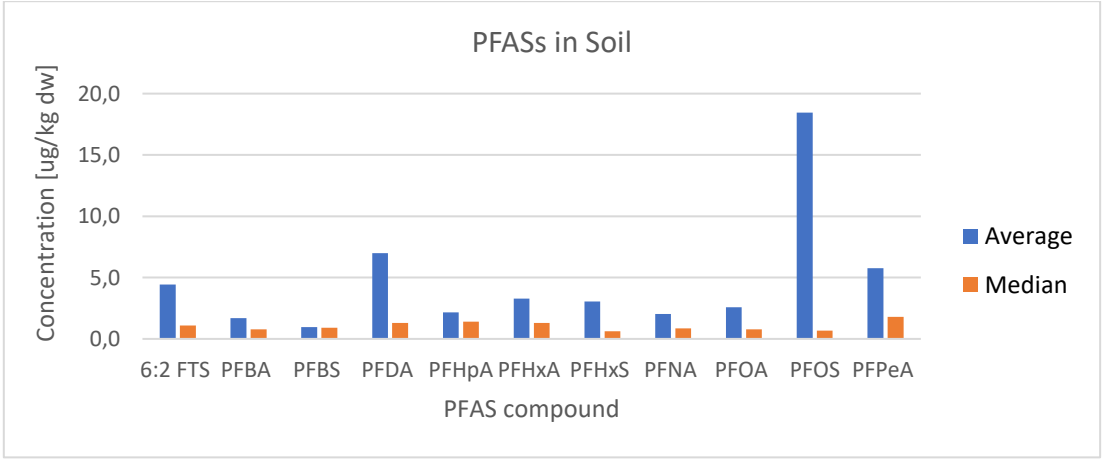


**Figure 11.** The average and median concentrations of PFASs in the soil.

## Groundwater

The groundwater samples were collected in the till layer at 17 different sampling locations, whereof 14 are WSP's (17Wxx and 18Wxx) and 3 are SWECO's (18Sxx), see Figure 12.

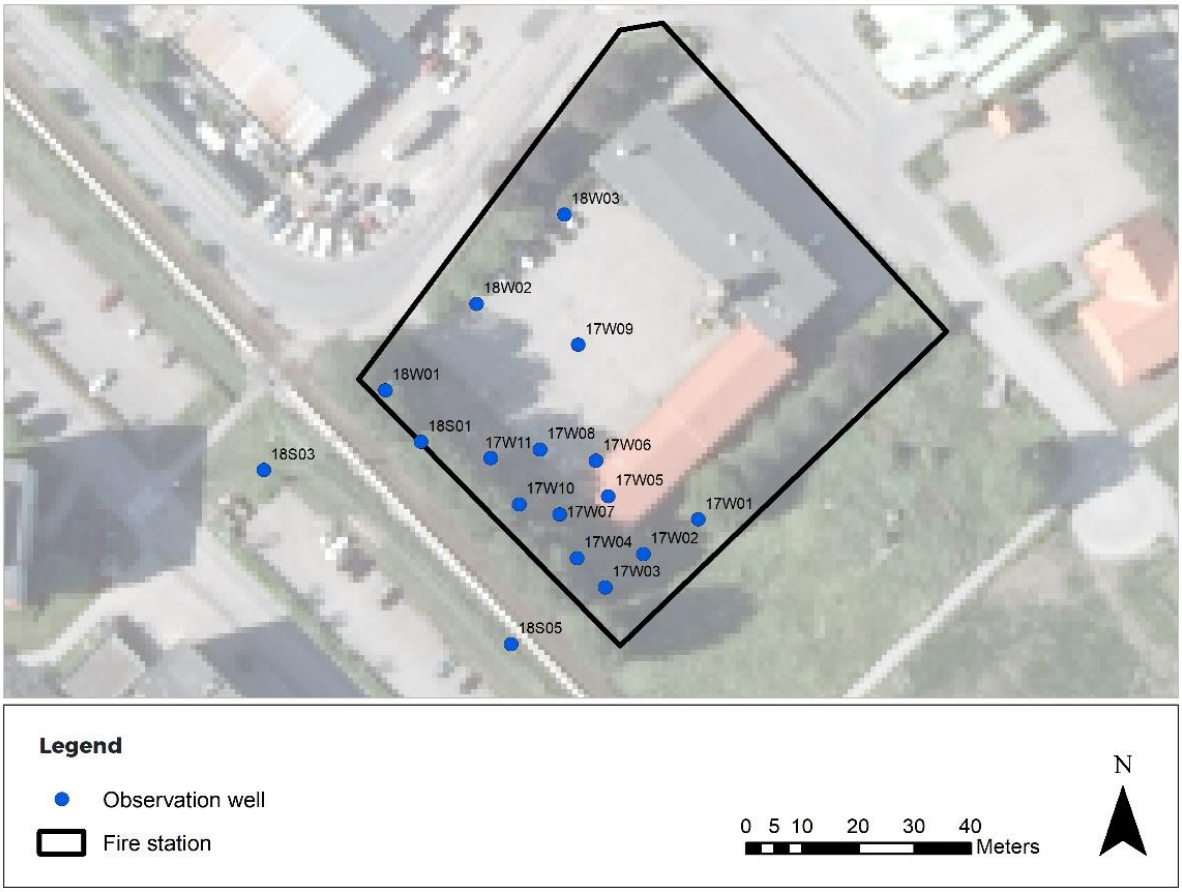


**Figure 12.** Observation wells in groundwater. Background map: GSD-Orthophoto, 1 m color © Lantmäteriet.

The laboratory results showed that PFASs could be detected in 16 of 17 sampling locations. The only sampling location where PFASs could not be detected was 18S05. The concentrations of observed PFASs11 in groundwater vary from 10 ng/l to 14000 ng/l. The highest PFASs11 concentration was observed at 17W11, which is also the sampling location where the highest concentration was detected for a specific PFAS homologue, PFPeA (5900 ng/l). The dominant PFAS homologues in groundwater are PFPeA, PFHxA, and 6:2 FTS (Figure 13).

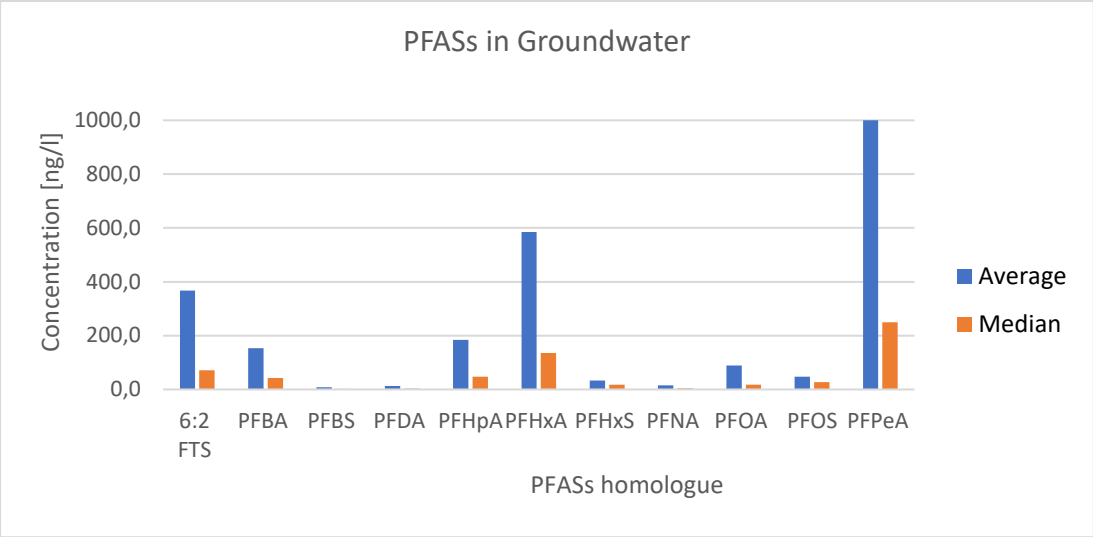


**Figure 13.** The average and median concentrations of PFASs in groundwater.

## 3.2. FIELDWORK

On the 18th of September 2018, fieldwork at the former fire station in Åkersberga was carried out. During the day groundwater level measurements and slug tests were performed in 17 observation wells, Figure 12.

### 3.2.1. Groundwater Level Measurement

The measurements of groundwater level in 17 observation wells were performed during the field investigation, using the Solinst 101 Water Level Meter with P7 Probe, Figure 14. The probe with sensor was led down the wells. When it reached the groundwater surface a signal was sent and the groundwater level was read and documented. The results of groundwater level measurement are presented in Appendix A, Table A1. In the same table, other measured groundwater levels from WSP, SWECO, SGU's well archive, and Geosigma can be seen.

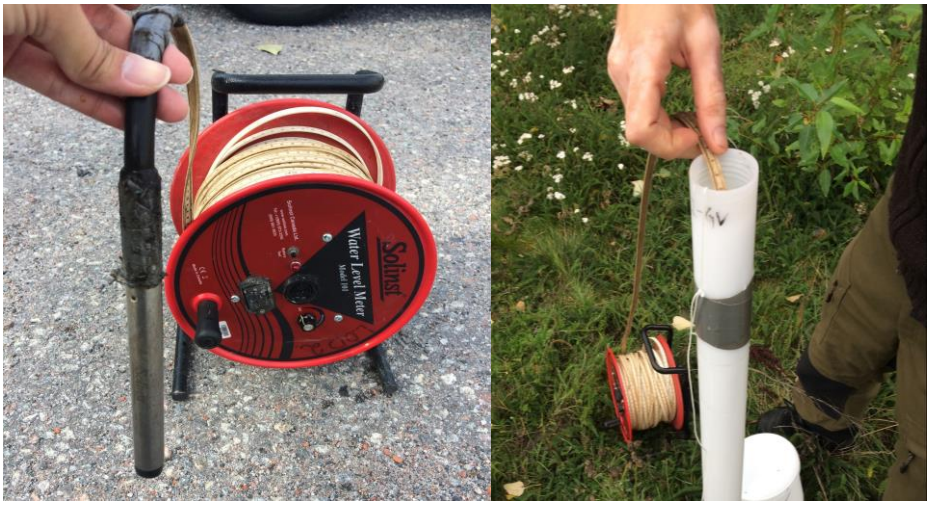


**Figure 14.** To the left, the Solinst 101 Water Level Meter with P7 Probe. To the right, when the Solinst was used to measure the groundwater level in a well.

### 3.2.2. Slug Test

The slug test was performed using Mini-Diver (DI 501) data logger and pressure transducer. The data logger and pressure transducer were programmed and read by the software Diver-Office 2018, Figure 15. Barometric compensation is usually made when the slug test is performed during a longer period. Since the slug tests in this project were carried out for only one day, no compensation was made to the obtained response data.

**Field operation**

The procedure of the slug test can be summarized as follow:

- The Mini-Diver pressure transducer was first programmed by the Diver-Office 2018 to measure the pressures due to the changes in water levels in a well. The recording interval was chosen to 0.5 seconds.
- With the known groundwater level, the pressure transducer was tied with lace long enough to place it under the water surface. The pressure transducer was then placed into the well.
- The change of water level was later created by rapidly adding a known amount, 1–2 liters, of water into the well (Figure 15).
- The pressure changes over time were recorded every 0.5 seconds for approximately 30 to 40 minutes by the pressure transducer. The values obtained by the pressure transducer were temperatures and pressures. The pressure here is equal to the "weight" of the water column above the transducer and it is measured in cm$H_2O$. Note that 1 cm$H_2O \approx$ 100 Pa.
- The pressure transducer was then removed from the well and the response data was uploaded to the Diver-Office 2018, using the Mini-Diver data logger.
- The same procedure was applied to all the wells.

**Figure 15.** To the left, Mini-Diver (DI 501) data logger and pressure transducer, connect to Diver-Office 2018 software (open in the laptop). To the right, two liters of water pouring rapidly into the well through a funnel.

Slug tests were performed at all the 17 wells. The response data plot of each well can be seen in Appendix B, Figure B1. From the response data, it can be noted that ten of the wells have too slow drawdown. They have therefore been excluded from the further analysis described below.

**Analysis of Response Data and Estimation of Hydraulic Conductivity**

The aquifer where slug test was performed is according to WSP's investigation *a confined aquifer*. The wells are also fully penetrating, which means that each well was drilled into and screened over the full thickness of the till layer (Butler, 1997). With these reasons, Hvorslev method has been chosen for estimation of the hydraulic conductivity in this area. The Hvorslev method consists of the following steps:

1. The values of $h_0$ and $h_t$ were calculated from the response data obtained from slug test.
2. The normalized head was calculated by computing the ratio $ht/h0$ at each time step. This normalized the head to values between 0 and 1, where 0 means that the head has reached back to its static water level.
3. The normalized head was then plotted on the y-axis with logarithm scale vs. the time on the x-axis. This resulted in a semilogarithmic plot of drawdown versus time.
4. A straight line was fitted to the data in semi logarithmic plot.
5. The slope of the fitted line was calculated by estimating the time at which a normalized head was 0.37. This gave the $t_{37}$-value.
6. The hydraulic conductivity was finally estimated with Equation (4) or Equation (5).

Table 5 represents the data of the seven approved wells. These data are needed for the estimation of hydraulic conductivity. The screen length ($L$) in each well is equal to the formation thickness of the till layer (aquifer thickness). The till layer was estimated by the interpolation with cokriging in ArcGIS, where the information of previous investigations was used (till thickness, bedrock elevation and till elevation).

For the observation wells where *L/R* was greater than 8, the analysis and estimation of hydraulic conductivity (step 1 to 6) were performed using the software program AquiferTest. The straight lines were fitted to normalized head between the interval of $ht/h0$ = 0.15 to 0.25. For the observation wells that did not fulfill the condition of *L/R* > 8 (18W03), the analysis and estimation of hydraulic conductivity (step 1 to 6) were manually performed in Excel and the straight line was limited to only fit the entire data set. The semi logarithmic plot and analysis of each well test are presented in Appendix B, Figure B2 and Figure B3. The results of estimated hydraulic conductivity (K) using Hvorslev method are summarized in Table 5. The estimated *K* values of till in confined aquifers varied from $1.39 \cdot 10^{-6}$ to $7.90 \cdot 10^{-5}$ m/s. The average and mthe edian value is $1.30 \cdot 10^{-5}$ m/s and $1.65 \cdot 10^{-6}$ m/s, respectively.

**Table 5.** The properties and estimated hydraulic conductivity of the seven approved wells

| Well | Radius of well casing, r [cm] | Radius of well screen, R [cm] | Estimated screen length, L [cm] | L/R | $K_{till}$ [m/s] |
|---|---|---|---|---|---|
| 17W01 | 2.05 | 3.1 | 25 | 8 | $5.30 \cdot 10^{-6}$ |
| 17W02 | 2.05 | 3.1 | 30 | 10 | $1.65 \cdot 10^{-6}$ |
| 17W03 | 2.05 | 3.1 | 30 | 10 | $1.11 \cdot 10^{-6}$ |
| 17W04 | 2.05 | 3.1 | 35 | 11 | $1.98 \cdot 10^{-6}$ |
| 17W06 | 2.05 | 3.1 | 50 | 16 | $1.39 \cdot 10^{-6}$ |
| 17W10 | 2.05 | 3.1 | 35 | 11 | $5.69 \cdot 10^{-6}$ |
| 18W03 | 2.05 | 3.1 | 10 | 3 | $7.90 \cdot 10^{-5}$ |

## 3.3. GROUNDWATER MODEL

### 3.3.1. Conceptual Groundwater Model

The conceptual groundwater model is representing pillars that will be included in the numerical model and is constructed with help from the information described in 3.1. SITE DESCRIPTION.

#### Model Demarcation

The model domain is presented in Figure 16. The demarcation of the model domain was determined with help from the information regarding topography, soil depth, and catchment area from SMHI. The starting point was to place the model boundaries along natural hydrogeologic and hydrologic boundaries, such as river or water divides, according to the recommendation by Domenico and Schwartz (1981). With the natural boundaries, it is easier to later define a boundary condition based on measurement or estimation and hence decrease the uncertainties in the model.

#### Boundary Conditions

The model boundaries with different distances are presented in Figure 16. The first model boundary (distance AB) is representing Åkers canal. The hypothesis is that PFASs spread from the former fire station through the railroad track and then further towards Åkers canal. It is therefore important to include Åkers canal in the model domain. Here the outflow from the

model domain will also take place. The next model boundary (distance AF) was mostly placed along the water divide that belongs to SMHI's catchment area and the assumption was made that no flow will be passing the boundary. This is because the flow normally moves away from a water divide. The same assumption was made for the model boundaries BC and DE since both lie along topographical ridges and therefore most likely form a water divide as well. For the model boundaries CD and EF, the elevation of the topography and the catchment area indicate that there is inflow through the boundaries from the northeast for distance CD and from the north for distance EF.

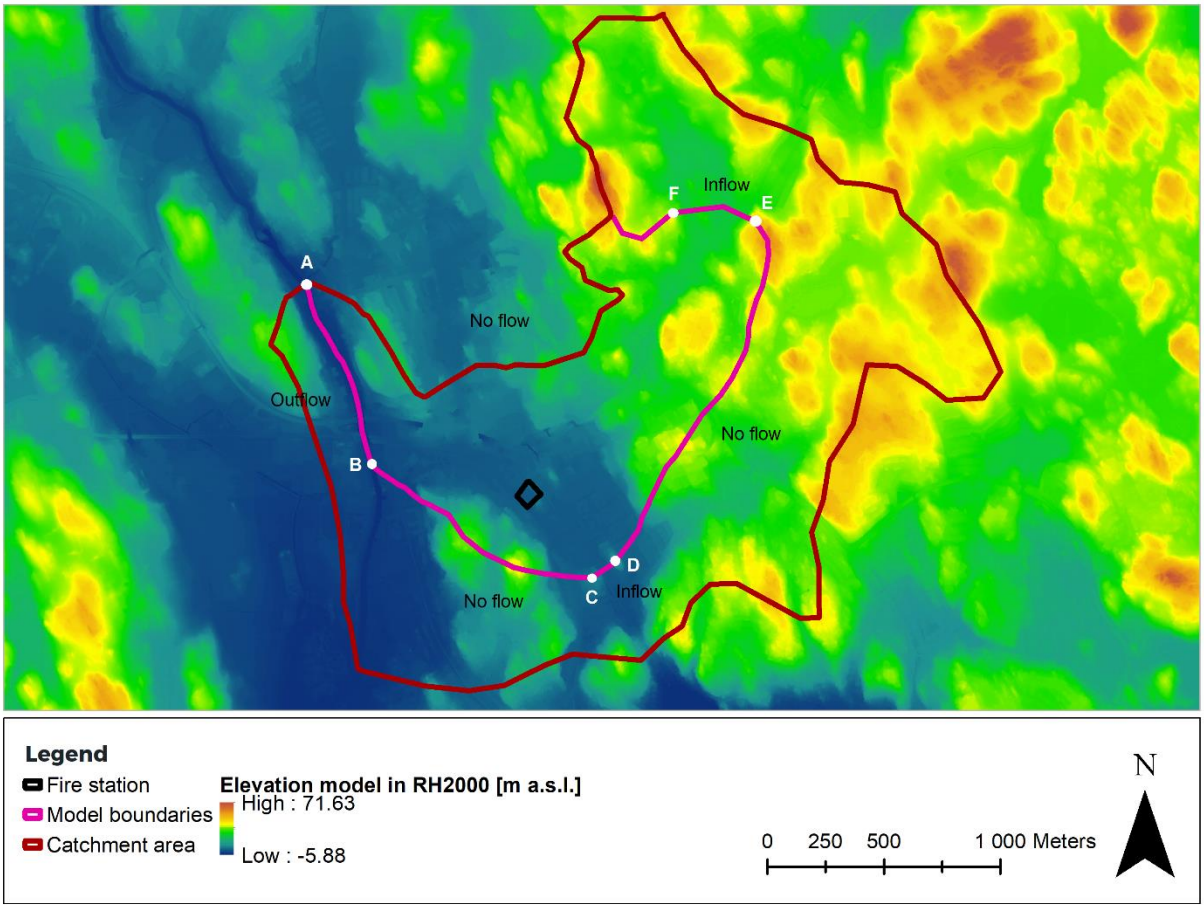


**Figure 16.** Chosen model boundaries and catchment area that the former fires station belongs to ©SMHI. Background map: GSD-Elevation data, grid 2+ ©Lantmäteriet.

## Geological Layers

The conceptual model of geological layers can be seen in Figure 17. The top layer consists of filling material and its thickness varied between 1 and 2 meters. The filling layer was in turn divided into two different groups, the first one for general filling and the other for filling in the railroad track. The second layer consists of clay and the third layer of till. The assumption was made that the till layer also has a thickness that varies between 1 and 2 meters. The bedrock has been divided into two different layers, where the shallow bedrock represents the top layer of bedrock with more cracks and fractures. Its thickness is estimated to be around 20 meters.

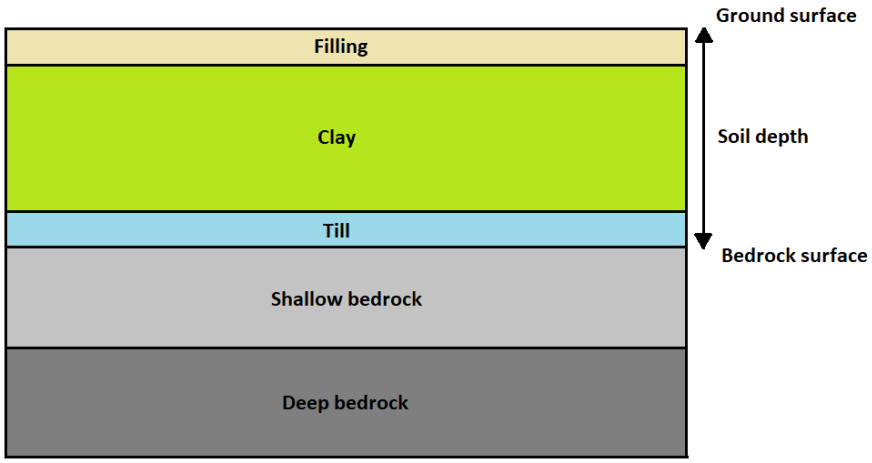


**Figure 17.** Geological conceptual model of soil and bedrock layers in the area. The picture is not according to scale.

As a basis for the construction of the groundwater model in Visual MODFLOW, a site-based bedrock level model was developed based on a compilation of ground elevation data (GSD-Elevation data from Lantmäteriet), soil depth data from SGU's well archive, and data from geotechnical investigations by WSP and SWECO.

Firstly, the soil depth data from SGU's well archive and geotechnical investigations performed by WSP and SWECO were used to interpolate a site-based soil depth map over the area. An interpolation with Kriging method was then performed in a software program called Surfer. The summary of soil depth data obtained from WSP and SWECO is presented in Appendix C, Table C1. Soil depth data obtained from WSP and SWECO. The result of interpolated soil depth in grid form of size 10·10 m can be seen in Appendix C, Figure C1.

Finally, the elevation of the bedrock surface was estimated by extracting soil depth from the ground elevation, see Figure 17. This operation was also performed in Surfer, by first converting the GSD-Elevation data with grid size 2·2 m to grid size 10·10 m. The elevation data was also clipped so that the same dimensions as the interpolated soil depth map was obtained. This is because the subtraction in Surfer can only be performed when the two maps have the exact same dimensions and grid sizes. The result of generated bedrock surface elevation in 3D can be seen in Figure 18.

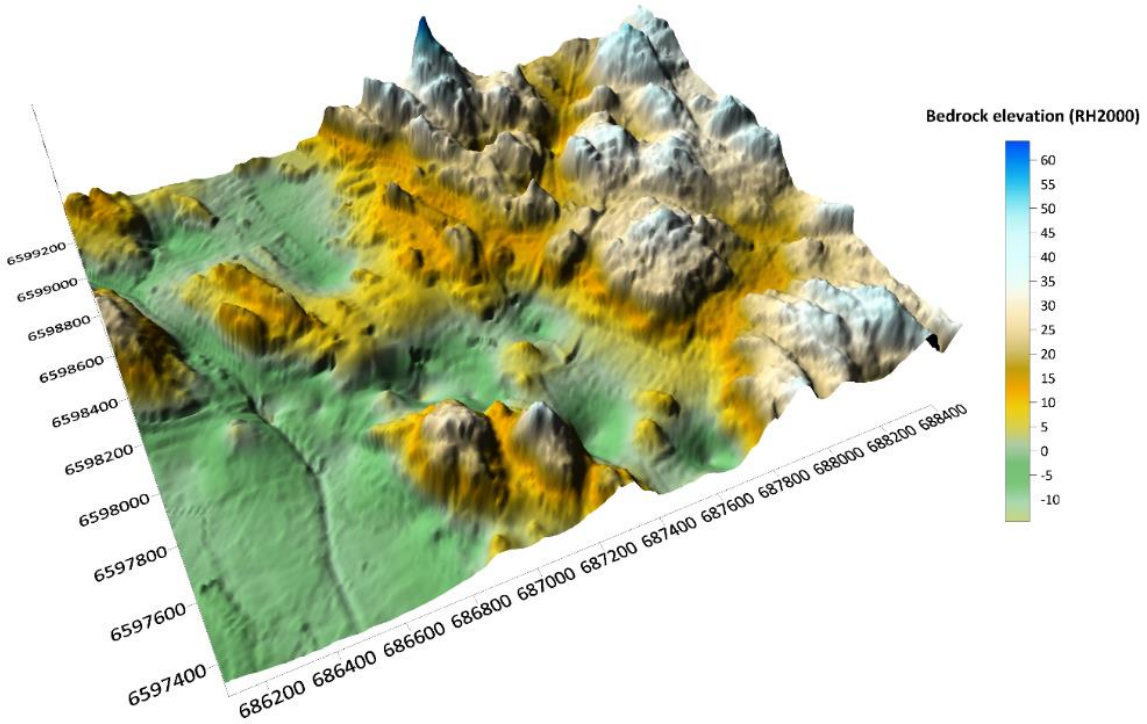


**Figure 18.** Generated bedrock surface elevation in 3D.

## Groundwater Recharge

The period of the modelling will be between 1969 and 2019. The initial value of groundwater recharge was therefore chosen to 175 mm/year. The value was chosen so that it lies between 180 and 168 mm/year according to Table 4. However, this value did not consider that some of the effective precipitation disappears in the drainage pipes in the urban environment. By considering the proportion of impermeable surfaces and roofs, an estimation of new groundwater recharge in the area was made. A division based on the degree of urbanization within the model domain is presented in Figure 19.

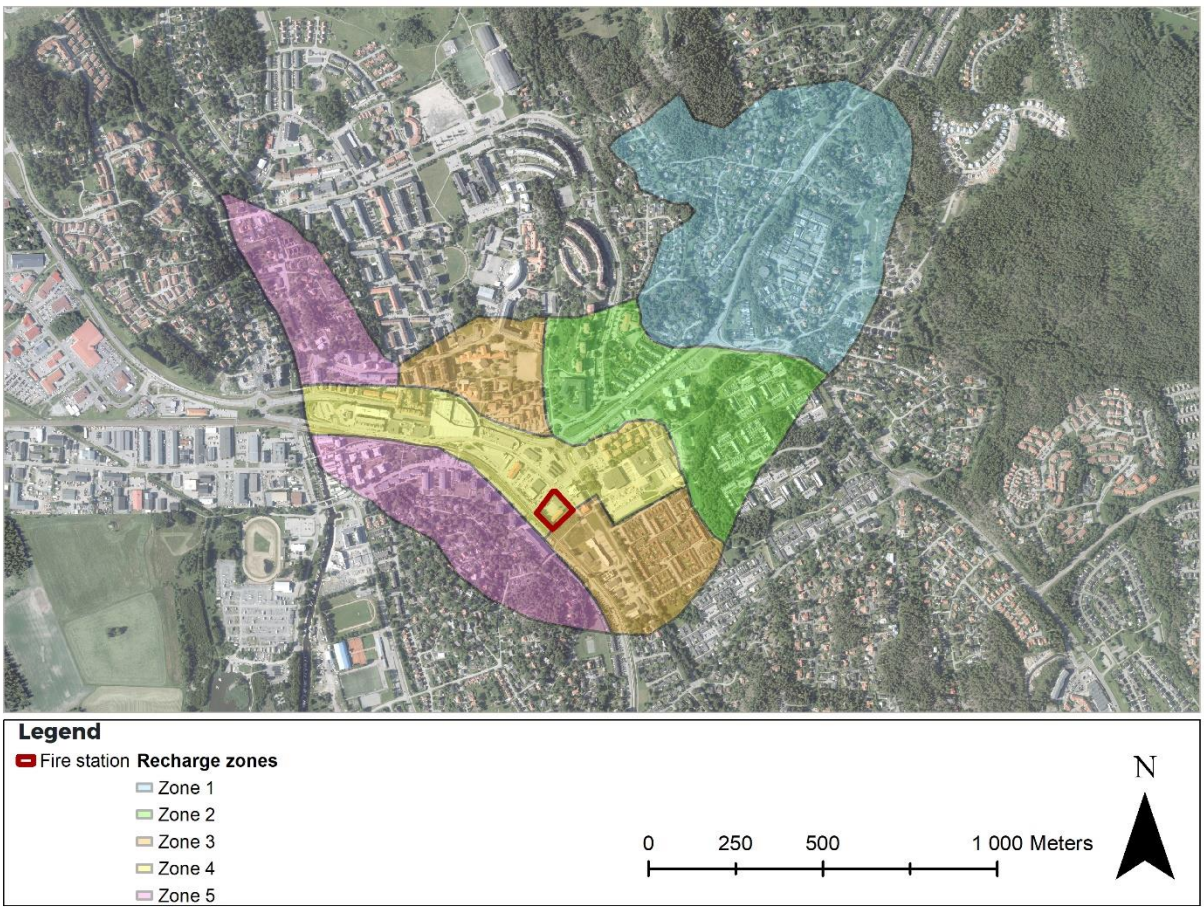


**Figure 19.** The recharge zones. Background map: GSD-Orthophoto, 1 m color ©Lantmäteriet.

The proportion of impermeable surfaces in each zone was estimated and the initial groundwater recharge was then used to recalculate groundwater recharge in each zone, see Table 6.

**Table 6.** Adjusted initial groundwater recharge based on the proportion of impermeable surface

| **Recharge zone** | **Proportion of impermeable surface** [%] | **Groundwater recharge** $[mm/year]$ |
|---|---|---|
| Zone 1 | 40 | 105 |
| Zone 2 | 60 | 70 |
| Zone 3 | 80 | 36 |
| Zone 4 | 95 | 9 |
| Zone 5 | 50 | 88 |

### 3.3.2. Numerical Groundwater Model

The groundwater model was created in Visual MODFLOW Classic, using MODFLOW-NWT as the flow engine. This section will summarize the process of model construction, based on the conceptual groundwater model and information from site description.

#### Model Design

The model domain was first created with 231 rows, 191 columns, and 5 layers. The model edges in xy-plane were defined according to Figure 16 and the grid cells outside it were assigned as inactive or no flow cells. In the inactive cells no calculations of flow, particle tracking, or contaminant transport were made. To get more detailed simulation results in the area of interest, the model grid around the former fire station was refined so that grid cells of size 10•10 m were obtained. The areas further away from the former station obtained larger model grids.

The model consists of 5 layers, whereof three are soil layers and two are bedrocks (see Figure 17). To create the layers, ground and bedrock surfaces that have been prepared in Surfer were imported to Visual MODFLOW. The thickness of layer 1 (filling) and layer 3 (till) were specified to vary between 1 and 2 meters. Layer 2 (clay) was determined to have a minimum thickness of 1 m. From the bedrock surface, the thickness of layer 4 (shallow bedrock) was specified to 20 m and the bottom of layer 5 (deep bedrock) was set to -60 m in RH 2000.

#### Aquifer Properties

The aquifer properties were assigned to the model grid based on the information from SGU's soil type map in Figure 7. There were however some exceptions made. Firstly, the assumption was made that clay in layer 1 consists of only dry crust clay. Secondly, the thin till layer on top of the bedrock that appears on the ground surface has been excluded from the model and instead the shallow bedrock was assigned to these areas. The assumption was then made that shallow till existed around those shallow bedrock's edges and enables the contact between layer 1 and layer 3, according to Figure 8. The result of the assigned soil types in layer 1 is presented in Figure 20.

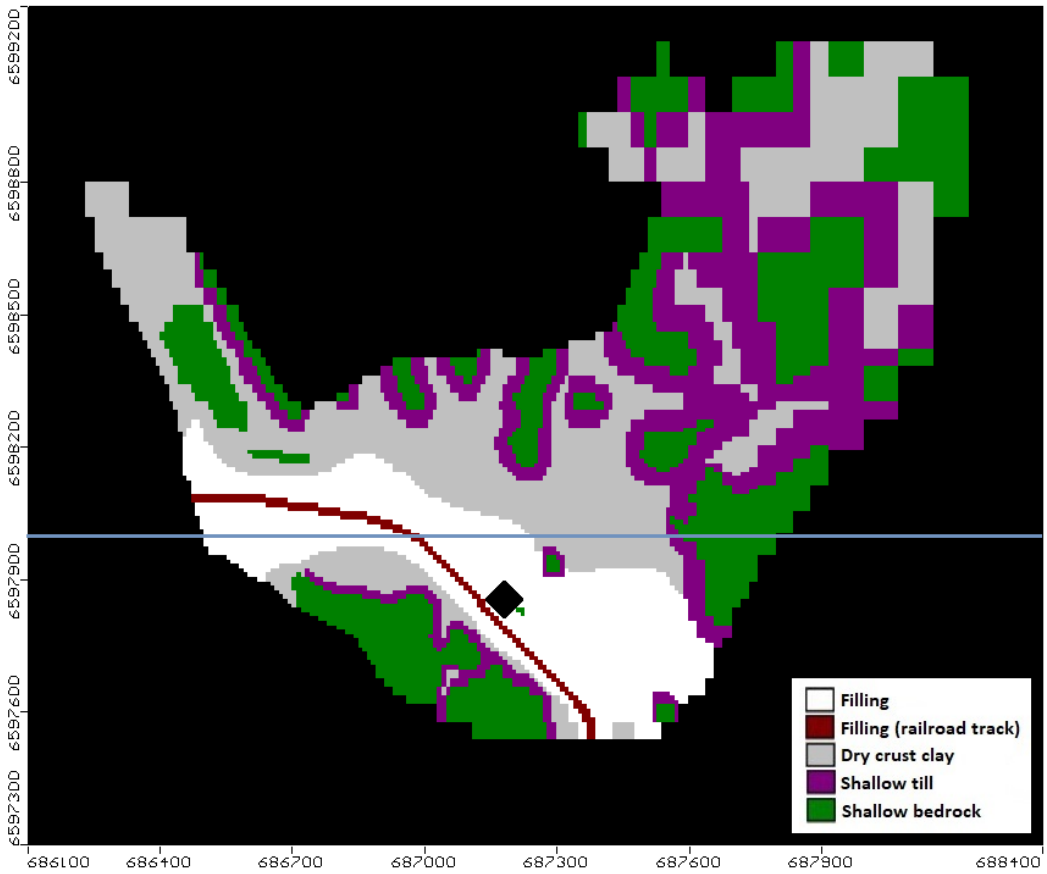


**Figure 20.** The assigned soil types in layer 1. The approximated location of the property is represented as a filled square in black. The location of row 48 where the cross-section was taken is presented as a horizontal blue line.

Clay was assigned to layer 2 and deep till was assigned to layer 3. The only exception is in the areas where shallow till or shallow bedrock appears on the surface in layer 1. After this, the same soil types were also assigned to layers 2 and 3. For layer 4 and layer 5, the aquifer properties of shallow bedrock and deep bedrock were assigned respectively. A cross-section of the model domain at row 48, where all the 5 layers are presented can be seen in Figure 21.

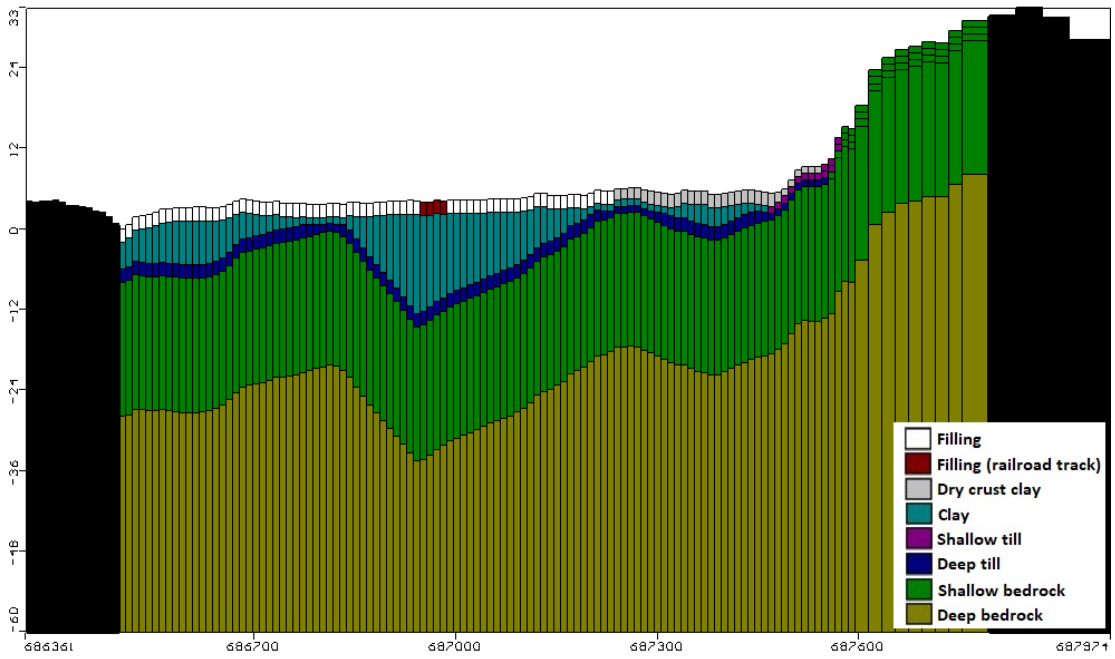


**Figure 21.** A cross-section of the model domain at row 48 (see Figure 20 for the location of row 48).

The hydraulic conductivities and storage properties that were assigned in the numerical model for each soil type before the calibration are presented in Table 7. The hydraulic conductivities of bedrock and till are site-based and were calculated with data from SGU's well archive and data from slug tests respectively. The other parameters were obtained from literature values that are summarized in Table 2.

**Table 7.** The initial values of hydraulic conductivities and storage properties for each soil

| **Soil type** | $K_x\ [m/s]$ | $K_y\ [m/s]$ | $K_z\ [m/s]$ | $n\ [-]$ | $n_e\ [-]$ | $S_s\ [\mathrm{m}^{-1}]$ | $S_y\ [-]$ |
|---|---|---|---|---|---|---|---|
| Filling (fine gravel) | $1 \cdot 10^{-4}$ | $1 \cdot 10^{-4}$ | $1 \cdot 10^{-4}$ | 0.34 | 0.05 | $9.87 \cdot 10^{-5}$ | 0.28 |
| Filling (coarse gravel) | $1 \cdot 10^{-3}$ | $1 \cdot 10^{-3}$ | $1 \cdot 10^{-3}$ | 0.28 | 0.05 | $1.63 \cdot 10^{-6}$ | 0.21 |
| Dry crust clay | $1 \cdot 10^{-9}$ | $1 \cdot 10^{-9}$ | $5 \cdot 10^{-10}$ | 0.5 | 0.01 | $9.81 \cdot 10^{-3}$ | 0.02 |
| Clay | $1 \cdot 10^{-9}$ | $1 \cdot 10^{-9}$ | $5 \cdot 10^{-10}$ | 0.5 | 0.01 | $9.81 \cdot 10^{-3}$ | 0.02 |
| Shallow till | $2 \cdot 10^{-6}$ | $2 \cdot 10^{-6}$ | $8 \cdot 10^{-7}$ | 0.31 | 0.05 | $5 \cdot 10^{-4}$ | 0.16 |
| Deep till | $2 \cdot 10^{-6}$ | $2 \cdot 10^{-6}$ | $8 \cdot 10^{-7}$ | 0.31 | 0.05 | $5 \cdot 10^{-4}$ | 0.16 |
| Shallow bedrock | $8 \cdot 10^{-7}$ | $8 \cdot 10^{-7}$ | $8 \cdot 10^{-7}$ | $1 \cdot 10^{-3}$ | $1 \cdot 10^{-3}$ | $1.63 \cdot 10^{-6}$ | $9 \cdot 10^{-4}$ |
| Deep bedrock | $4 \cdot 10^{-7}$ | $4 \cdot 10^{-7}$ | $4 \cdot 10^{-7}$ | $1 \cdot 10^{-3}$ | $1 \cdot 10^{-3}$ | $1.63 \cdot 10^{-6}$ | $9 \cdot 10^{-4}$ |

**Boundary Conditions**

The flow boundary conditions were assigned to the groundwater model to describe the exchange of flow between the model and the outside world. There were three different boundary conditions that were used.

*Constant Head (CDH)*

The constant head boundary condition is a specified head boundary. It was used to fix the head values in all the soil layers along the model boundaries AB, CD, and EF (Figure 16). As mentioned in 2.4.2. Numerical Model, the constant head boundary can act as sources (where water enters the model) or as sinks (where water leaves the model). For Åkers canal (distance AB) that works as a sink, the specified head value of 0.13 m was assigned after the canal's approximated water level. The distance CD and EF, on the other hand, were assigned as sources of water entering the model. The specified head values of 6 m and 25 m were assigned to the distance CD and distance EF respectively. These values were chosen after the nearest groundwater level observations.

*Drain (DRN)*

The drain boundary condition was used to simulate the effects of artificial drainage that exists in the model domain. The area within the model domain is quite urban with buildings and impermeable surfaces such as roads and ceiling. It was therefore considered important not to disregard the drainage pipes that exist because of these surfaces. Since the exact locations of drainage pipes were not known, the "general" drain was applied everywhere in the model domain, in layer 1. The drain elevation was assigned at 0.5 m b.g.l., note that the drain boundary would not have any effects if the head in the model is below this level.

*Recharge (RCH)*

The recharge boundary condition was used to generate the groundwater recharge, which is the amount of precipitation that enters the groundwater aquifer through infiltration. The initial groundwater recharge was calculated to 175 mm/year. Since groundwater recharge is often prevented by impermeable surfaces such as roofs and asphalt in the urban environment. The new groundwater recharge based on the proportion of impermeable surfaces were therefore calculated in 3.3.1. Conceptual Groundwater Model. Based on Figure 19 and Table 6, the groundwater recharge was assigned to the model domain in layer 1.

**Groundwater Flow and Calibration**

Groundwater flow was simulated using MODFLOW-NWT as the numeric engine and the results of the calculated head were then compared and calibrated to the observed head in the area. The initial parameters of hydraulic conductivity, recharge rate, drain, and constant head value were manually adjusted within the limits in Table 2 until calculated heads best matched observed heads. The calibration considered to be good when the residual mean of 0.5 m or less was obtained. Since the observed groundwater levels in previous surveys came from different occasions and seasons, they have been compiled and divided after high or low season. High

season is the period between January and May, while low season is between June and December. It was considered important not to mix the groundwater measurements from different seasons because the differences can be large and hence affect the reliability of the model. The observed groundwater levels that were used during the calibration can be seen in Appendix A, Table A1.

**Water Balance**

To study the inflow and outflow through the model, the function *zone budget* in Visual MODFLOW was used. The model was divided into different *zone budget* zones. Inflow and outflow generated from constant heads, drains, and recharge were studied.

## 3.4. TRANSPORT MODEL

### 3.4.1. Conceptual Transport Model

As a basis for the construction of the transport model in Visual MODFLOW, a contaminant distribution map in soil was developed for PFOS, PFOA, 6:2 FTS, and PFPeA. The contaminant distribution maps were based on the detected concentrations on site (between 0 and 1 m b.g.l.) and the interpolation was performed in ArcMap 10.4.1 using Inverse Distance Weighting (IDW) method.

The concentration of PFASs in the soil is divided into intervals from low (in green) to high (in red). Furthermore, dark green represents the sampling location where PFASs concentration is below the limit of detection (LOD). Light green represents the interval of concentration below the guideline value for sensitive land use, 3 µg/kg dw (SGI, 2015). Yellow represents the interval of concentrations below the guideline value for less sensitive land use, 20 µg/kg dw (SGI, 2015) when the rest exceed these values. The concentrations that exceed PFOS's guideline value for less sensitive land use is referred to as a hotspot in this project. Note that the guideline values for PFOS have been used for each PFAS compound since it is the only existing guideline value for groundwater.

PFOS distribution map in soil is presented in Figure 22. There are two hotspots that can be observed on the map. The first one is around sampling location 17W10, where the detected PFOS concentration was 630 µg/kg dw. The second hotspot was observed around 18W05, with a detected concentration of 150 µg/kg dw. The LOD for PFOS is 0.1 µg/kg dw and the sampling location where detected concentration was below this threshold value was 17W14.

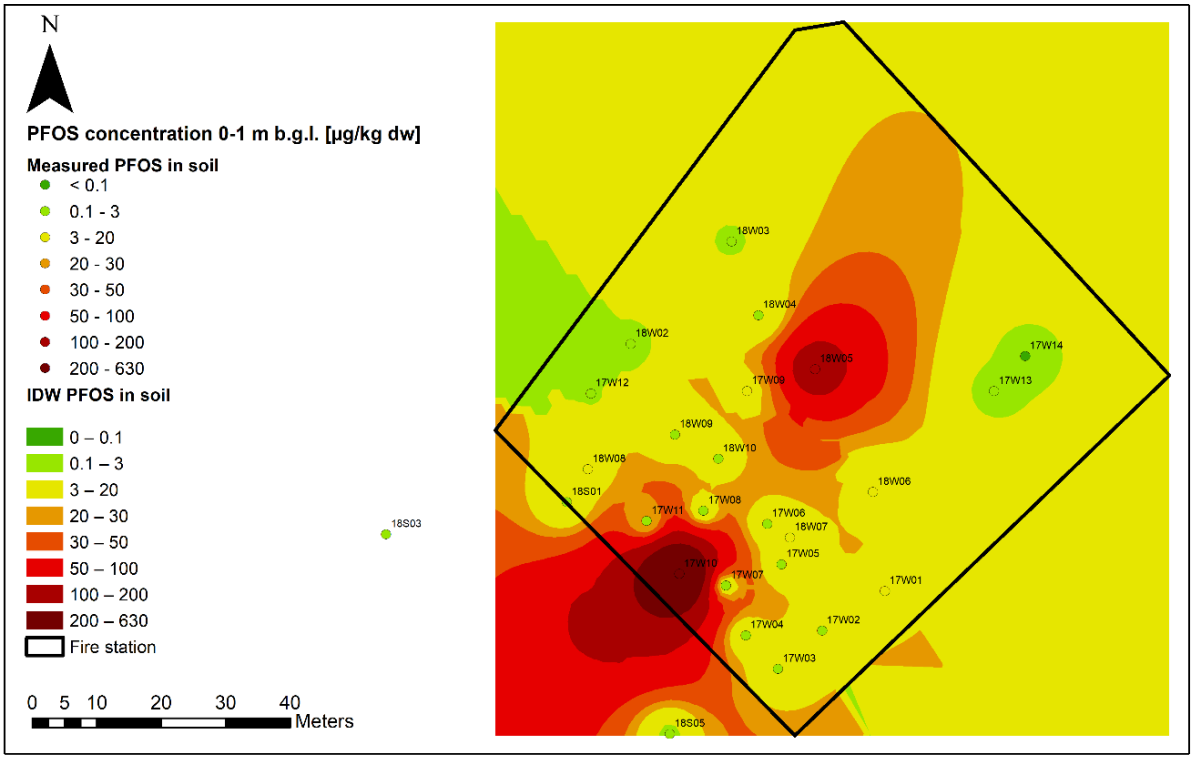


**Figure 22.** The contaminant distribution map of PFOS in soil (0-1 m b.g.l.).

PFOA distribution map in soil is presented in Figure 23. Higher concentrations can be observed in the southwest of the fire station with hotspot around sampling location 17W11, there the detected PFOA concentration was 27 µg/kg dw. The LOD for PFOA is 0.1 µg/kg dw and there are eight sampling locations where detected concentration is below this threshold. The concentrations are especially low in the northwest around sampling locations 17W13 and 17W14, where no PFOA has been detected.

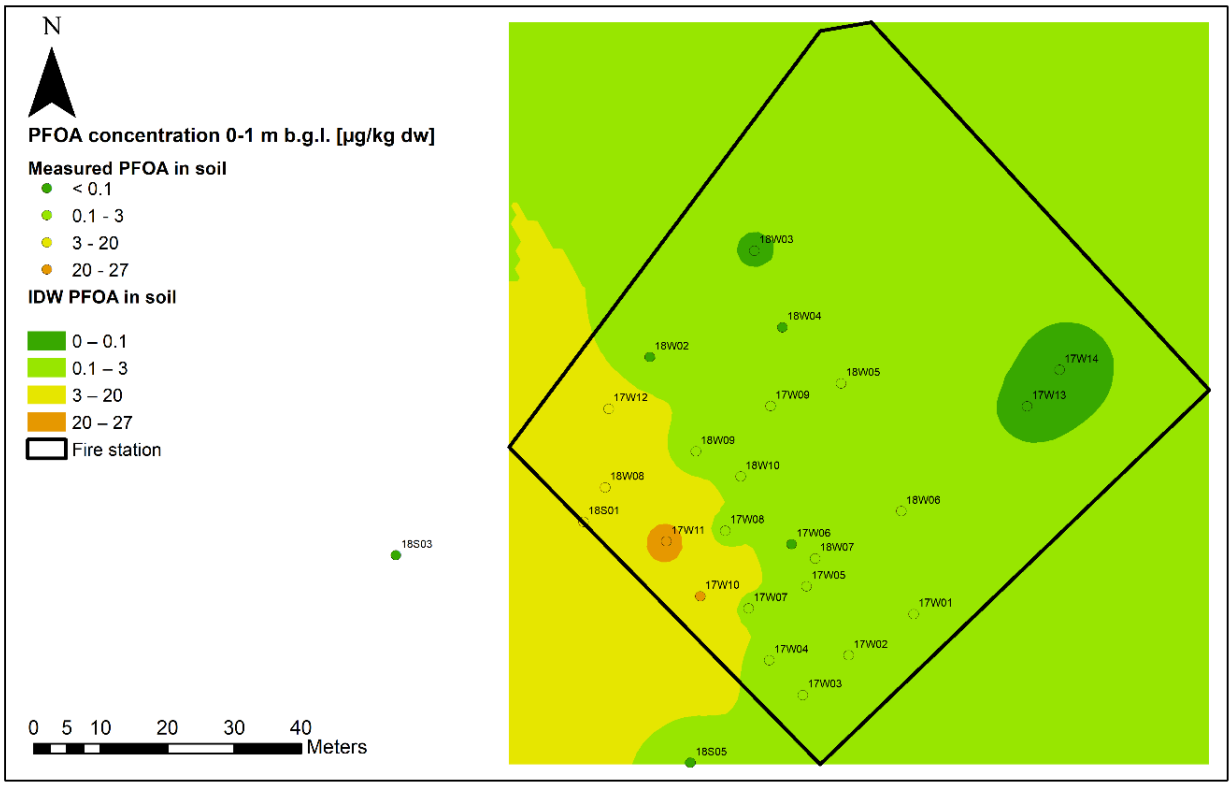


**Figure 23.** The contaminant distribution map of PFOA in soil (0-1 m b.g.l.).

6:2 FTS distribution map is presented in Figure 24. Higher concentrations can be observed in the southwest of the fire station with hotspot around sampling location 18W06, there the detected 6:2 FTS concentration was 27 µg/kg dw. The LOD for 6:2 FTS is 0.2 µg/kg dw and there are nine sampling locations where detected concentration is below this threshold. Similar to PFOA, the concentrations of 6:2 FTS are especially low in the northwest around sampling locations 17W13 and 17W14, where no 6:2 FTS has been detected.

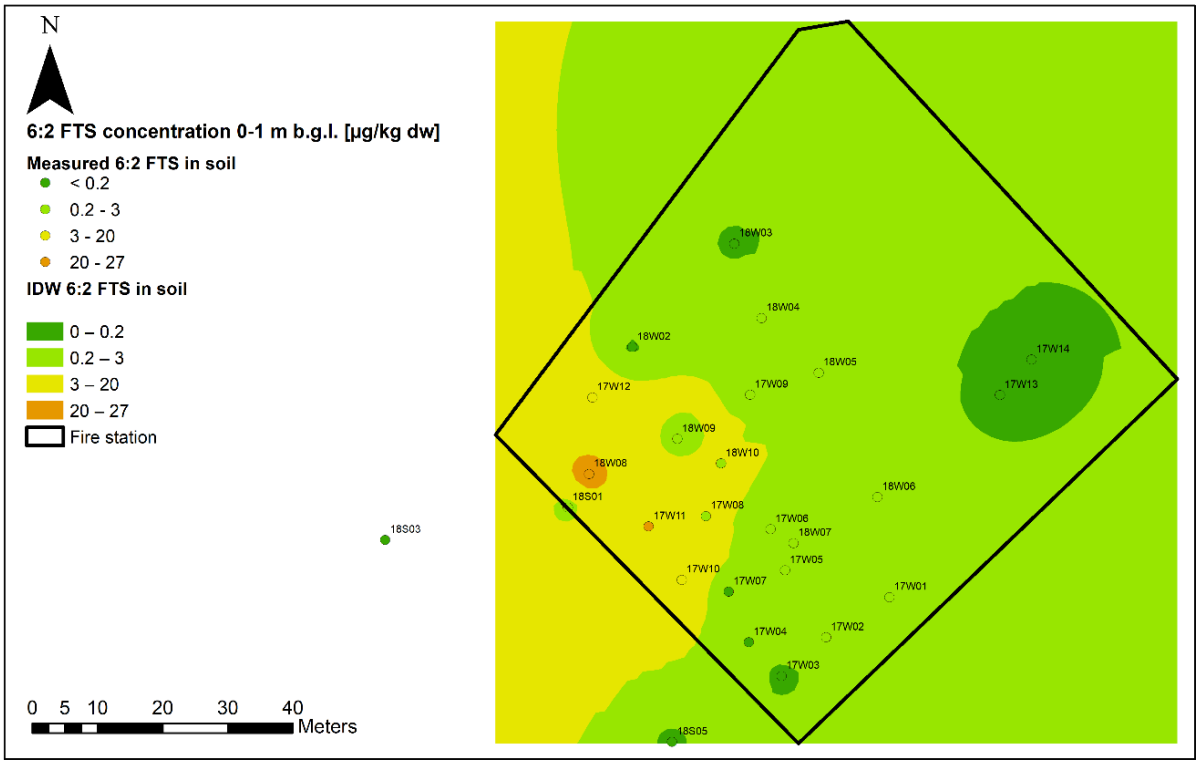


**Figure 24.** The contaminant distribution map of 6:2 FTS in soil (0-1 m b.g.l.).

The last contaminant is PFPeA and its contaminant distribution map is presented in Figure 25. High concentrations can be observed in the southwest of the fire station. The hotspot is located around sampling location 18S01, where the detected concentration is 34 µg/kg dw. The LOD for PFPeA is 0.2 µg/kg dw and there are eight sampling locations where detected concentration is below this threshold. Similar to PFOA and 6:2 FTS, the concentrations of PFPeA are especially low in the northwest around sampling locations 17W13 and 17W14, where no PFPeA has been detected.

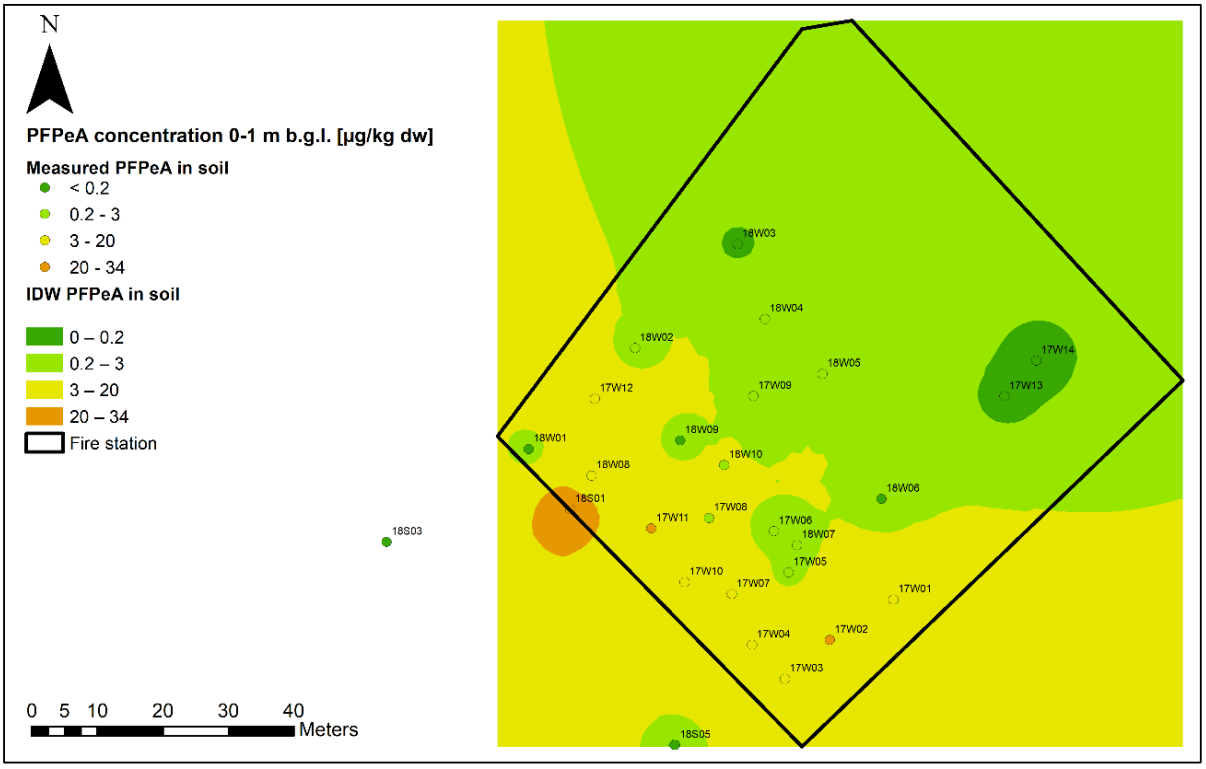


**Figure 25.** The contaminant distribution map of PFPeA in soil (0-1 m b.g.l.).

### 3.4.2. Numerical Transport Model

The numerical transport model uses the output of the steady-state groundwater flow simulation as a basis to simulate particle tracking and contaminant transport of the four PFAS homologues. The contaminant transport of PFOS, PFOA, 6:2 FTS, and PFPeA was constructed based on the conceptual transport model.

#### Particle Tracking

Within the former fire station, 130 imaginary particles were assigned to each soil layer (layer 1 to 3). With MODPATH the forward particle tracking was then performed. Results of the particle tracking included particles advective pathlines and travel times.

#### Transport of PFASs

The contaminant transport of PFOS, PFOA, 6:2 FTS, and PFPeA was modeled with the module MT3DMS, using the conceptual transport model as the basis. The length of the model simulation was 50 years (1969 to 2019) and the default parameter value of longitudinal dispersivity (10 m) was used. For sorption, the linear isotherm (equilibrium-controlled) method was applied and the distribution coefficient ($K_d$) was assigned for each investigated PFAS homologue. No reaction or degradation was modeled. The concentrations of the four PFAS homologues have been assigned to layer 1 (filling) with the constant concentration boundary. The constant concentration boundary acted as a contaminant source where a known concentration of the contaminant releases to the model domain. The assigned concentrations of

each homologue were based on the measured concentrations in soil, because no water samples had been taken in the top soil layer. Concentrations in soil were recalculated to concentrations in water with Equation (1) and $K_d$ values for each homologue presented in Table 8. $K_d$ values were selected based on the fraction of organic carbon (%) in the soil, because it is an important factor that affects the transport of PFASs. Fraction of organic carbon in layer 1 (filling) is generally less than 1%. Therefore, the $K_d$ values from a Danish site, called Jynnevad, with foc = 1% were used for PFOS and PFOA (Enevoldsen and Juhler, 2010). Due to the difficulties of finding a representative $K_d$ values for 6:2 FTS and PFPeA, the median values from IVL's study at Stockholm Arlanda Airport were applied (Rosenqvist et al., 2017).

The concentrations were assigned to layer 1 based on the hotspots from the generated IDW map in Figure 22 to Figure 25, conceptual transport model. As previously mentioned, a hotspot is here referred to the concentrations that exceed PFOS's guideline value for less sensitive land use (20 µg/kg dw), interval orange and above on the IDW maps. In other words, only the concentrations above 20 µg/kg dw were modeled in Visual MODFLOW. Chosen concentration in soil is the highest concentration detected at each hotspot. For PFOS, two hotspots could be observed. One of the hotspots (around sampling location 17W10) was considered large, therefore it has been divided into two intervals. For the compilation of values used in the numerical transport model see Table 8. Finally, contaminant transport of PFOS, PFOA, 6:2 FTS, and PFPeA were simulated using MT3DMS as transport engine and the results of calculated concentrations were then compared to the observed concentrations in layer 3 (till). However, no initial parameters were adjusted during the comparison.

**Table 8.** The compilation of values that were used in the numerical transport model.

| PFASs | $K_d$ [L/kg] | Concentration in soil [µg/kg dw] | Assigned concentrations [µg/L] | Assigned locations |
|---|---|---|---|---|
| PFOS | 15 | 630 | 42 | 17W10 |
| | | 50 | 3.3 | Around 17W10 |
| | | 150 | 10 | 18W05 |
| PFOA | 1.1 | 27 | 24.5 | 17W11 |
| 6:2 FTS | 0.65 | 27 | 41.5 | 18W08 |
| PFPeA | 0.49 | 34 | 69.4 | 18S01 |

# 4. RESULTS

## 4.1. NUMERICAL GROUNDWATER MODEL

### 4.1.1. Groundwater Flow

The result of groundwater flow simulation can be seen in Figure 26, where calculated head equipotential and velocity vectors for layer 5 are presented. Velocity vectors represent the speed and direction of the groundwater flow, where red arrows mean that the flow is moving downward and black that the flow is moving upward in the model. The velocity vectors indicate that groundwater from the northeast (high area) is flowing towards the southwest. When the flow reaches the lower area, where the former fire station is also located, its direction is instead changed towards the west to Åkers canal. Similar groundwater flow can be observed in the other layers except from the dry cells that have been generated in parts of the area in layer 1 to layer 4. Dry cells mostly occur in the higher areas and for example, consist of hills and in those areas no flow was calculated.

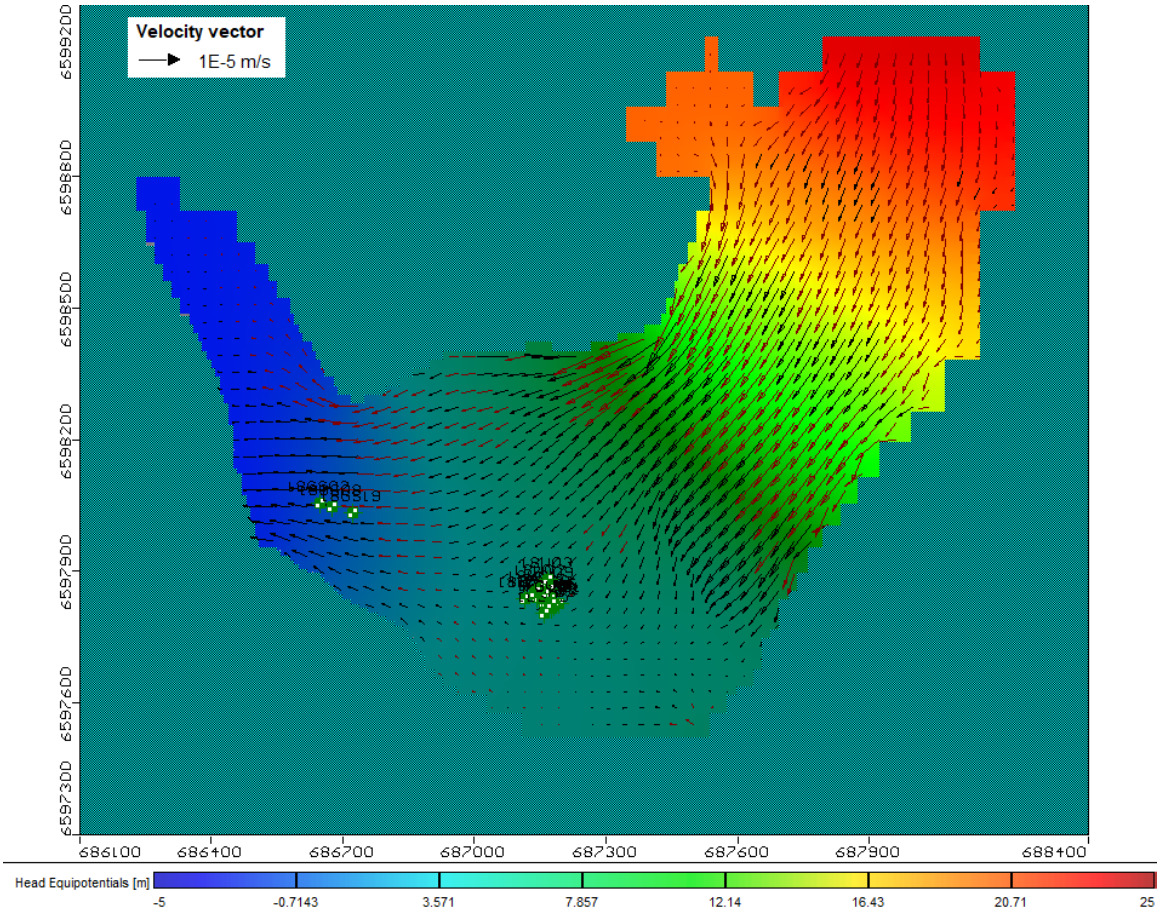


**Figure 26.** Calculated head equipotential and velocity vectors for layer 5 in the model. Red arrows mean that the flow is moving downward and black that the flow is moving upward in the model. Green circles represent observation wells that were used during the calibration.

From the former fire station, the groundwater flows to the southwest and then further towards Åkers canal, see Figure 27. The flow can be observed to move upwards around the former fire station.

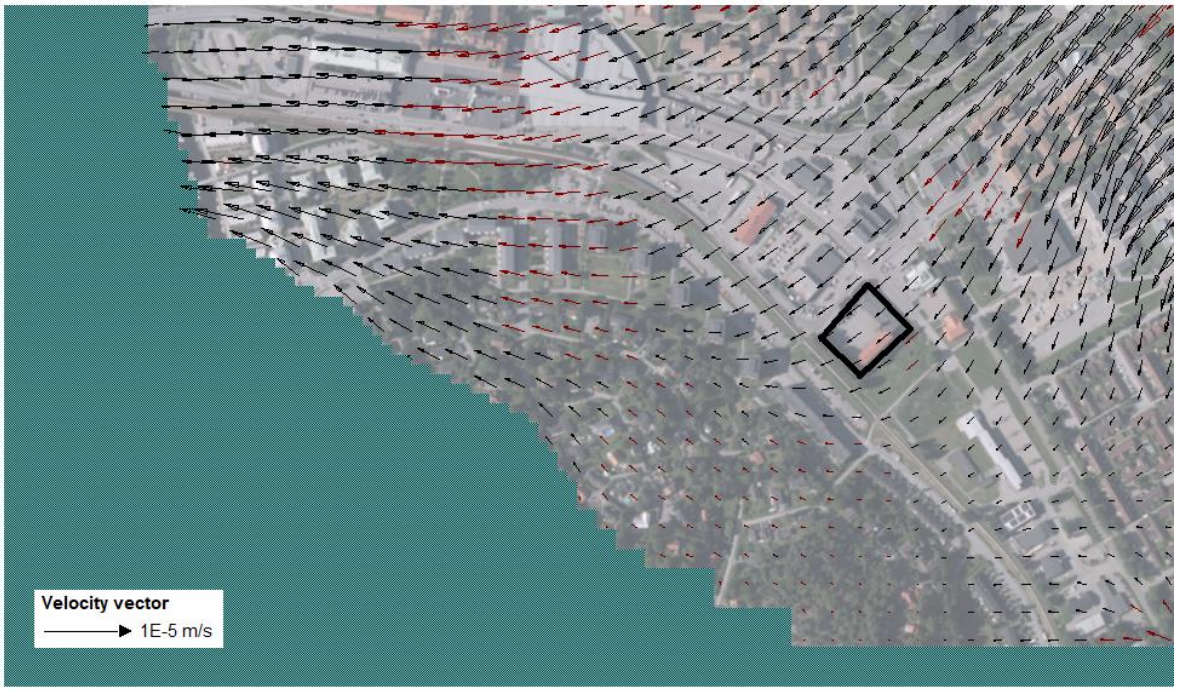


**Figure 27.** Groundwater flows from the former fire station (marked in black) in layer 5. Red arrows mean that the flow is moving downward and black that the flow is moving upward in the model. Background map: GSD-Orthophoto, 1 m color ©Lantmäteriet.

Calibration was performed for 19 observation wells, whereof 16 of them are located within or around the former fire station, and 3 are located closer to Åkers canal (Figure 26). The comparison between the calculated and observed heads after the calibration is presented in Figure 28. The symbols of red squares and blue circles illustrate the compared head levels in layer 2 and layer 3 respectively, and the closer they are to the blue straight line the better the calculated values are compared to the observed ones. The symbols above the blue straight line mean that the calculated head levels are larger than the observed head levels, and vice versa. From Figure 28, it can be said that the calculated heads are in general still overestimated after the calibration, especially for the observation wells in or around the former fire station (blue circles). The worst match was obtained for well 18S01. The best match was obtained for well 18GS02, which is the well located closest to Åkers canal. After the calibration, the residual mean of 0.49 m was obtained.

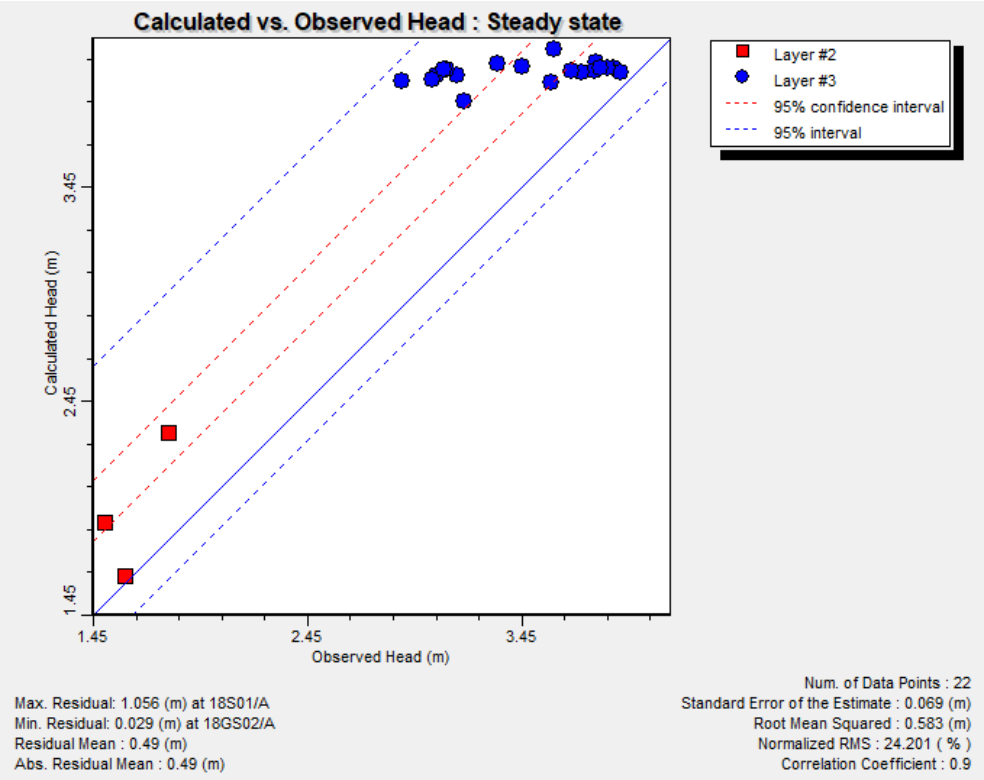


**Figure 28.** Comparison between calculated heads (Y-axis) and observed heads (X-axis) after the calibration. The blue line represents an ideal calibration scenario, where X=Y. The 95% confidence interval is the range where there is a 95% chance that the calculated heads will be acceptable for a given observed head. The 95% interval is the range where 95% of the head values are expected to occur.

The value of the drain boundary condition was 0.9 m b.g.l. after the calibration. For constant head boundary, the values of 0, 5, and 22.1 m were obtained as specified head for distance AB, CD, and EF respectively. Finally, the values of recharge rate and hydraulic conductivity after the calibration can be seen in Table 9 and Table 10. In general, the recharge rates within the model domain have been markedly decreased, where the differences were calculated to at least 86% (for zone 3) and at 94% as maximum (for zone 5).

**Table 9.** Recharge rate in zone 1 to zone 5 after calibration

| **Recharge Zone** | **Recharge rate** [**mm/year**] | **Difference** [%] |
|---|---|---|
| Zone 1 | 12 | 89 |
| Zone 2 | 9 | 87 |
| Zone 3 | 5 | 86 |
| Zone 4 | 1 | 89 |
| Zone 5 | 5 | 94 |

The hydraulic conductivities have been adjusted for most of the soil types, except the filling (fine gravel) and the two bedrock layers. To obtain a good match between the calculated head and observed head, the hydraulic conductivities of filling (coarse gravel), dry crust clay, clay, and the two till layers needed to be increased, Table 10.

**Table 10.** The hydraulic conductivity for each soil type in the model after calibration

| Soil type | $K_x\ [m/s]$ | $K_y\ [m/s]$ | $K_z\ [m/s]$ |
|---|---|---|---|
| Filling (fine gravel) | $1 \cdot 10^{-4}$ | $1 \cdot 10^{-4}$ | $1 \cdot 10^{-4}$ |
| Filling (coarse gravel) | $9 \cdot 10^{-3}$ | $9 \cdot 10^{-3}$ | $9 \cdot 10^{-3}$ |
| Dry crust clay | $9 \cdot 10^{-7}$ | $9 \cdot 10^{-7}$ | $9 \cdot 10^{-7}$ |
| Clay | $5 \cdot 10^{-9}$ | $5 \cdot 10^{-9}$ | $1 \cdot 10^{-9}$ |
| Shallow till | $4 \cdot 10^{-5}$ | $4 \cdot 10^{-5}$ | $9 \cdot 10^{-6}$ |
| Deep till | $8 \cdot 10^{-6}$ | $8 \cdot 10^{-6}$ | $9 \cdot 10^{-7}$ |
| Shallow bedrock | $8 \cdot 10^{-7}$ | $8 \cdot 10^{-7}$ | $8 \cdot 10^{-7}$ |
| Deep bedrock | $4 \cdot 10^{-7}$ | $4 \cdot 10^{-7}$ | $4 \cdot 10^{-7}$ |

### 4.1.2. Water Balance

The water balance obtained from the function zone budget in Visual MODFLOW shows that inflow to the model domain occurs via two sources. The first one is via constant head boundaries CD and EF (Figure 29) that stands for approximately half of total inflow. The other half of inflow is generated from recharge. Outflow from the model domain occurs via two ways, constant head boundary AB (Åkers canal) and drain. Here the outflow occurs mainly via drain.

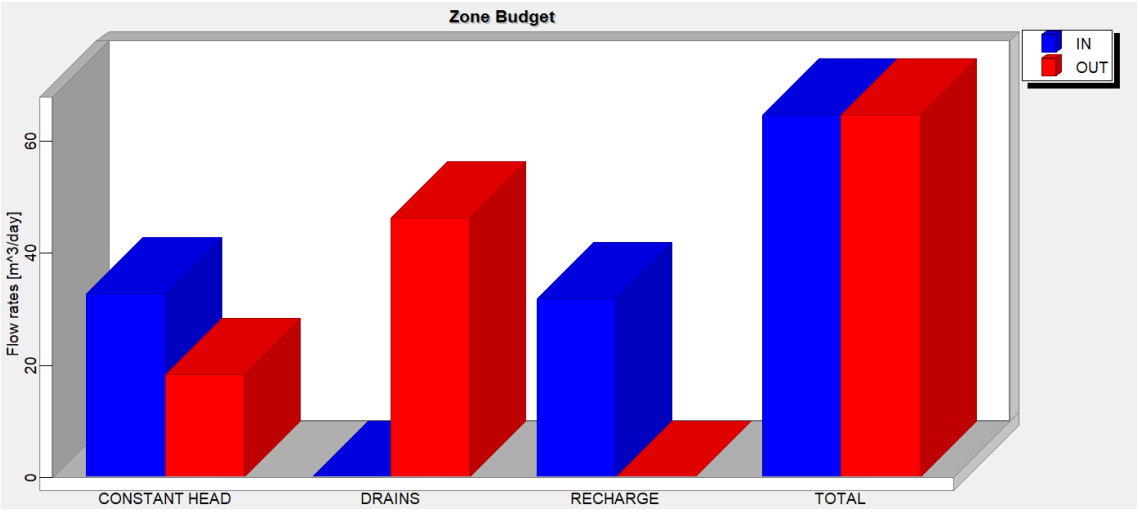


**Figure 29.** Water balance, generated from zone budget, over the model domain.

## 4.2. NUMERICAL TRANSPORT MODEL

### 4.2.1. Particle Tracking

The results of particle tracking after 130 imaginary particles have been assigned to layer 1, layer 2, and layer 3 are presented in Figure 30. The time markers appear after every 1 year, and the red color means that the pathline is going downward while blue color means that the pathline is going upward in the model.

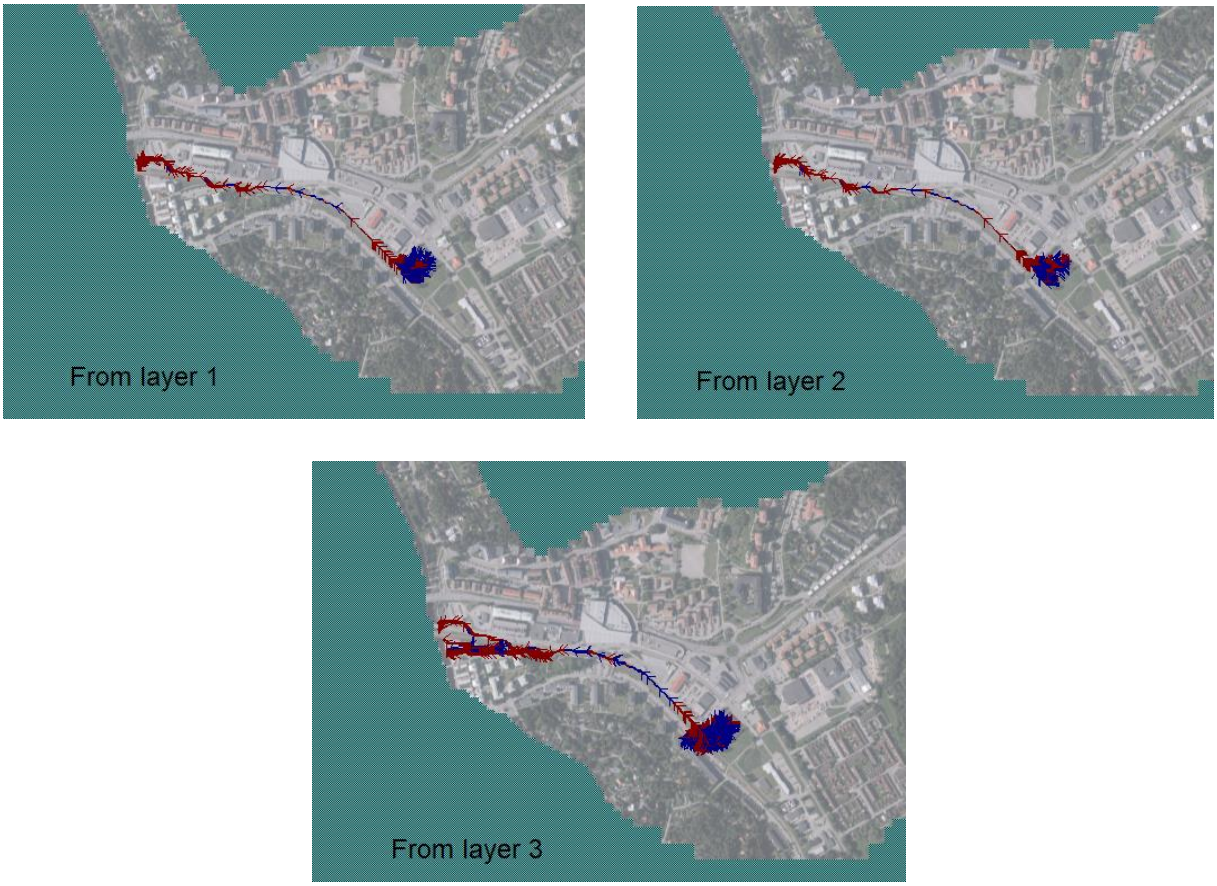


**Figure 30.** Pathlines of particles released from layer 1 (top left), layer 2 (top right), and layer 3 (bottom). The time markers are appearing after every 1 year and the red color means that the pathline is going downward while blue color means that the pathline is going upward in the model. Background map: GSD-Orthophoto, 1 m color ©Lantmäteriet.

The pathlines of the particles are very similar for the three layers, and although 130 different particles were assigned in the former fire station not many differences could be seen regarding the particle pathways. It can be noted from Figure 30 that the particles in all layers are travelling from the former fire station to Åkers canal via the railroad track in the southwest. In layer 2 the particles have traveled straight up to layer 1 before they travel via the railroad track to Åkers canal. Similar particle pathways could be observed from layer 3. The only difference is that the particles first travel to the southwest before they eventually find their way up to layer 1 and travel via the railroad track.

The travel time of an imaginary particle from the former fire station to Åkers canal was approximated to nearly 2 years for a particle released in layer 1 and layer 2. For a particle released in layer 3, the travel time was approximated to nearly 4 years. The approximated velocity of a particle is 400 m/year from filling and 270 m/year from till.

### 4.2.2. Transport of PFASs

This section will summarize the results of the transient transport model for PFOS, PFOA, 6:2 FTS, and PFPeA. The plots with contaminant plume and its concentration will be presented, where orange and red represent the interval of concentration that exceeds the guideline value for PFOS in groundwater ($4.5 \cdot 10^{-5}$mg/L).

**PFOS**

The transport of PFOS from the former fire station after 50 years in layer 1 is presented in Figure 31. The highest PFOS concentration ($> 4.5 \cdot 10^{-5}$mg/L) has moved about 30 m northwest from the former fire station and PFOS can be observed to spread in the direction where the railroad track is located. A lower concentration of PFOS ($\approx 1 \cdot 10^{-8}$mg/L) travels approximately 150 m from the former fire station after 50 years. The approximated velocity of PFOS plume for the concentration $4.5 \cdot 10^{-5}$mg/L is 0.6 m/year in filling.

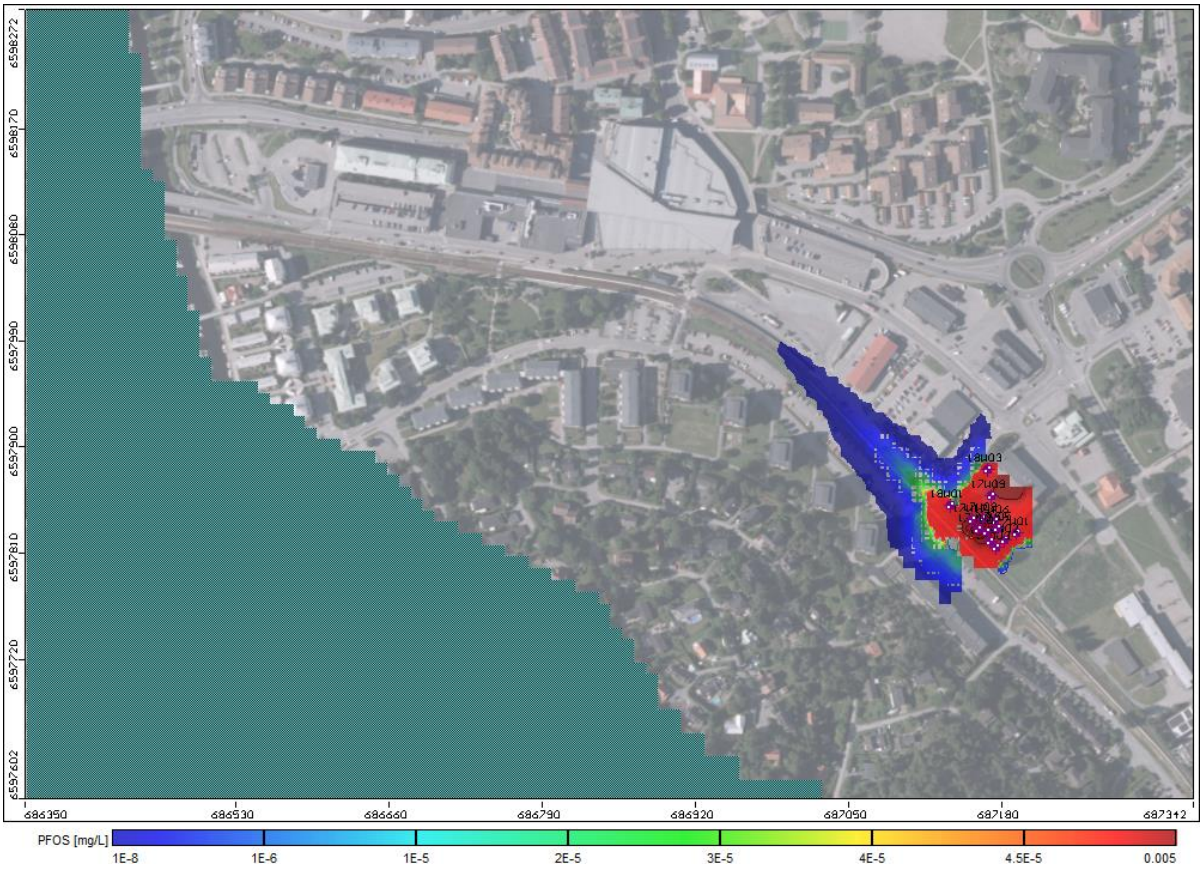


**Figure 31.** PFOS transport from the former fire station, after 50 years in layer 1. Purple circles illustrate the location of observation wells used during the calibration. Background map: GSD-Orthophoto, 1 m color ©Lantmäteriet.

The comparison of the calculated concentrations with observed concentrations was performed for 13 observation wells in layer 3, where PFOS has been observed. The calibration plot in Figure 32 shows quite a good match between the calculated and observed PFOS concentrations in layer 3. However, most of the calculated PFOS concentrations have been slightly underestimated. Especially, for the concentration in one of the observation wells (17W05).

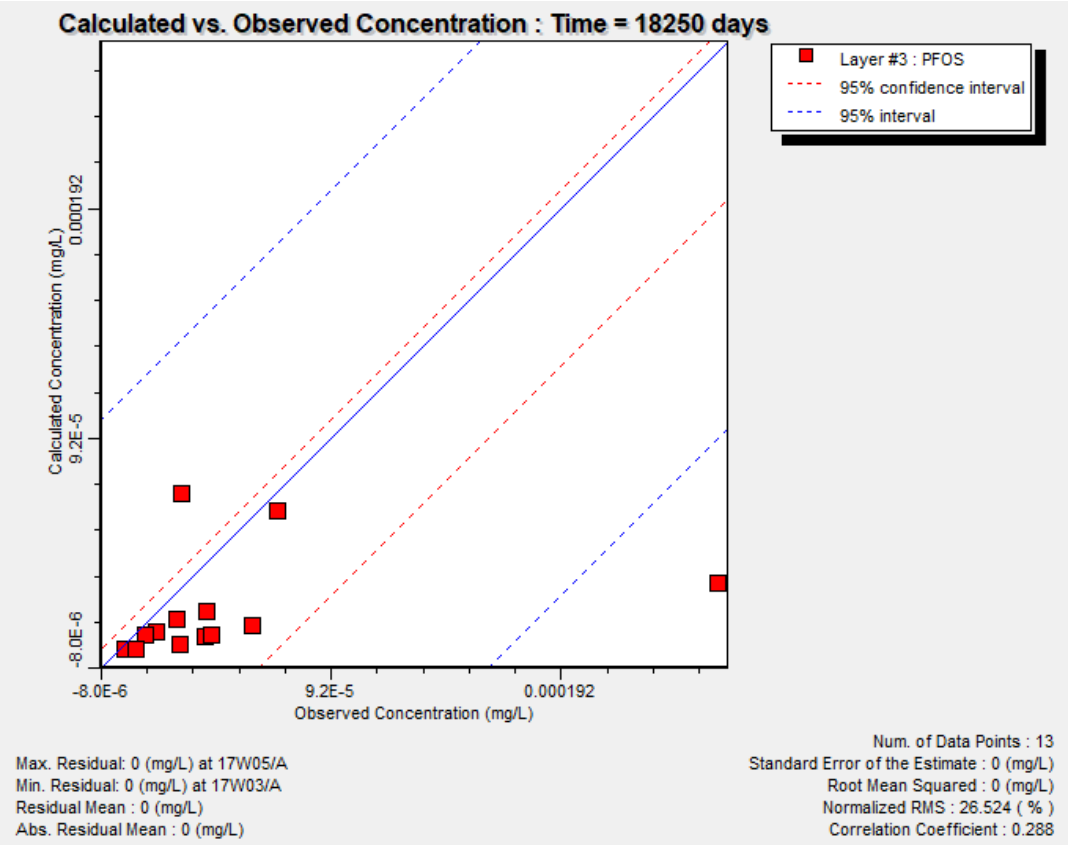


**Figure 32.** Comparison between calculated (Y-axis) and observed PFOS concentrations (X-axis) after 18250 days or 50 years. The blue line represents an ideal calibration scenario, where X=Y. The 95% confidence interval is the range where there is a 95% chance that the calculated concentrations will be acceptable for a given observed concentration. The 95% interval is the range where 95% of the concentration values are expected to occur.

### PFOA

The transport of PFOA from the former station after 50 years in layer 1 is presented in Figure 33. The PFOA plume with concentration higher than $4.5 \cdot 10^{-5}$mg/L can be observed to spread via the railroad track to Åkers canal. This concentration interval reaches about 150 m away from the former fire station, and a lower concentration of PFOA ($1 \cdot 10^{-8} - 1 \cdot 10^{-7}$ mg/L) reaches Åkers canal after 50 years. The approximated velocity of PFOA plume for the concentration $4.5 \cdot 10^{-5}$mg/L is 3 m/year in filling.

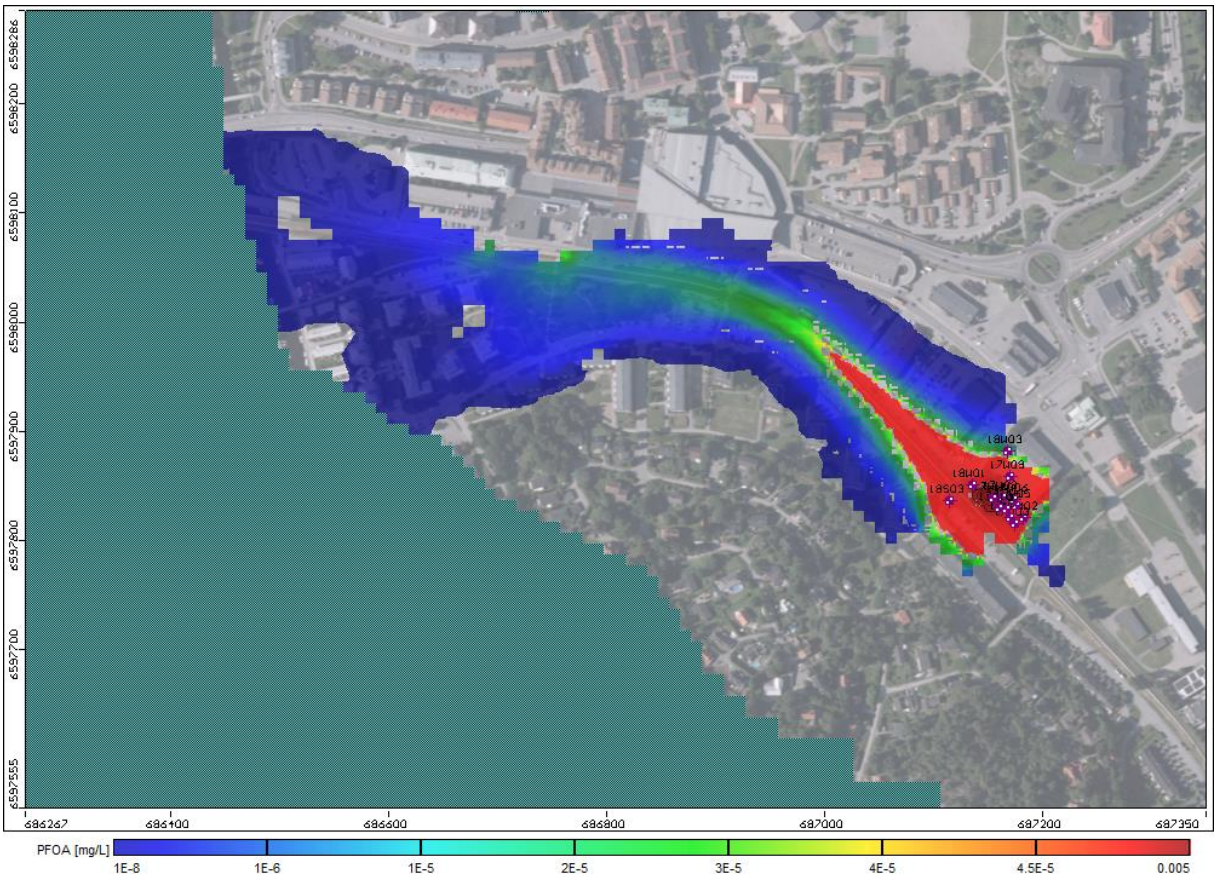


**Figure 33.** PFOA transport from the former fire station, after 50 years in layer 1. Background map: GSD-Orthophoto, 1 m color ©Lantmäteriet.

The comparison of the calculated concentrations with observed concentrations was performed for 13 observation wells in layer 3, where PFOA has been observed. The calibration plot in Figure 34 shows that all of the data points except one match the observed concentrations quite well. Although the calculated PFOA concentrations generally are a little bit overestimated, since 16 of 19 observation wells obtained higher calculated concentrations than the observed ones. The observation well that has the worse matching is 17W11.

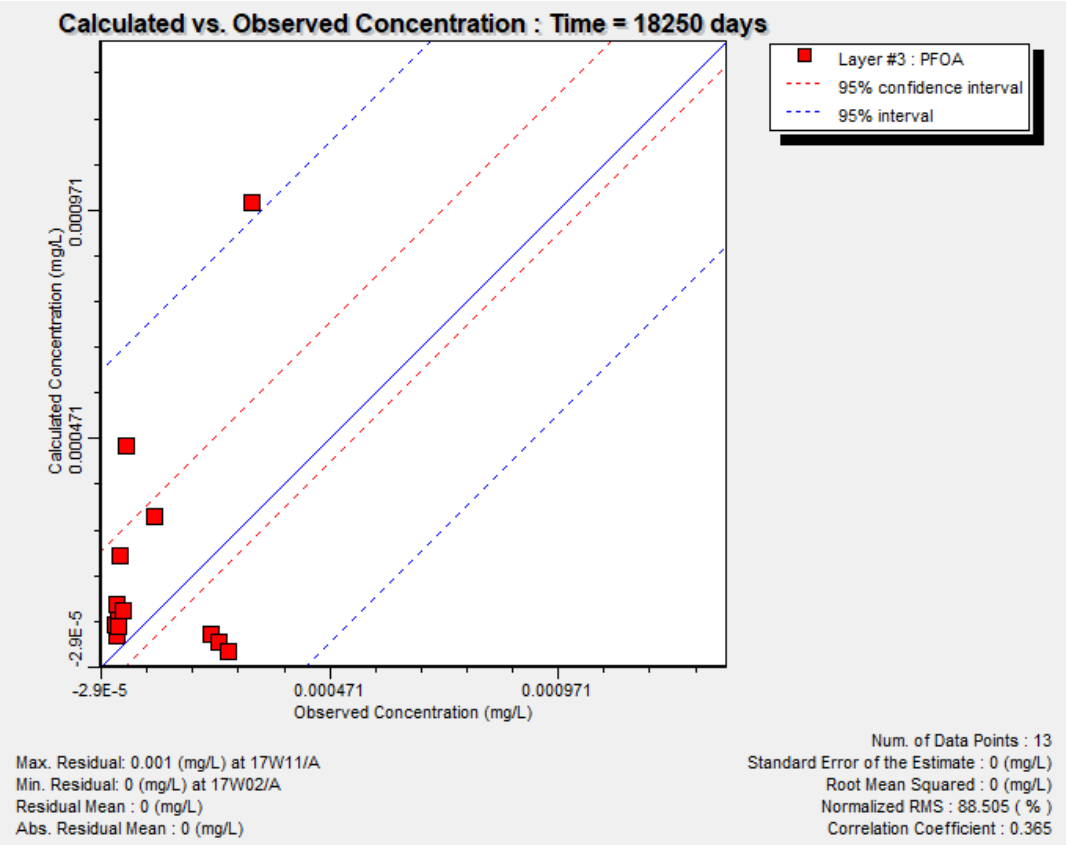


**Figure 34.** Comparison between calculated (Y-axis) and observed PFOA concentrations (X-axis) after 18250 days or 50 years. The blue line represents an ideal calibration scenario, where X=Y. The 95% confidence interval is the range where there is a 95% chance that the calculated concentrations will be acceptable for a given observed concentration. The 95% interval is the range where 95% of the concentration values are expected to occur.

### 6:2 FTS

The transport of 6:2 FTS from the former station after 50 years in layer 1 is presented in Figure 35. The 6:2 FTS plume with a concentration higher than $4.5 \cdot 10^{-5}$mg/L can be observed to spread via the railroad track to Åkers canal. This concentration interval travels about 400 meters from the fire station and the concentration of approximately $1 \cdot 10^{-6}$ mg/L reaches Åkers canal after 50 years. The approximated velocity of 6:2 FTS plume for the concentration $4.5 \cdot 10^{-5}$mg/L is 8 m/year in filling.

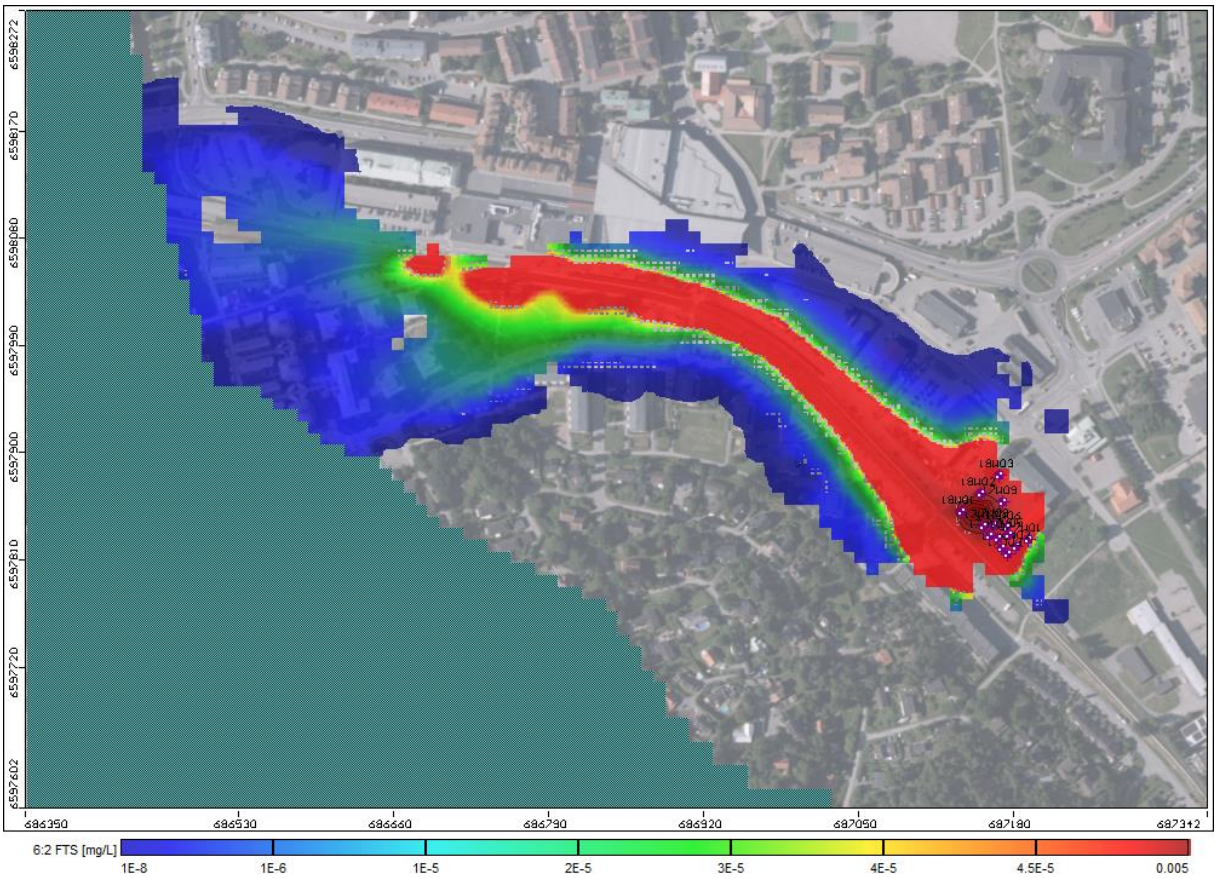


**Figure 35.** 6:2 FTS transport from the former fire station, after 50 years in layer 1. Background map: GSD-Orthophoto, 1 m color ©Lantmäteriet.

The comparison of the calculated concentrations with observed concentrations was performed for 14 observation wells in layer 3, where 6:2 FTS has been observed. The calibration plot in Figure 36 shows a good match for 11 of 14 observation wells. The worse matching is obtained for the observation well 17W09, whereas very good matching is obtained for 17W01.

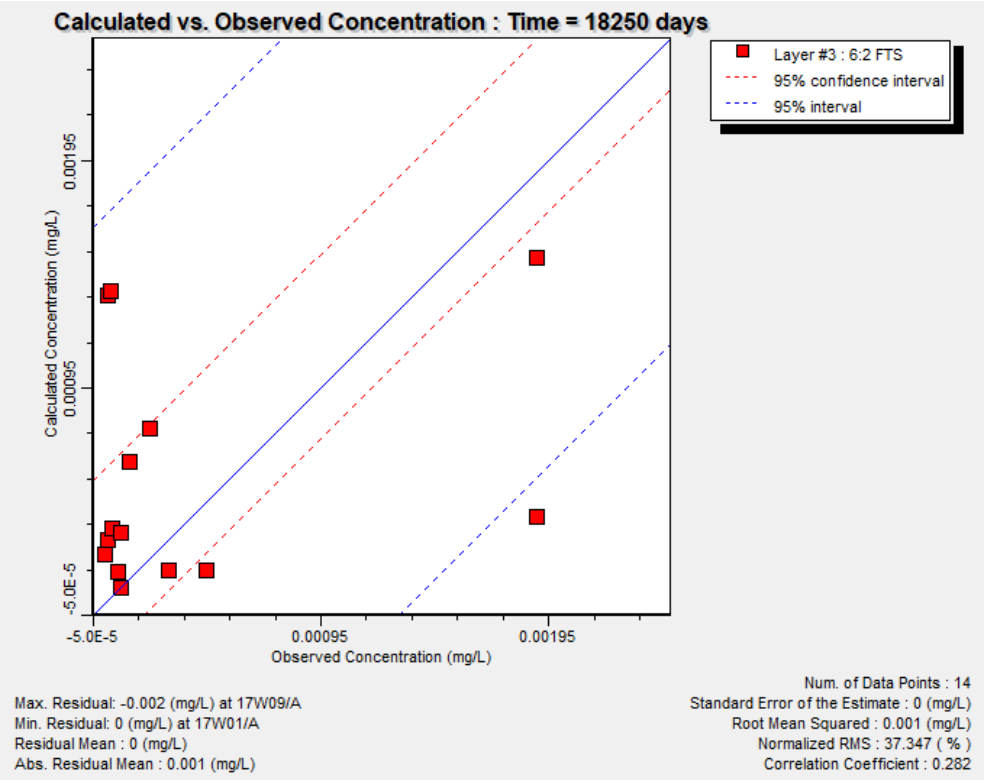


**Figure 36.** Comparison between calculated (Y-axis) and observed 6:2 FTS concentrations (X-axis) after 18250 days or 50 years. The blue line represents an ideal calibration scenario, where X=Y. The 95% confidence interval is the range where there is a 95% chance that the calculated concentrations will be acceptable for a given observed concentration. The 95% interval is the range where 95% of the concentration values are expected to occur.

### PFPeA

The transport of PFPeA from the former station after 50 years in layer 1 is presented in Figure 37. The PFPeA plume with concentration higher than $4.5 \cdot 10^{-5}$mg/L can be observed to spread via the railroad track and to nearly reach Åkers canal after 50 years. The concentration of PFPeA that can be observed to reach Åkers canal after 50 years is approximately $4 \cdot 10^{-5}$mg/L. The approximated velocity of PFPeA plume for the concentration $4.5 \cdot 10^{-5}$mg/L is 16 m/year in filling.

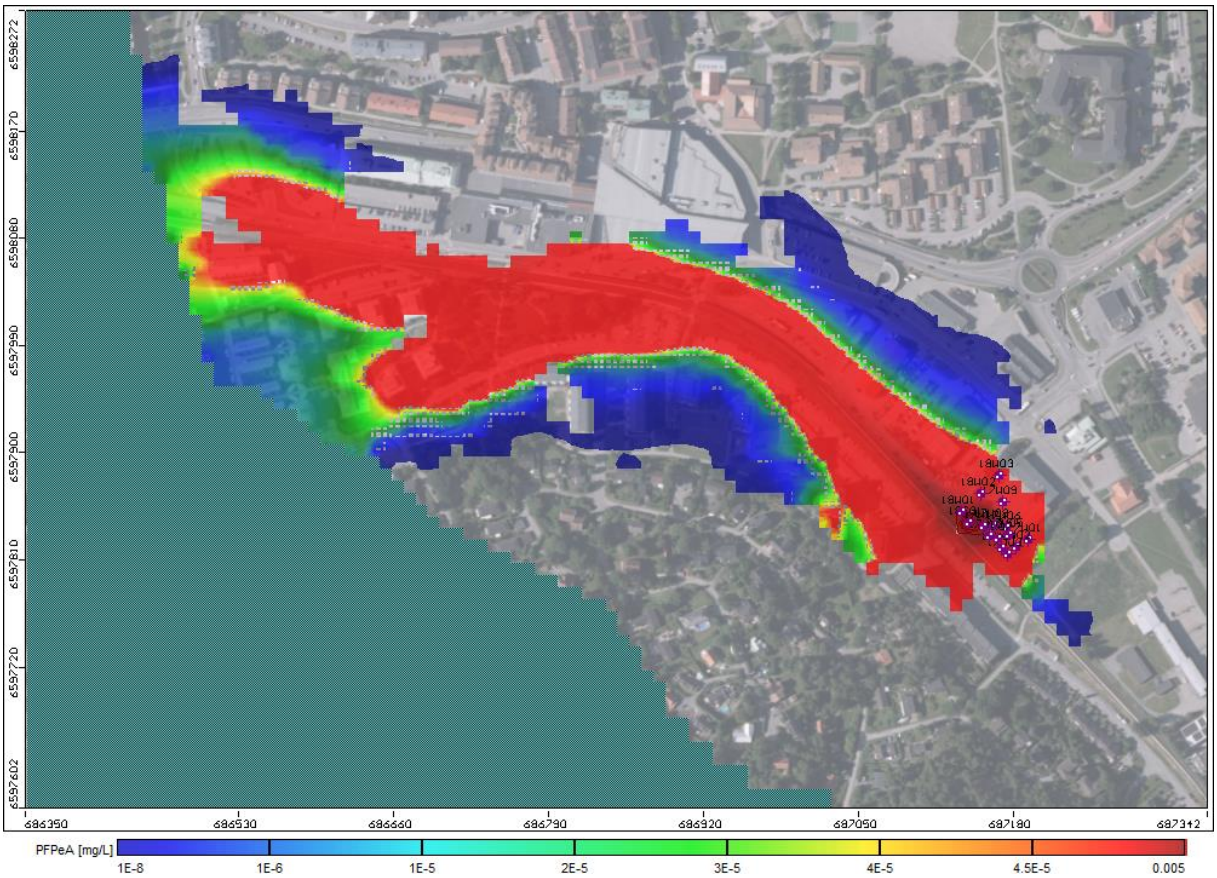


**Figure 37.** PFPeA transport from the former fire station, after 50 years in layer 1. Background map: GSD-Orthophoto, 1 m color ©Lantmäteriet.

The comparison of the calculated concentrations with observed concentrations was performed for 14 observation wells in layer 3, where PFPeA has been observed. The calibration plot is presented in Figure 38 and the calculated concentrations can be seen to spread both above and below the blue line. In general, the model generated a good calculated concentration. Although, some of the concentrations are quite underestimated, among them 17W11 is the worst.

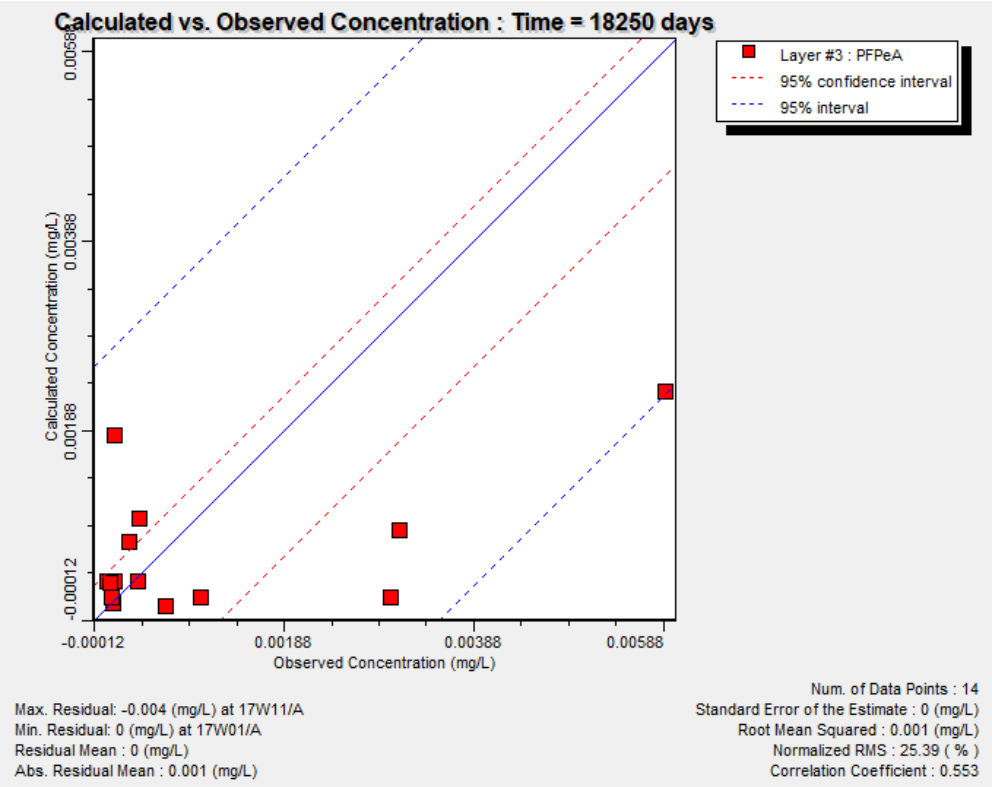


**Figure 38.** Comparison between calculated (Y-axis) and observed PFPeA concentrations (X-axis) after 18250 days or 50 years. The blue line represents an ideal calibration scenario, where X=Y. The 95% confidence interval is the range where there is a 95% chance that the calculated concentrations will be acceptable for a given observed concentration. The 95% interval is the range where 95% of the concentration values are expected to occur.

# 5. DISCUSSION

## 5.1. GROUNDWATER MODEL

Groundwater model was created in Visual MODFLOW with an aim to study the groundwater flow in the area. A groundwater model is a simplified representation of a real groundwater system therefore many simplifications and assumptions were made.

### 5.1.1. Numerical Groundwater Model

The groundwater flow model reproduces the observed groundwater levels with residual mean 0.49 m (Figure 28), which is within the criteria set for the calibration. On the other hand, all the calculated groundwater levels were overestimated compared to the observed levels. This despite the very low recharge rates (Table 9) and drain at 0.9 m below ground level. There could be several reasons for this result. One reason could be the assumption that the clay layer in layer 2 is continuous except the area where bedrock and till exist. In the low area (Figure 6) where the former fire station is located, a large amount of precipitation is therefore prevented from being infiltrated and consequently groundwater level raises in this area. Another reason could be the water from the high area in the northeast (Figure 6). In the high area, most of the assigned recharge infiltrates and almost nothing drains. Instead, the water flows down the hill and enter the low area and as a result, also heightens the groundwater level there (Figure 39). A third reason that could have influenced the overestimation of groundwater levels is the thickness of the till layer. The till's thickness varies between 1 and 2 meters. This is not much compared to the amount of the water that enters the model and consequently, not much groundwater can drain through this "natural drain".

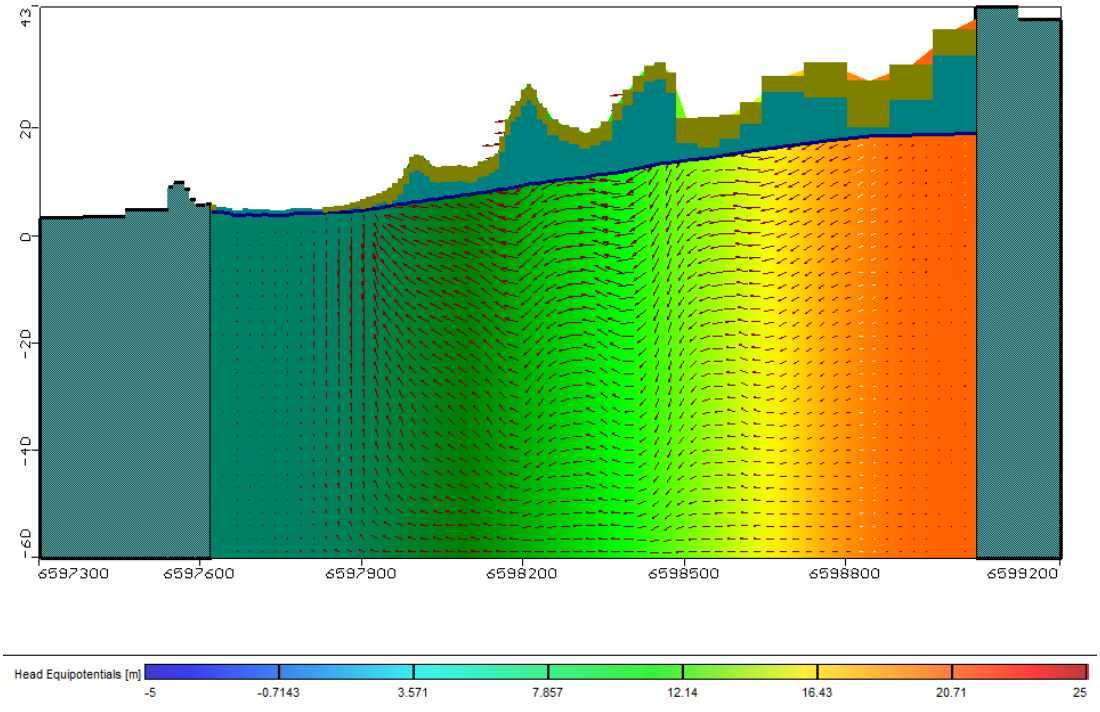


**Figure 39.** Water from the high area infiltrates and flows towards the lower area.

The calculated velocity vectors in Figure 26 indicate that the groundwater is flowing to the southwest from the former fire station. This result is in line with the observed groundwater levels and the estimated groundwater flow directions modeled by WSP. Furthermore, the calculated groundwater flow indicates an upward direction around the former fire station. This could be reasonable. Firstly, because the former fire station is in a low area surrounded by high areas with higher groundwater potentials to the southeast and northeast (Figure 6). This means that groundwater will flow to the former fire station since water flows from high to low water potential. The upward groundwater flow could consequently be caused by the high differences in the water potentials. Secondly, because of the higher inflows from constant head boundaries CD and EF compared to the recharge (Figure 29), as a large amount of water is entering the model through the sides. In reality, the water that is believed to enter the model through boundaries CD and EF may be a smaller amount or entering the model domain through drainage pipes, and hence do not affect the groundwater level as much as calculated. The last thing that might influence this flow behavior is the thickness of the till and the clay layer. The till layer consists of a material with higher hydraulic conductivity compared to clay and bedrock. This means that the groundwater preferably flows through the layer ("natural drain"). But, since its thickness is only limited to 2 meters as maximum, not much groundwater can flow through it in the low area. This combined with a thick clay layer to the northwest of the former fire station may also cause the groundwater to flow upwards to the filling material, where it can easily move.

### 5.1.2. Uncertainties

The first step in the modelling process was to develop a conceptual model, based on all available data and knowledge of the area. During this step, many simplifications and assumptions were made. The first assumption was made during the model demarcation, where the model domain was assumed to have inflow from boundary CD and boundary EF, Figure 16. This was considered important in order to limit the extent of the model domain. The decision was mainly based on the elevation model from Lantmäteriet. The assigned constant heads in the two boundaries were based on the measured groundwater levels from SGU's well archive. The reliability of groundwater level measurements from SGU's well archive was considered low because no clear documentation exists regarding their method of drilling or measuring. Therefore, the constant head values were calibrated to match the observed groundwater level in the area. However, how the groundwater in those areas behaves in reality is very difficult to know since the area is quite urban. The precipitation that falls into the area north of boundary EF could for example drain to the stormwater drainage system and as a result, not much water from those areas would enter the area through this boundary.

The next simplification that yield uncertainties was that the model's geological layers only consisted of 5 layers, whereof 3 are soil layers and 2 are bedrocks. The soil layers were assumed to consist of filling, clay, and till over the entire model domain. This assumption is very rough because the decision is mainly based on the information of geological survey performed within the former fire station and along the railroad track towards Åkers canal. Since no data regarding soil layers were available for the area east of the former fire station, this assumption was

necessary to make. Another uncertainty, caused by the lack of geological data outside the former fire station, is that the soil layers were assumed to be continuous. Soil types in different layers were assigned partly after SGU's soil type map in Figure 7, and the assumption was accordingly made that the clay in layer 2 is continuous. This is in fact not certain because SGU's soil map is only based on a few drilling points with known geological layers. Clay can block the movement of groundwater as described in 3.1.2. Hydrogeology, its continuity is therefore very important for the groundwater flow. However, since no better information was available the SGU's soil map was considered as the most suitable source.

Furthermore, the assumption was made that clay in layer 1 consists of dry crust clay with higher hydraulic conductivity compared to normal clay. The geological survey supports that dry crust clay exists in the area, and although clay theoretically has a hydraulic conductivity of less than $10^{-9}$ m/s, aggregate formation, cracks, and strata in the soil have a great influence on its permeability (Bovin et al., 2015). Larsson (2008) has also emphasized that through desiccation, frosting, and weathering dry crust clay could be formed in the upper clay layer. With these reasons, the decision was made that dry crust clay would be included in the model and a higher hydraulic conductivity than normal clay has been assigned.

To determine the hydraulic conductivities for different geologic materials in the study area, the literature study, slug test, and calculation with data from SGU's well archive were performed. Slug test was performed to determine the hydraulic conductivity of the till within the former fire station. Out of the 17 observation wells that slug test was performed only 7 of them were approved for further analysis. The reason that so many wells had too slow drawdown is probably because the screen (filter part where water can flow into the well) has been blocked by silt/clay material, which was observed during the field work. Also, because the wells were installed as sampling wells with the primary task to monitor groundwater level and deliver water for sampling and not to have the perfect function with regards to surrounding hydraulic conditions. The results of slug tests were then used to assign the values of hydraulic conductivity in shallow and deep till in the groundwater model. An assumption has therefore been made that the hydraulic conductivity of till outside the former fire station obtains a similar value as slug test results. In reality, a slug test only gives the effect very close to the observation well that is being tested and the result from a slug test should only be seen as an indication of the hydraulic conductivity closest to the tested well. Nevertheless, the results of the slug test were still considered to give a better insight of the area's hydraulic conductivity compared to the literature values.

The hydraulic conductivity of bedrock was determined through the calculation with data from SGU's well archive. For the population with well depth below 50 m, not many data points were available and the result therefore was not considered to be reliable. Therefore, the results calculated with well depth below 100 m and 210 m have been used in the groundwater model.

Construction of the railroad track and its hydraulic conductivity are important factors that affect the groundwater flow. In the groundwater model, the thickness of the railroad track has been assumed to vary between 1 and 2 meters (like other soil types in layer 1). Normally, a railroad

track consists of ballast material. Ballast is typically made of crushed stone and its hydraulic conductivity was therefore assigned as coarse gravel in this model. Based on the available information about Roslagsbanan, the thickness of the railroad track is approximately 1 m. The assumption that the thickness of the railroad track varies between 1 and 2 meters may therefore be an overestimation. However, such estimation can reflect a worst-case scenario and may therefore be considered better than if an underestimation is made.

The next uncertainty is a result of insufficient groundwater level measurements. Firstly, more equally distributed groundwater level measurements within the model domain are needed. The existing groundwater level data are mostly located around the former fire station and some closer to Åkers canal, Figure 26. Calculated groundwater levels in the northeast area are consequently more or less unknown and depend entirely on the groundwater levels in the south. Four groundwater level measurements from SGU's well archive have been used to assign the initial constant head values. But they have been excluded from the calibration process because their reliability was considered low. Secondly, to calibrate the model, groundwater levels from February and April were used. This is because no groundwater levels for longer time series existed for the wells, and to avoid the mixture of groundwater levels from different seasons. Groundwater levels undergo seasonal variation during a year. For the area where the model domain is located high groundwater levels could be observed during Spring, while low groundwater levels could be observed during Autumn. A division of groundwater levels with regards to high respective low seasons was made accordingly and the data from the Spring period was chosen because most measurements were done during that time. The groundwater flow was simulated under steady-state conditions, meaning that the groundwater level and flow do not change over time.

Drain boundary condition was assigned to the first layer of the model domain. The uncertainty that comes with it, is its depth below ground level. Generally, drainage pipes are located approximately 1 to 2 m b.g.l. (Dittlau, 2005), but in this model drain was assigned at 0.9 m b.g.l. which is quite shallow. Since the minimum thickness of layer 1 is 1 m it was not possible to assign the drain below this level (in layer 1). Therefore, the drain depth was limited to 1 m as the deepest. Another assumption was made regarding the location of the drainage pipes. The area is considered urban but the exact locations of drainage pipes are unknown, the concept of general drain has therefore been adopted where the drain boundary condition was applied everywhere in layer 1 of the model domain, except where constant heads exist.

## 5.2. TRANSPORT MODEL

Based on the result of the groundwater flow modelling, the contaminant transport was developed for PFOS, PFOA, 6:2 FTS, and PFPeA. The construction of the transport model was in turn based on the contaminant distribution map in soil that was developed in the conceptual transport model.

### 5.2.1. Numerical Transport Model

#### Particle Tracking

The result of particle tracking shows that the water molecules are traveling to Åkers canal via the railroad track. A difference in the particle's travel times between different layers was observed. For the particles released from layer 1 and layer 2, the travel time was approximated to 2 years. The reason that the travel times for the two layers are almost equally is because the particles from layer 2 are going up to layer 1 (upward groundwater flow) before the horizontal transport is taken place in the filling material. The transport of particles released from the till (layer 3) took up to nearly 4 years, although a large part of transport also occurs in filling. This shows that the advective transport of water molecules in the till layer is much slower compared to the transport through filling.

#### Transport of PFASs

For each transport model, calculated concentrations of PFASs were observed in layer 3 although the contaminant was applied only in layer 1. This, although the local upward groundwater flow was generated from the groundwater model, where the advective transport occurs in layer 3 to layer 1 direction. The transport of PFASs in this model can therefore be said to not only follow the advective process because then calculated PFASs concentration would not have been observed in layer 3. The reasons that PFASs spread to the other layers is therefore probably due to diffusion and dispersion.

The transport of PFOS has the most limited extent compared to the other three homologues that were modeled (Figure 31). This could be because of the higher $K_d$ value, and hence a higher amount of PFOS is absorbed to the soil. The higher concentration compared to the other three homologues can also be due to the precursors that can degrade to PFOS. Generally, the calculated PFOS concentrations in layer 3 are lower than the observed concentration (Figure 32). This could possibly be because too high $K_d$ value was assigned and therefore too much PFOS was bound to the soil in layer 1 and layer 2. Why the calculated concentration at sampling location 17W05 is so underestimated compared to the other locations could not really be explained.

Furthermore, the transport model showed that FFOA has traveled further away from the former fire station compared to PFOS (Figure 33), although the assigned concentration is smaller. Low concentration of PFOA can also be observed to have reached Åkers canal after 50 years. This is probably due to the lower $K_d$ value and consequently PFOA is not bound to the soil as hard as PFOS. Moreover, the calculated PFOA concentrations were generally overestimated (Figure 34). The reason of overestimation is probably also due to the assigned $K_d$ value. For PFOA, the $K_d$ value might have been slightly too low in layer 1 and layer 2. The highest residual mean was obtained for the sampling location 17W11, which is the location where PFOA was assigned in the model. The high calculated concentration at this location in layer 3 could be because of $K_d$ value in layer 1 and 2 was underestimated.

For 6:2 FTS, the plume has reached more extension than both PFOS and PFOA (Figure 35). This is because 6:2 FTS is more water soluble and therefore do not bind as hard to the soil. With this reason, the $K_d$ value of 6:2 FTS was also chosen to be lower than both PFOS and PFOA. The calibration plot in Figure 36 shows that the calculated concentrations match the observed concentrations quite well, except from the calculated concentration at sampling location 17W09 that obtain an underestimated result.

For the last contaminant, PFPeA has obtained the most extensive contaminant plume with the highest concentration compared to the previous three homologues (Figure 37). The reason that such high concentrations of PFPeA has traveled from the fire station is probably because of the low $K_d$ value. PFPeA is the most water-soluble contaminant out of the four PFAS homologues and it was therefore expected that PFPeA would have been the contaminant that traveled the furthest. 6:2 FTS can also degrade to PFPeA, this was however not included in the modelling. If the degradation of 6:2 FTS to PFPeA had been taking into consideration, it would probably have resulted in higher concentration of PFPeA and lower concentration of 6:2 FTS.

With regard to the travel times of the contaminant plume, the velocity from low to high are as followed: PFOS, PFOA, 6:2 FTS and PFPeA. The slowest velocity was obtained for PFOS at 0.6 m/year and fastest for PFPeA at 16m/year. This shows that shorter chain PFASs with low $K_d$ value can travel faster than the longer chain PFASs. It is therefore important that studies are conducted to investigate the properties of these shorter chain PFASs.

As mentioned, the assigned concentrations are possibly underestimated, at the same time the $K_d$ values in layer 2 and layer 3 may also be underestimated. These two uncertainties in the model might cancel each other out, where the low $K_d$ values compensate for the low assigned concentrations (low $K_d$ value means less sorption). Furthermore, the longitudinal dispersivity value of 10 m was used during the transport modelling. This value could have caused the spread of PFASs in the direction perpendicular to the groundwater flow. Finally, due to the fact that the groundwater level generally was overestimated. It is therefore possible that the transport of PFASs would have looked differently if the groundwater level drops half a meter. This could, for example, mean that the transport through the top layer (filling) is more limited and thus does not reached the extent it currently does. However, the results of this project should only be seen as an indication of how transport of PFASs could have looked like from the property, rather than showing an exact extent of PFAS concentrations.

### 5.2.2. Uncertainties

As a basis for the construction of the transport model, contaminant distribution maps were developed for the four PFAS homologues. With contaminant distribution maps, the extent of different PFASs could be studied and the concentrations were then assigned based on these maps.

The first uncertainty comes with the distribution maps that use the observed concentrations for interpolation. The method used during the interpolation was inverse distance weighting (IDW).

From Figure 22 to Figure 25, the extension of PFASs seems to be overestimated to the southwest of the property. For example, in Figure 22 the hotspot from sampling location 17W10 seem to have overestimated the concentration towards the southwest. Two observation wells exist outside the former fire station and they have an observed concentration in the light green interval, therefore the hotspot's extent should not have been as extensive as the interpolation result shows. Similar behavior could be observed in the other three figures. However, the distribution maps have only been used as a guideline when assigning the concentration in Visual MODFLOW and should therefore not be seen as an actual transport of PFASs.

Based on the different hotspots that could be observed on each distribution maps and the detected concentrations in soil, the concentrations in water were calculated. This was done because MODFLOW requires the initial contaminant concentration to be assigned in the water and water analysis have only been done in the till layer. The source of PFASs that leach into the groundwater in the till has its origin from the filling/top soil layer, therefore it was important that the transport is being mapped from there. This method of course implies uncertainties to the transport model. One of the uncertainties comes from the $K_d$ values that are based on the literature. Although, the choice was made regarding the fraction of the organic carbon in the soil, there are still other factors that can affect the $K_d$ values, such as pH and fraction of clay. The values of $K_d$ can vary significantly between different sites, therefore site-based values are recommended. This was however not possible in this project, because no soil and groundwater samples from the same layer was analyzed except from one point. Furthermore, the assumption was also made that the same $K_d$ value was obtained for each soil layer. As previously discussed, the value of $K_d$ vary depending on what soil type it is. The $K_d$ values were chosen for filling material, which are generally lower than for example clay. It was considered "safer" to choose a smaller $K_d$ to reflect a worst-case scenario where transport of PFASs overestimated rather than underestimated.

The initial concentration of each PFAS homologue was then assigned to the top soil layer, using the constant concentration boundary. The assumption was consequently made that the same concentration was released to the model from layer 1 in the period of 50 years. This is considered reasonable although the training with AFFFs was carried out until 1969 and 1997. Because PFASs can bind to the soil even after the trainings have stopped, the leaching from the unsaturated surface soil to the groundwater would therefore still occur. Furthermore, the concentration observed in the soil today was used to calculate the leached concentration in groundwater. This approach might have underestimated the historical contribution from the property as concentrations probably are lower today than it was when firefighting exercises still performed, due to the dilution. However, the results of the transport model have not shown a significant underestimation of the calculated concentrations.

## 5.3. RECOMMENDATIONS FOR FURTHER STUDIES

To construct a more reliable transport modelling of PFASs, more information and data are needed. Therefore, the following is recommended:

- More equally distributed observation wells and more groundwater level measurements need to be conducted so that the modeled groundwater level and flow can better be verified.

- Perform groundwater level measurements in different soil layers.

- Perform a geologic investigation so that soil types layer to the bedrock can be identified outside the former fire station.

- Get more detail data regarding the railroad track's construction.

- Perform pair sampling and analysis of soil and groundwater in different soil layer (both top and bottom soil layers). By doing this, site-based $K_d$ values can be calculated for the specific PFASs compounds and soil types. The recalculation will neither need to be done for the assigned concentrations.

- Install observation wells in or near the railroad track to the west of the fire station. So that analysis can be made and used for the calibration of the transport model.

For further studies, modelling of future scenario could be performed for another 50 or 100 years from now. How would the transport of PFASs look like if no remediation is taken place? The sensitivity analysis should also be conducted to study how different parameters affect the result of the model simulation. Lastly, the mass of PFASs that spread from the former fire station can be estimated, based on this model or by constructing a new model based on additional information and data listed above.

# 6. CONCLUSIONS

Literature study, fieldwork, and groundwater flow model over the study area combined with a transport model of PFOS, PFOA, 6:2 FTS, and PFPeA were constructed in this master's thesis. According to the results produced during this project the following has been concluded:

- The important property of PFASs that should be taken into consideration when constructing a transport model is the compounds' sorption in soil that can be described with the distribution coefficient ($K_d$).

- The site-based hydraulic conductivity of till was calculated with the slug test to vary between $1.4 \cdot 10^{-6}$ and $7.9 \cdot 10^{-5}$ m/s. For bedrock, the hydraulic conductivity was estimated within the interval of $3.8 \cdot 10^{-7}$ and $7.8 \cdot 10^{-7}$ m/s.

- The result of the groundwater flow simulation shows that groundwater flows towards the southwest from the former fire station and then further towards Åkers canal. The approximated velocity of a water molecule released from the property varies between 270 m/year and 400 m/year.

- The transport modelling shows that the four PFAS homologues (PFOS, PFOA, 6:2 FTS, and PFPeA) travel towards Åkers canal via the railroad track. The approximated velocity of the contaminant plume is 0.6 m/year for PFOS, 3 m/year for PFOA, 8 m/year for 6:2 FTS, and 16 m/year for PFPeA.

# REFERENCE


Ahrens, L., Norström, K., Viktor, T., Cousins, A.P., Josefsson, S., 2015. Stockholm Arlanda Airport as a source of per- and polyfluoroalkyl substances to water, sediment and fish. *Chemosphere*, [e-journal] 129, 33–38. Available through: Uppsala University Library website https://doi.org/10.1016/j.chemosphere.2014.03.136 [Accessed 1 December 2018].

Andersson, M.P., Woessner, W.W., Hunt, R.J., 2015. *Applied Groundwater Modeling - Simulation of Flow and Advective Transport*. 2nd ed. [e-book] Elsevier. Available through: Uppsala University Library website https://app.knovel.com/web/toc.v/cid:kpAGMSFAT1/viewerType:toc/root_slug:applied-groundwater-modeling?kpromoter=federation [Accessed 7 December 2018].

AquiferTest, 2019. *AquiferTest Pro 9.0 Help.* [online]. Available at: https://www.waterloohydrogeologic.com/help/aquifertest/index.html?_hvorslev_slug_test.htm [Accessed 6 December 2019].

Bear, J., Verruijt, A., 1987. *Modeling Groundwater Flow and Pollution.* Dordrecht: D. Reidel Publishing Company.

Bovin, K., Vikberg, E., Morén, I., 2015. *Tätande jordlager – en kunskapssammanställning.* [pdf] Uppsala: Sveriges geologiska undersökning. Available at: http://resource.sgu.se/produkter/sgurapp/s1532-rapport.pdf [Accessed 31 January 2019].

Brömssen, M. von, Gunnemyr, L., Lindstrand, O., Jonasson, S., 2006. *Modeller för transport och spridning av föroreningar fas 1. Förstudie - Användning av numeriska beräkningsmodeller för beskrivning av transport och spridning av föroreningar i grundvatten.* [pdf] Stockholm: Naturvårdsverket. Available at: https://www.naturvardsverket.se/Documents/publikationer/620-5541-0.pdf [Accessed 2 December 2018].

Buck, R.C., Murphy, P.M., Pabon, M., 2012. Chemistry, Properties, and Uses of Commercial Fluorinated Surfactants. In: Knepper, T.P., Lange, F.T., 2012. *Polyfluorinated Chemicals and Transformation Products.* New York: Springer. pp. 1-24.

Butler, J.J., Jr., 1997. *The Design, Performance, and Analysis of Slug Tests.* Boca Raton: CRC Press.

Dittlau, P., 2005. *Kapitel D Avvattning och dränering 48.* [pdf] Trafikverket. Available at: https://www.trafikverket.se/contentassets/c19c23215b0f477a8e179c8aa4082c98/kapitel_d_avvattning_och_dranering.pdf [Accessed 1 March 2019].

Domenico, P.A., Schwartz, F.W., 1998. *Physical and chemical hydrogeology.* 2nd ed. New York: Wiley, cop.

EFSA, 2018. *Minutes of the expert meeting on perfluooroctane sulfonic acid and perfluorooctanoic acid in food assessment.* [pdf]. Available at:

https://www.efsa.europa.eu/sites/default/files/news/efsa-contam-3503.pdf [Accessed 1 December 2018].

Encyclopedia Britannica, 2018. *Continuity principle | physics.* [online] Available at: https://www.britannica.com/science/continuity-principle [Accessed 11 November 2018].

Enevoldsen, R., Juhler, R.K., 2010. Perfluorinated compounds (PFCs) in groundwater and aqueous soil extracts: using inline SPE-LC-MS/MS for screening and sorption characterisation of perfluorooctane sulphonate and related compounds. A*nalytical and Bioanalytical Chemistry* 398, 1161–1172. Available at: https://doi.org/10.1007/s00216-010-4066-0 [Accessed 28 January 2019].

Espeby, B., Gustafsson, J.P., 1997. *Vatten och ämnestransport i den omättade zonen: en kunskapsöversikt*, Trita-AMI. Report, 1400-1306;3038. Stockholm: Kungl. Tekniska högskolan.

Eveborn, D., Vikberg, E., Thunholm, B., 2016. *Grundvattenbildning och grundvattentillgång i Sverige.* [pdf] Uppsala: Sveriges Geologisk Undersökning. Available at: http://resource.sgu.se/produkter/regeringsrapporter/2017/RR1709.pdf [Accessed 19 January 2019].

Fetter, C.W., 2001. *Applied Hydrogeology.* 4th ed. Upper Saddle River: Prentice-Hall.

Filipovic, M., Woldegiorgis, A., Norström, K., Bibi, M., Lindberg, M., Österås, A.-H., 2015. Historical usage of aqueous film forming foam: A case study of the widespread distribution of perfluoroalkyl acids from a military airport to groundwater, lakes, soils and fish. *Chemosphere,* [e-journal] 129, 39–45. Available through: Uppsala University Library website https://doi.org/10.1016/j.chemosphere.2014.09.005 [Accessed 1 December 2018].

Frost, C., Lissel, M.B., Nordlund, J., Ågren, C., 2018. *Översvämningshantering Östra kanalstaden etapp 2 - Översvämning av Östersjön.* Stockholm: Structor Miljöbyrån Stockholm AB.

Gellrich, V., Stahl, T., Knepper, T.P., 2012. Behavior of perfluorinated compounds in soils during leaching experiments. *Chemosphere,* [e-journal] 87(9), 1052–1056. Available through: Uppsala University Library website https://doi.org/10.1016/j.chemosphere.2012.02.011 [Accessed 1 December 2018].

Harbaugh, A.W., 2005. *MODFLOW-2005, The U.S. Geological Survey Modular Ground-Water Model—the Ground-Water Flow Process.* Virginia: U.S. Geological Survey Techniques and Methods 6-A16.

Heath, R.C., 1983. *Basic Ground-Water Hydrology.* Virginia: U.S. Geological Survey.

Hvorslev, M.J., 1951. Time Lag and Soil Permeability in Ground-Water Observations. [pdf] Vicksburg, Mississippi: Corps of Engineers, U.S. Army. Available at: http://acwc.sdp.sirsi.net/client/en_US/default/index.assetbox.assetactionicon.view/100

4497/?rm=GENERAL+REPORTS0%7C%7C%7C1%7C%7C%7C0%7C%7C%7Ctrue [Accessed 6 February 2019].

HydroSOLVE, 2018. *Slug Tests.* [online]. Available at: http://www.aqtesolv.com/slug-tests/slug-tests.htm#Slug_Test_Initiation [Accessed 7 December 2018].

HydroSOLVE, 2016. *Representative Values of Hydraulic Properties*. [online]. Available at: http://www.aqtesolv.com/aquifer-tests/aquifer_properties.htm [Accessed 7 December 2018).

Jonasson, S., Brömssen, M. von, Gunnemyr, L., Lindstrand, O., 2007. *Modeller för transport och spridning av föroreningar fas 2.* [pdf] Stockholm: Naturvårdsverket. Available at: https://www.naturvardsverket.se/Documents/publikationer/620-5692-1.pdf [Accessed 2 December 2018].

Kemikalieinspektionen, 2018. *Högfluorerade ämnen – PFAS.* [online]. Available at: https://www.kemi.se/kemiska-amnen-och-material/hogfluorerade-amnen-pfas [Accessed 1 December 2018].

Kemikalieinspektionen, 2013. PM 5/13 - Brandskum som möjlig förorenare av dricksvattentäkter. [pdf] Sundbyberg: Kemikalieinspektionen. Available at: https://www.kemi.se/global/pm/2013/pm-5-13.pdf [Accessed 1 December 2018].

Kissa, E., 2001. Fluorinated Surfactants and Repellents. Marcel Dekker, New York, Revised and Expanded Surfactant Science Series 97.

Knutsson, G., Morfeldt, C.-O., 1993. *Grundvatten: teori & tillämpning.* Stockholm: Svenskt Tryck AB.

Larsson, M., Johansson, I., Rigard, K., 2016. *Förorenad mark och hydrogeologisk bedömning - Åkersberga station och Båthamnsvägens ersättning.* Uppdragsnummer 10199742. [pdf] Stockholm: WSP Samhällsbyggnad. Available at: http://www.osteraker.se/download/18.63fdc4101582444d7e517ecb/1480058714832/F%C3%B6rorenad+mark+och+hydrogeologisk+bed%C3%B6mning+161026.pdf [Accessed 15 January 2019].

Larsson, R., 2008. *Jords egenskaper.* [pdf] Linköping: Statens Geotekniska Institut. Available at: http://www.swedgeo.se/globalassets/publikationer/info/pdf/sgi-i1.pdf [Accessed 4 February 2019].

Livsmedelsverket, 2018. *Riskhantering - PFAS i dricksvatten och fisk.* [online] Available at: https://www.livsmedelsverket.se/livsmedel-och-innehall/oonskade-amnen/miljogifter/pfas-poly-och-perfluorerade-alkylsubstanser/riskhantering-pfaa-i-dricksvatten [Accessed 2 December 2018].

Lutze, H., Panglisch, S., Bergmann, A., Schmidt, T.C., 2012. Treatment Options for the Removal and Degradation of Polyfluorinated Chemicals. In: Knepper, T.P., Lange, F.T., 2012. *Polyfluorinated Chemicals and Transformation Products.* New York: Springer. pp. 103-125.

Matheron, G., 1967. “Eléments pour une théorie des milieux poreux.” Masson, Paris, France.

Morris, D.A., Johnson, A.I., 1967. *Physical Properties of Rock and Soil Materials, as Analyzed of the U.S. Geological Survey.* [pdf] Washington: United States Department of The Interior. Available at: https://pubs.usgs.gov/wsp/1839d/report.pdf [Accessed 19 January 2019].

Naturvårdsverket, 2018. *Högfluorerade ämnen i miljön.* [online]. Available at: https://www.naturvardsverket.se/Sa-mar-miljon/Manniska/Miljogifter/Organiska-miljogifter/Perfluorerade-amnen/ [Accessed 1 December 2018].

Pettersson, M., Ländell, M., Ohlsson, Y., Kleja, D.B., Tiberg, C., 2015. *Preliminära riktvärden för högfluorerade ämnen (PFAS) i mark och grundvatten.* [pdf] Linköping: Statens Geotekniska Institut. Available at: http://www.swedgeo.se/globalassets/publikationer/sgi-publikation/sgi-p21.pdf [Accessed 2 December 2018].

Pollock, D.W., 2012. *User Guide for MODPATH Version 6 - A Particle-Tracking Model for MODFLOW.* [pdf] Reston, Virginia: U.S. Geological Survey. Available at: https://pubs.usgs.gov/tm/6a41/pdf/TM_6A_41.pdf [Accessed 3 February 2019].

Pollock, D.W., 1989. *Documentation of computer programs to compute and display pathlines using results from the U.S. geological survey modular three-dimensional finite-difference ground-water flow model.* [pdf] Reston, Virginia: U.S. Geological Survey. Available at: https://pubs.usgs.gov/of/1989/0381/report.pdf [Accessed 3 February 2019].

Rigardt, K., Nilsson, E., 2015. Roslagsbanans Utbyggnad (RBU) Österskärsgrenen Delen Åkersberga vändspår 28028, km 25+900 - 27+600. [pdf] Stockholm: AB Storstockholms Lokaltrafik.

Rosenqvist, L., Vestergren, R., Westberg, E., Eliaeson, K., Norström, K., Liljeberg, M., Strandberg, J., Rahmberg, M., 2017. *Spridning av högfluorerade ämnen i mark från Stockholm Arlanda Airport.* [pdf] Stockholm: IVL Svenska Miljöinstitutet. Available at: https://www.ivl.se/download/18.1369484715f59ce4babf2/1509550871689/B2289.pdf [Accessed 28 January 2019].

Ryd, E., 2017. *Samband mellan kapacitet vid borrning och transmissivitet i kristallint och sedimentärt berg.* M.Sc.Eng. Uppsala University. Available at: http://www.w-program.nu/filer/exjobb/ellinor_ryd.pdf [Accessed 1 February 2019].

SGI, 2018. *Högfluorerade ämnen - PFAS.* [online]. Available at: http://www.swedgeo.se/sv/vagledning-i-arbetet/fororenade-omraden/hogfluorerade-amnen-pfas/ [Accessed 4 January 2019].

SGU, 2018. *SGUs kartvisare - About mapviewer.* [online] Available at: https://apps.sgu.se/kartvisare/kartvisare-brunnar.html [Accessed 2 December 2018].

U.S. EPA, 2018. *Basic Information on PFAS.* [online]. Available at: https://www.epa.gov/pfas/basic-information-pfas [Accessed 1 December 2018].

Woldegiorgis, A., Regazzoni, L., Inkapööl, J., 2017. *Miljöteknisk markundersökning - Åkersberga brandstation.* Uppdragsnummer 10255262. Stockholm: WSP Environmental Sverige.

Younger, P.L., 1993. Simple generalized methods for estimating aquifer storage parameters. *Quarterly Journal of Engineering Geology.* [pdf] 26, 127–135. [Accessed 25 October 2018].

Zheng, C., Wang, P.P., 1999. *MT3DMS: A Modular Three-Dimensional Multispecies Transport Model for Simulation of Advection, Dispersion, and Chemical Reactions of Contaminants in Groundwater Systems; Documentation and User's Guide.* [pdf] U.S. Army Corps of Engineers. Available at: https://hydro.geo.ua.edu/mt3d/mt3dmanual.pdf [Accessed 4 February 2019].

# APPENDIX

## A. GROUNDWATER LEVELS

**Table A1.** Measured groundwater level from WSP, SWECO, SGU's well archive, and Geosigma. The locations of the wells are in coordinate system SWEREF 99 TM and the groundwater levels are presented in height system RH 2000. Red and blue mark all the levels measured during low and high seasons, respectively. Yellow highlight marks the groundwater levels used for calibration

| Well | X | Y | Date of measurement | | | | | | | | | | | | | |
|---|---|---|---|---|---|---|---|---|---|---|---|---|---|---|---|---|
| | | | 19990527 | 20081127 | 20121004 | 20130311 | 20171115 | 20171210 | 20180208 | 20180220 | 20180404 | 20180830 | 20180912 | 20180918 | 20180919 | 20181017 |
| 17W01 | 6597827 | 687191 | | | | | 3.70 | 3.65 | 3.80 | 3.58 | | | | 3.11 | | |
| 17W02 | 6597821 | 687181 | | | | | 3.81 | 3.66 | 3.88 | 3.71 | | | | 3.41 | | |
| 17W03 | 6597815 | 687174 | | | | | 3.76 | 3.75 | 3.79 | 3.67 | | | | 3.32 | | |
| 17W04 | 6597820 | 687169 | | | | | 3.75 | 3.71 | 3.91 | 3.66 | | | | 3.36 | | |
| 17W05 | 6597831 | 68717 | | | | | | 3.49 | 3.85 | 3.73 | | | | 3.39 | | |
| 17W06 | 6597837 | 687173 | | | | | 3.78 | 3.73 | 3.82 | | | | | 3.54 | | |
| 17W07 | 6597828 | 687166 | | | | | 3.57 | 3.34 | 3.73 | 3.68 | | | | 3.15 | | |
| 17W08 | 6597839 | 687163 | | | | | 3.40 | 2.75 | 3.68 | 3.65 | | | | 3.28 | | |
| 17W09 | 6597858 | 687169 | | | | | | 3.30 | 3.34 | | | | | 3.03 | | |
| 17W10 | 6597829 | 687159 | | | | | 3.09 | 3.01 | 3.15 | 3.06 | | | | 2.77 | | |
| 17W11 | 6597838 | 687154 | | | | | 2.89 | 2.88 | 3.05 | 3.25 | | | | 2.97 | | |
| GV1 | 6597827 | 687174 | | | | | 3.05 | 3.06 | 3.10 | 3.01 | | | | | | |
| GV2 | 6597827 | 687175 | | | | | 3.03 | 2.93 | 3.09 | 2.99 | | | | | | |
| 18W01 | 6597850 | 687135 | | | | | | | | 3.59 | | | | 3.74 | | |

| Well | X | Y | Date of measurement | | | | | | | | | | | | | |
|---|---|---|---|---|---|---|---|---|---|---|---|---|---|---|---|---|
| | | | 19990527 | 20081127 | 20121004 | 20130311 | 20171115 | 20171210 | 20180208 | 20180220 | 20180404 | 20180830 | 20180912 | 20180918 | 20180919 | 20181017 |
| 18W02 | 6597865 | 687151 | | | | | | | | 3.45 | | | | 2.94 | | |
| 18W03 | 6597881 | 687167 | | | | | | | | 3.60 | | | | 3.25 | | |
| 18S01 | 6597841 | 687142 | | | | | | | | | | | 2.32 | 2.89 | | |
| 18S03 | 6597836 | 687114 | | | | | | | | | | | 3.18 | 3.06 | | |
| 18S05 | 6597805 | 687158 | | | | | | | | | | | 3.03 | 1.93 | | |
| 913519163 | 6598856 | 687821 | | | | 19.45 | | | | | | | | | | |
| 912815103 | 6598139 | 687400 | | | 2.39 | | | | | | | | | | | |
| 908636642 | 6598949 | 688037 | | 20.90 | | | | | | | | | | | | |
| 999056286 | 6598599 | 686370 | 3.72 | | | | | | | | | | | | | |
| 18GS02 | 6598055 | 686649 | | | | | | | | | 1.60 | | | | | |
| 18GS08 | 6598047 | 686676 | | | | | | | | | 1.50 | 1.20 | | | | |
| 18GS19 | 6598032 | 686724 | | | | | | | | | 1.80 | 1.30 | | | 1.40 | 1.20 |

## B. SLUG TEST

Response data from the slug test in well 17W01 - 17W11, 18W01 - 18W03, 18S01, 18S03, and 18S05 are in Figure B1a to Figure B1p.

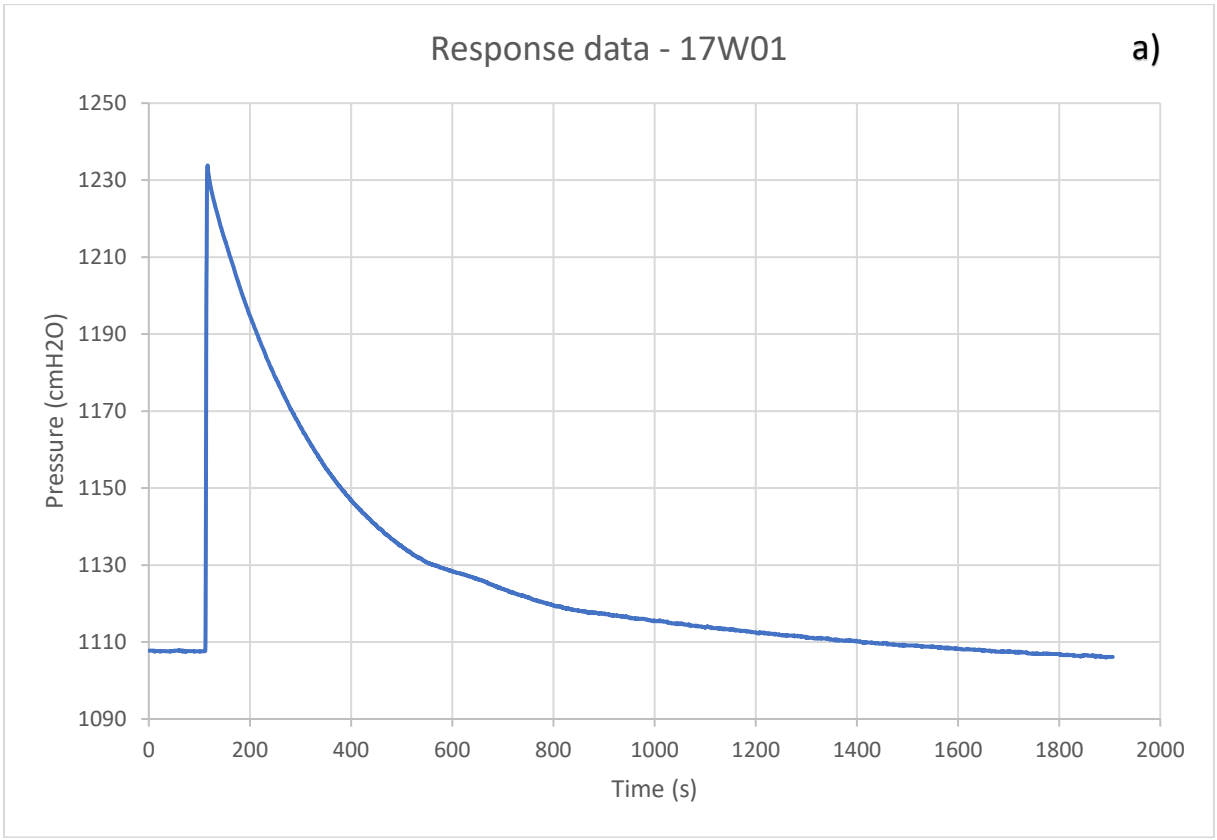


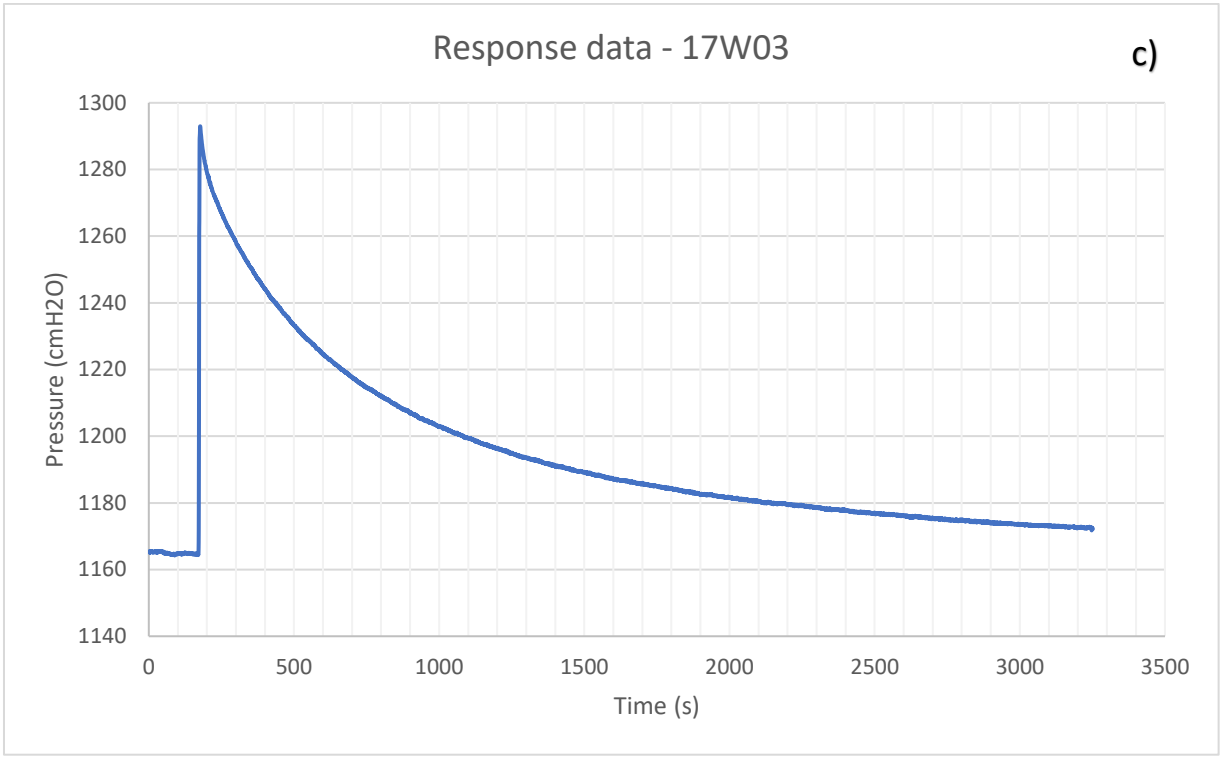
Response data - 17W03
c)
Pressure (cmH2O)
1300
1280
1260
1240
1220
1200
1180
1160
1140
0
500
1000
1500
2000
2500
3000
3500
Time (s)

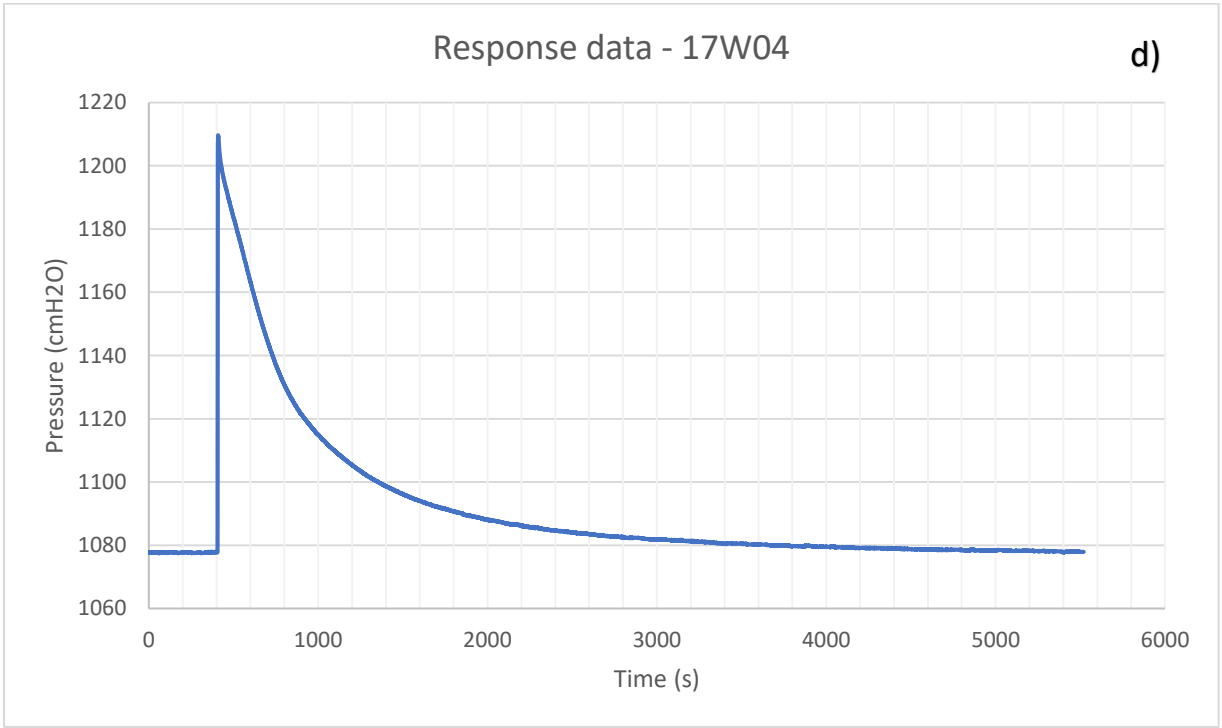
Response data - 17W04
d)
Pressure (cmH2O)
1220
1200
1180
1160
1140
1120
1100
1080
1060
0
1000
2000
3000
4000
5000
6000
Time (s)

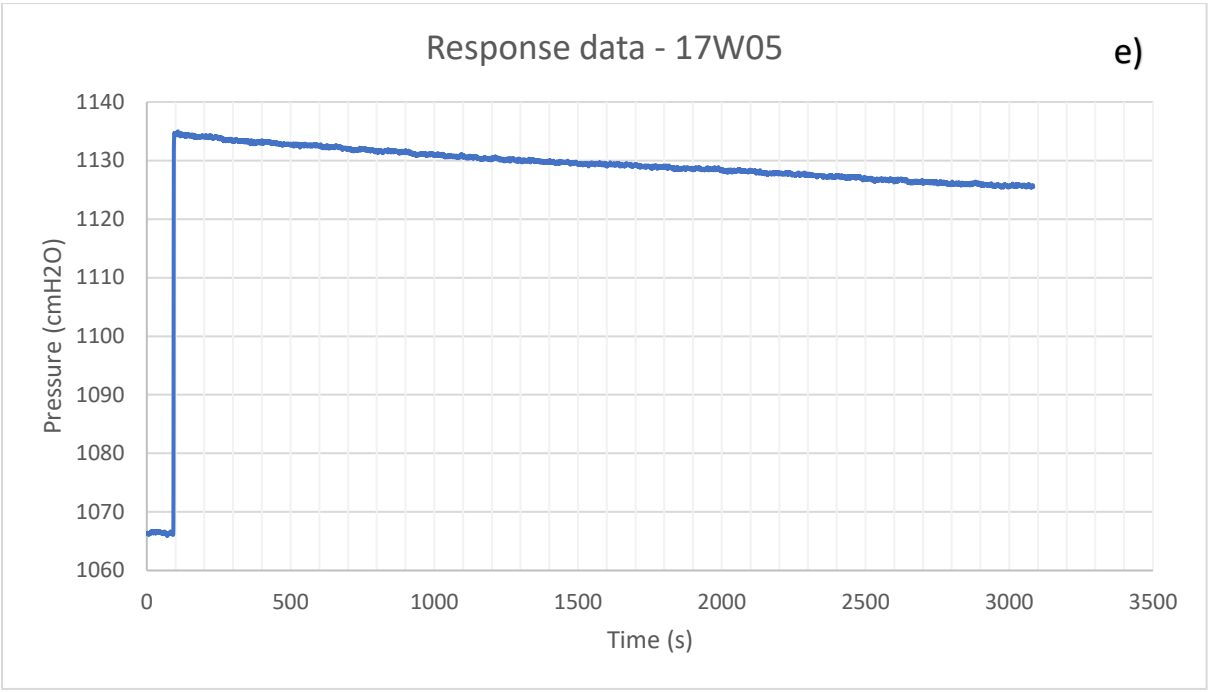
Response data - 17W05
e)
Pressure (cmH2O)
1140
1130
1120
1110
1100
1090
1080
1070
1060
0
500
1000
1500
2000
2500
3000
3500
Time (s)


Response data - 17W06
f)
Pressure (cmH2O)
1160
1150
1140
1130
1120
1110
1100
1090
1080
1070
0
500
1000
1500
2000
2500
3000
3500
Time (s)


Response data - 17W07
g)
Presure (cmH2O)
1240
1220
1200
1180
1160
1140
1120
1100
0
500
1000
1500
2000
2500
3000
Time (s)

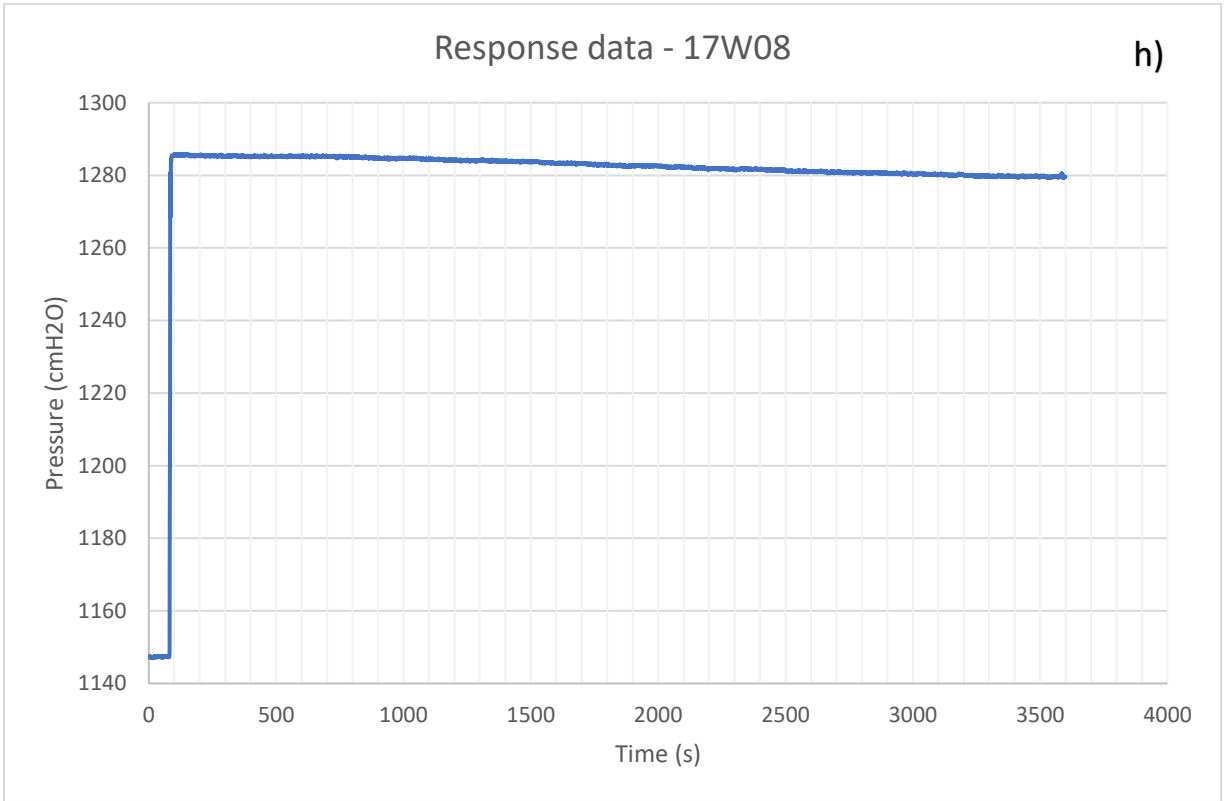
Response data - 17W08
h)
Pressure (cmH2O)
1300
1280
1260
1240
1220
1200
1180
1160
1140
0
500
1000
1500
2000
2500
3000
3500
4000
Time (s)

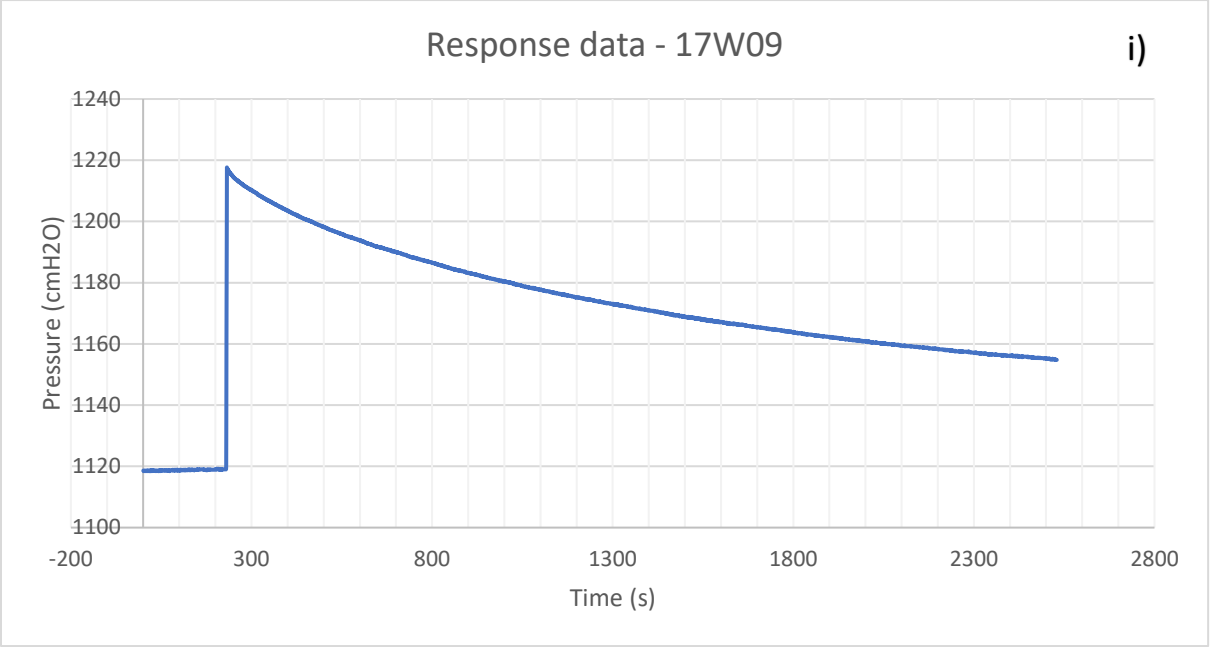
Response data - 17W09
i)
Pressure (cmH2O)
1240
1220
1200
1180
1160
1140
1120
1100
-200
300
800
1300
1800
2300
2800
Time (s)

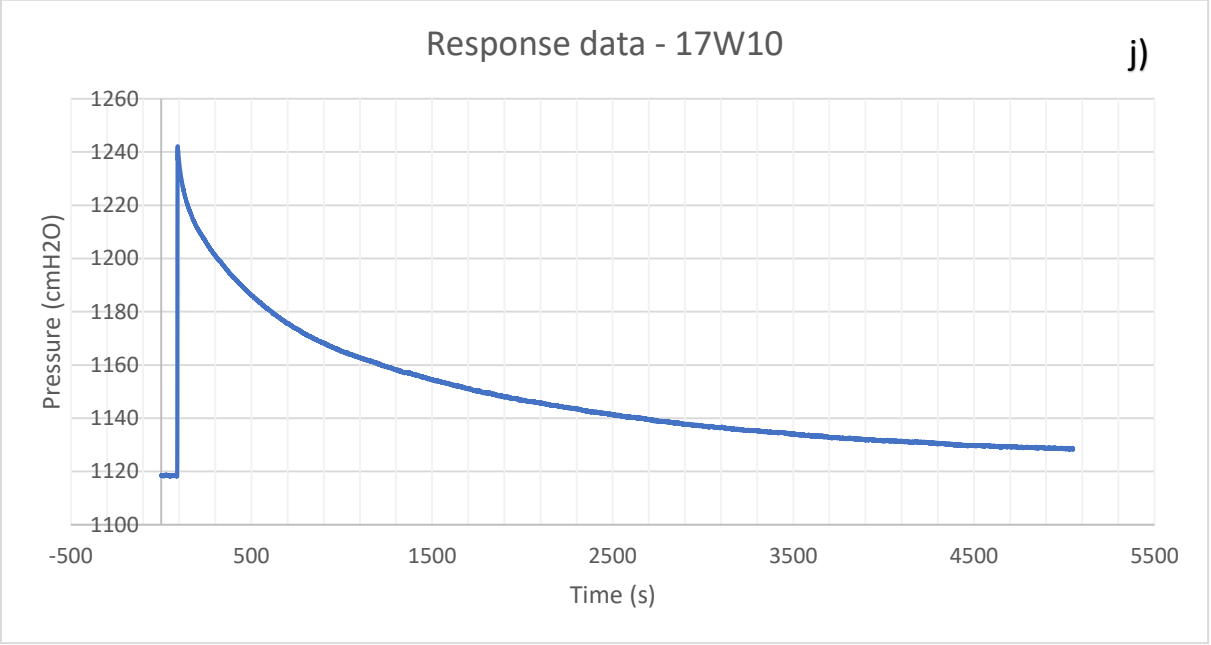
Response data - 17W10
j)
Pressure (cmH2O)
1260
1240
1220
1200
1180
1160
1140
1120
1100
-500
500
1500
2500
3500
4500
5500
Time (s)

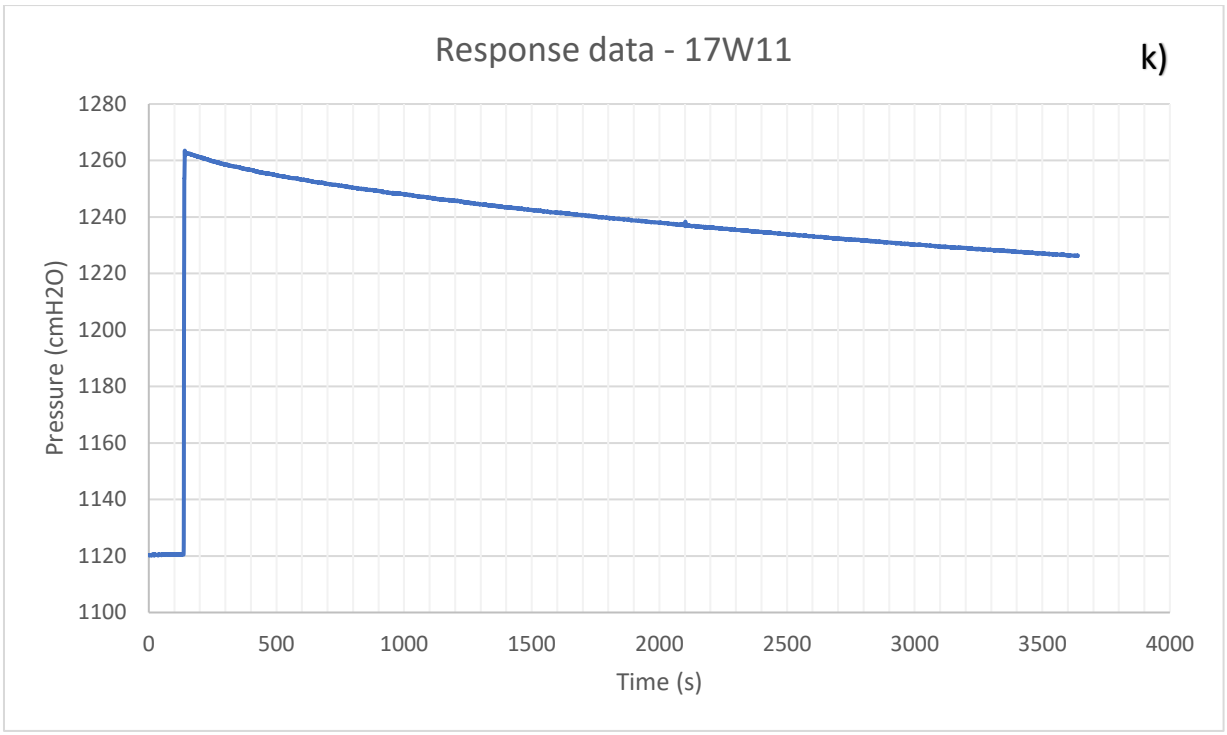
Response data - 17W11
k)
Pressure (cmH2O)
1280
1260
1240
1220
1200
1180
1160
1140
1120
1100
0
500
1000
1500
2000
2500
3000
3500
4000
Time (s)

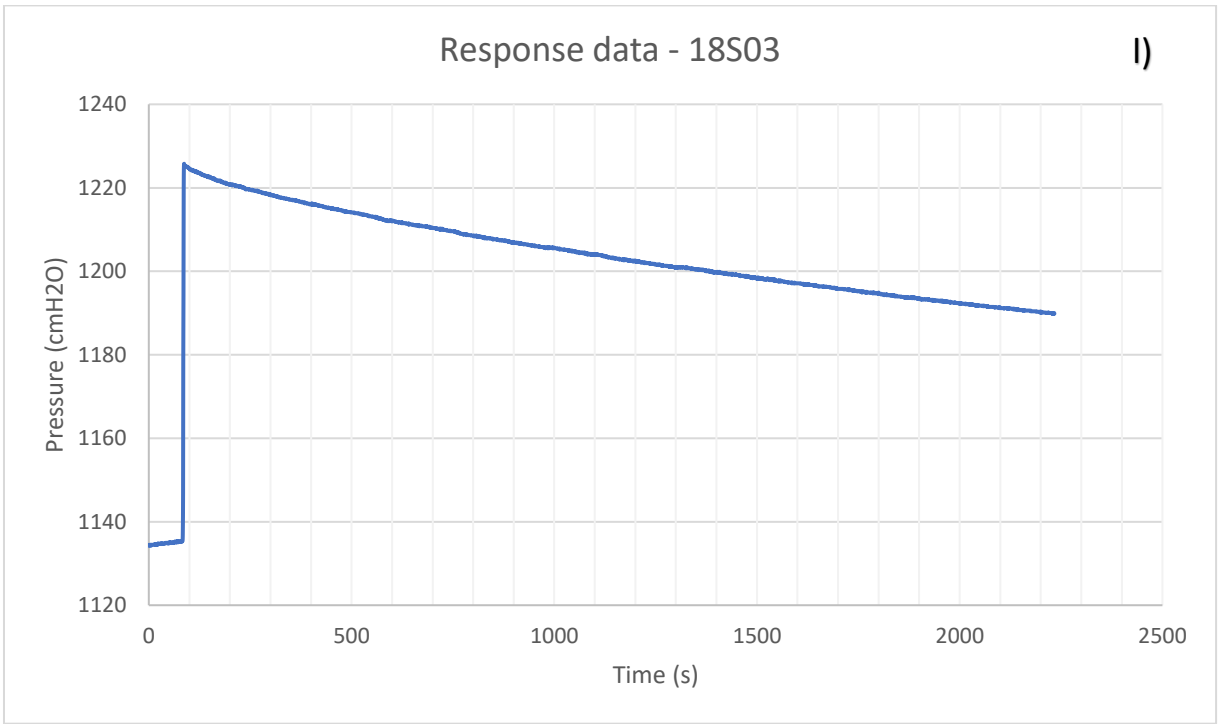
Response data - 18S03
l)
Pressure (cmH2O)
1240
1220
1200
1180
1160
1140
1120
0
500
1000
1500
2000
2500
Time (s)

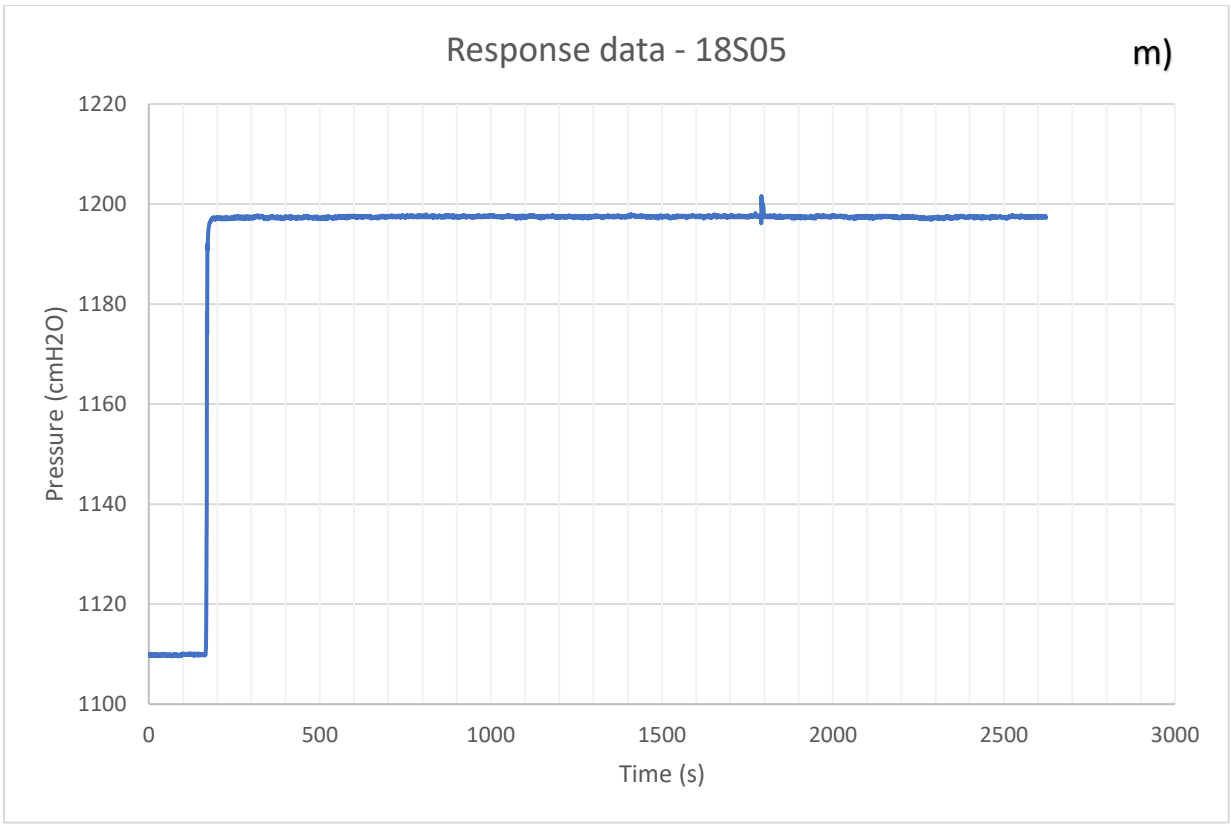
Response data - 18S05
m)
Pressure (cmH2O)
1220
1200
1180
1160
1140
1120
1100
0
500
1000
1500
2000
2500
3000
Time (s)


Response data - 18W01
n)
Pressure (cmH2O)
1280
1260
1240
1220
1200
1180
1160
1140
1120
0
500
1000
1500
2000
2500
Time (s)

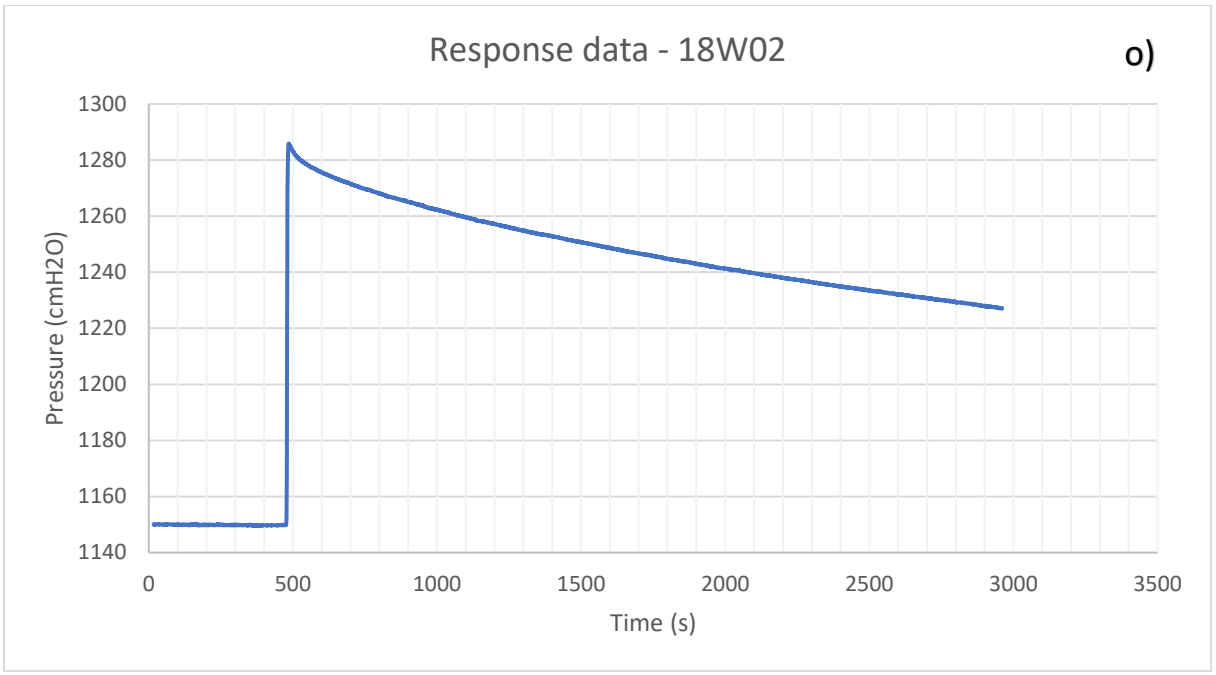


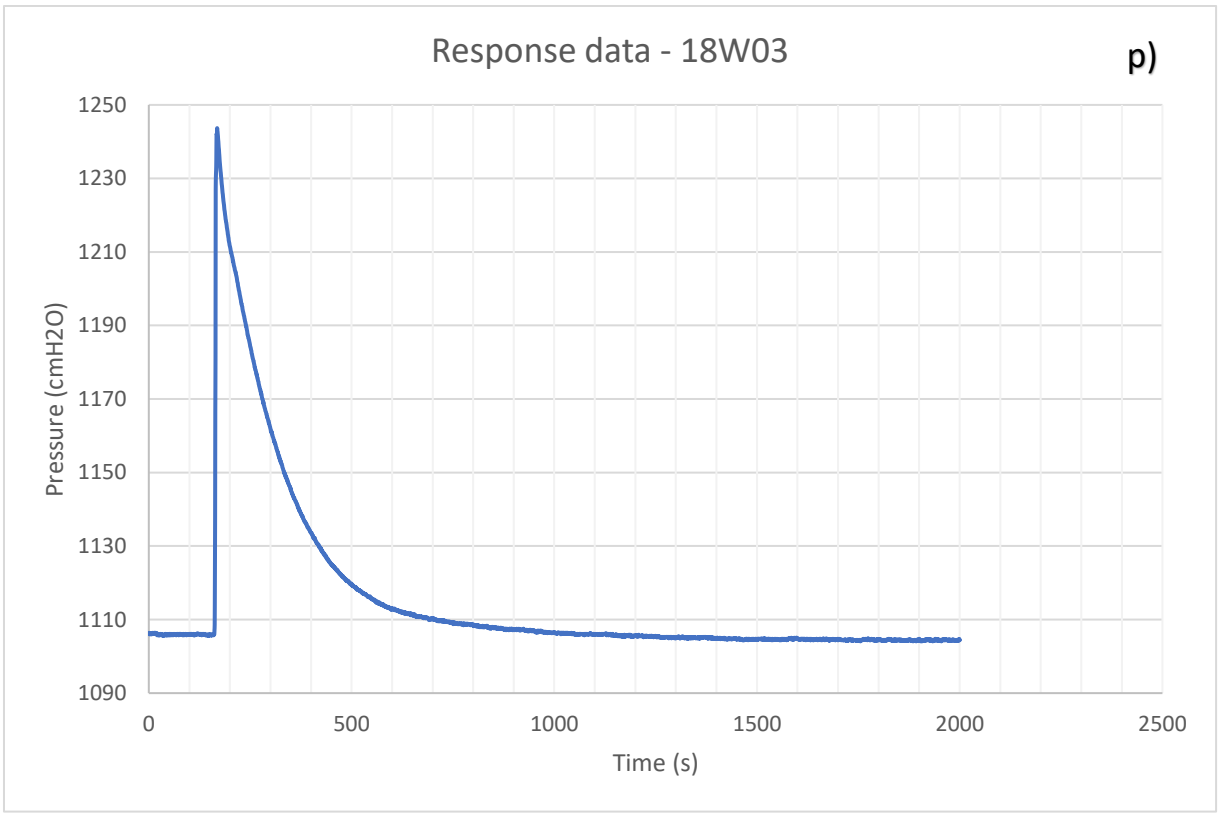


**Figure B1.** Response data from slug test in well 17W01 - 17W11, 18W01 - 18W03, 18S01, 18S03, and 18S05.

The results of semi-logarithmic plot and analysis of the approved wells performed in Aquifer test (17W01, 17W02, 17W03, 17W04, 17W06, 17W10) are presented in Figure B2a to Figure B2f.

a)

**Semi-log plot of drawdown versus time - 17W01**

Project:

Number:

Client:

| | | |
|---|---|---|
| Location: Åkersbega | Slug Test: 17W01 | Test Well: 17W01 |
| Test Conducted by: WB | | Test Date: 2018-09-18 |
| Analysis Performed by: WB | | Analysis Date: 2018-10-03 |
| Aquifer Thickness: 25,00 cm | | |

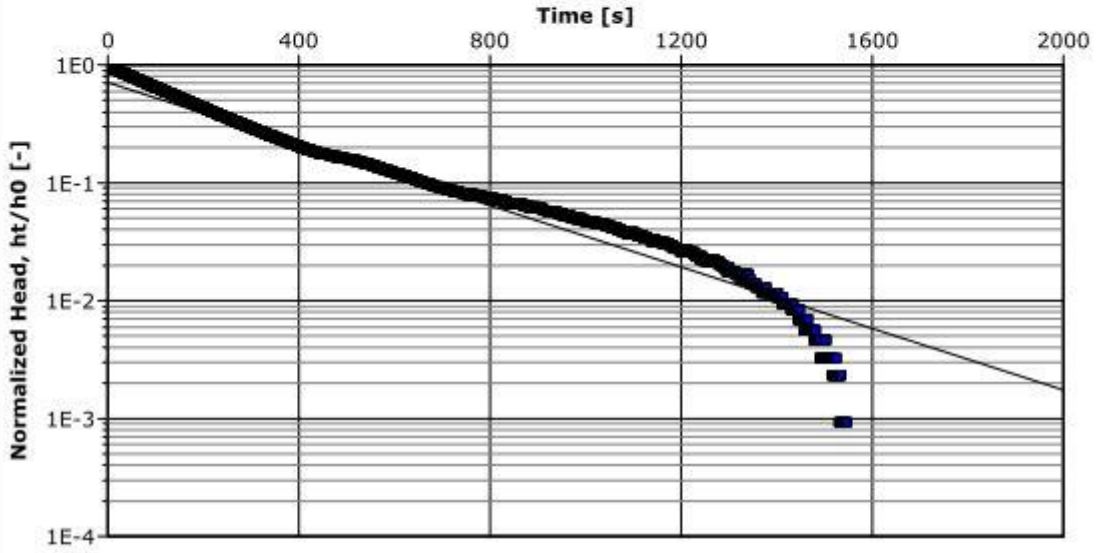


Calculation using Hvorslev

| Observation Well | Hydraulic Conductivity [m/s] |
|---|---|
| 17W01 | $5{,}30 \times 10^{-6}$ |

b)

| | |
|---|---|
| | **Semi-log plot of drawdown versus time - 17W02** |
| | Project: |
| | Number: |
| | Client: |

| | | |
|---|---|---|
| Location: Åkersberga | Slug Test: 17W02 | Test Well: 17W02 |
| Test Conducted by: WB | | Test Date: 2018-09-18 |
| Analysis Performed by: WB | | Analysis Date: 2018-10-03 |
| Aquifer Thickness: 30,00 cm | | |

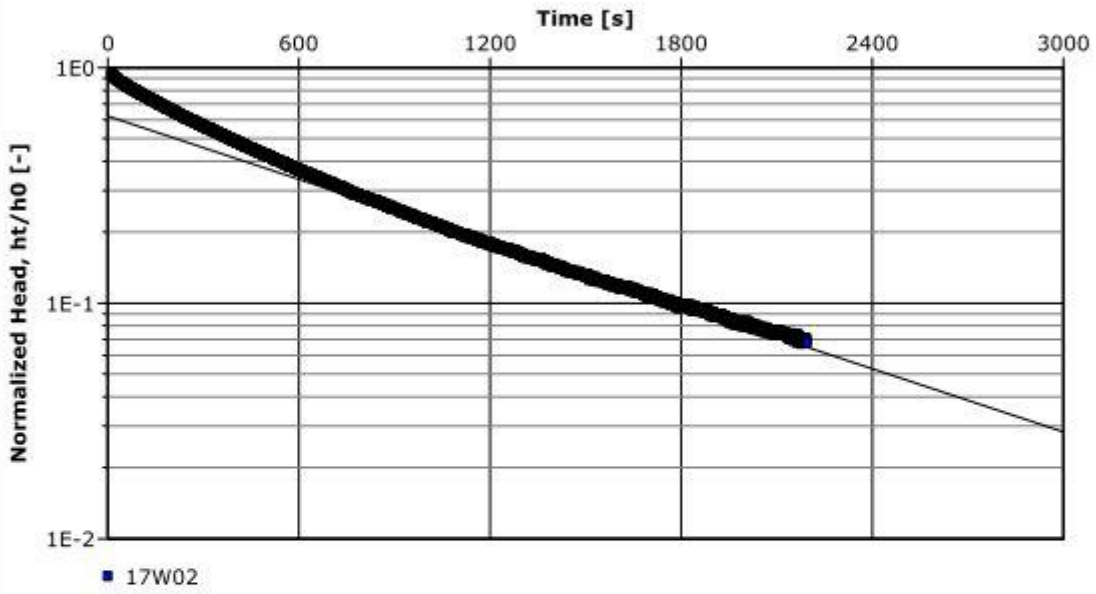


Calculation using Hvorslev

| Observation Well | Hydraulic Conductivity [m/s] | |
|---|---|---|
| 17W02 | $1{,}65 \times 10^{-6}$ | |

c)

| | |
|---|---|
| | **Semi-log plot of drawdown versus time - 17W03** |
| | Project: |
| | Number: |
| | Client: |

| | | |
|---|---|---|
| Location: Åkersberga | Slug Test: 17W03 | Test Well: 17W03 |
| Test Conducted by: WB | | Test Date: 2018-09-18 |
| Analysis Performed by: WB | | Analysis Date: 2018-10-03 |
| Aquifer Thickness: 30,00 cm | | |

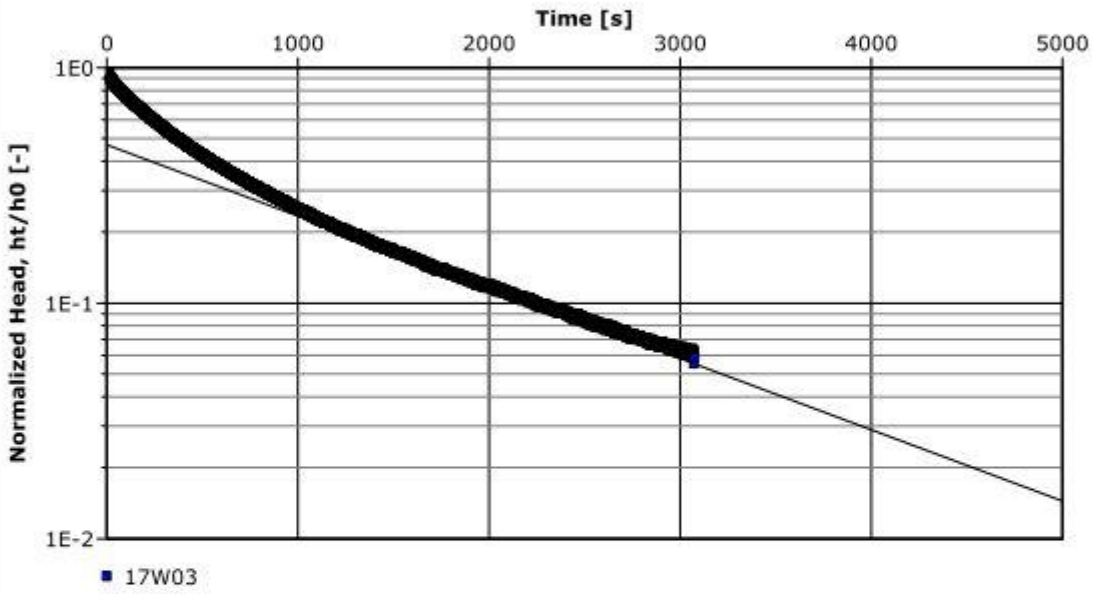


Calculation using Hvorslev

| Observation Well | Hydraulic Conductivity [m/s] | |
|---|---|---|
| 17W03 | $1{,}11 \times 10^{-6}$ | |

d)

| | | |
|---|---|---|
| | **Semi-log plot of drawdown versus time - 17W04** | |
| | Project: | |
| | Number: | |
| | Client: | |
| Location: Åkersberga | Slug Test: 17W04 | Test Well: 17W04 |
| Test Conducted by: WB | | Test Date: 2018-09-18 |
| Analysis Performed by: WB | | Analysis Date: 2018-10-03 |
| Aquifer Thickness: 35,00 cm | | |

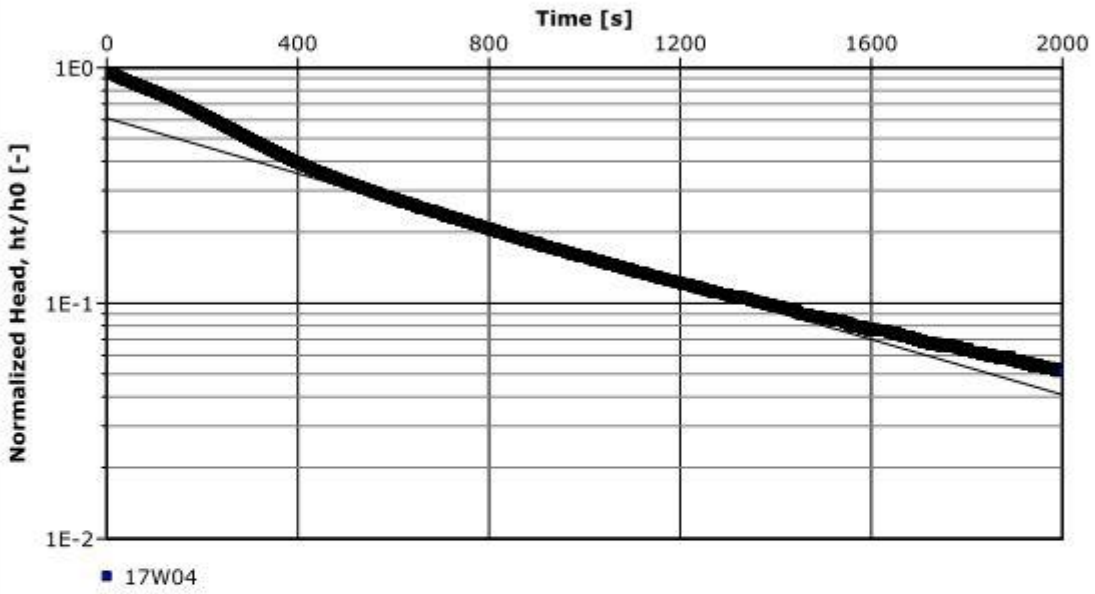


Calculation using Hvorslev

| Observation Well | Hydraulic Conductivity [m/s] | |
|---|---|---|
| 17W04 | $1{,}98 \times 10^{-6}$ | |

e)

| | |
|---|---|
| **Semi-log plot of drawdown vesus time - 17W06** | |
| Project: | |
| Number: | |
| Client: | |

| | | |
|---|---|---|
| Location: Åkersberga | Slug Test: 17W06 | Test Well: 17W06 |
| Test Conducted by: WB | | Test Date: 2018-09-18 |
| Analysis Performed by: WB | | Analysis Date: 2019-01-10 |
| Aquifer Thickness: 50,00 cm | | |

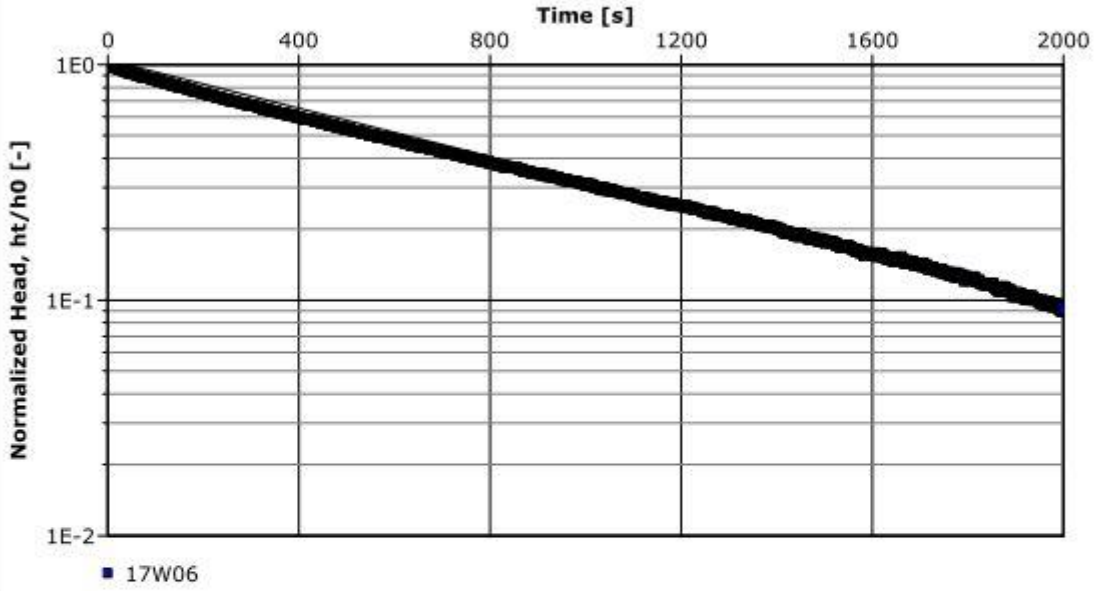


Calculation using Hvorslev

| Observation Well | Hydraulic Conductivity [m/s] | |
|---|---|---|
| 17W06 | $1{,}39 \times 10^{-6}$ | |

f)

**Semi-log plot of drawdown versus time - 17W10**

Project:

Number:

Client:

| | | |
|---|---|---|
| Location: Åkersberga | Slug Test: 17W10 | Test Well: 17W10 |
| Test Conducted by: WB | | Test Date: 2018-09-18 |
| Analysis Performed by: WB | | Analysis Date: 2018-10-04 |
| Aquifer Thickness: 35,00 cm | | |

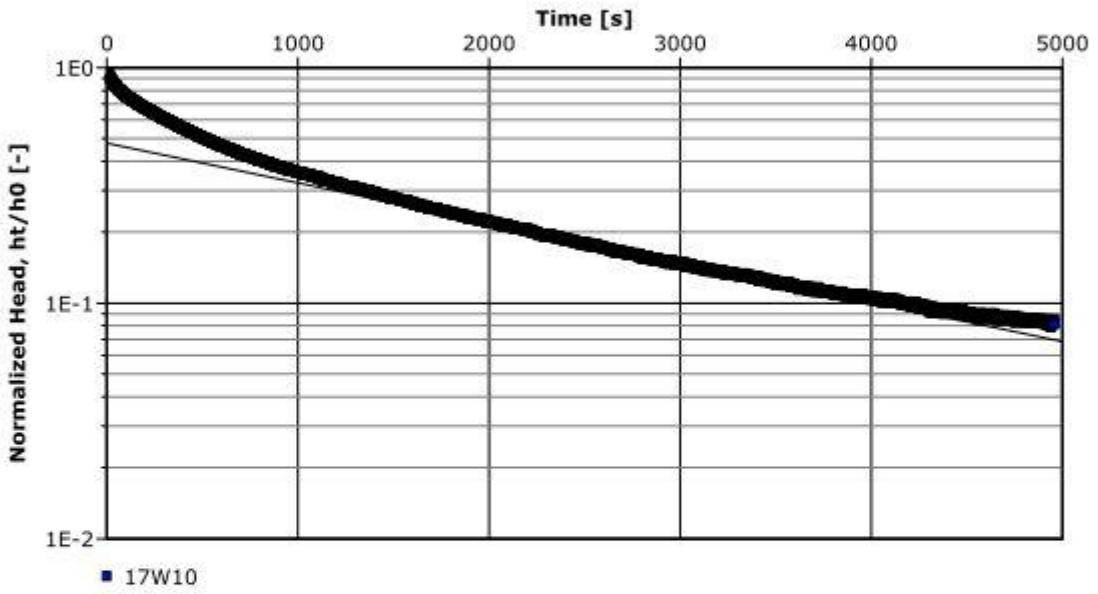


Calculation using Hvorslev

| Observation Well | Hydraulic Conductivity [m/s] | |
|---|---|---|
| 17W10 | $5{,}69 \times 10^{-7}$ | |

**Figure B2.** Semi logarithmic plot and analysis performed in AquiferTest for wells 17W01, 17W02, 17W03, 17W04, 17W06, and 17W10.

The result of semi-logarithmic plot and analysis performed manually in Excel for well 18W03 are presented in Figure B3. From the Equation of the fitted straight line, the value of $t_{37}$ was calculated to 140.86 s. With the values of *r* and *L* of well 18W03, which summarized in Table 5, the estimated hydraulic conductivity was then calculated with Equation (5) to $7.90 \cdot 10^{-5}$ m/s.

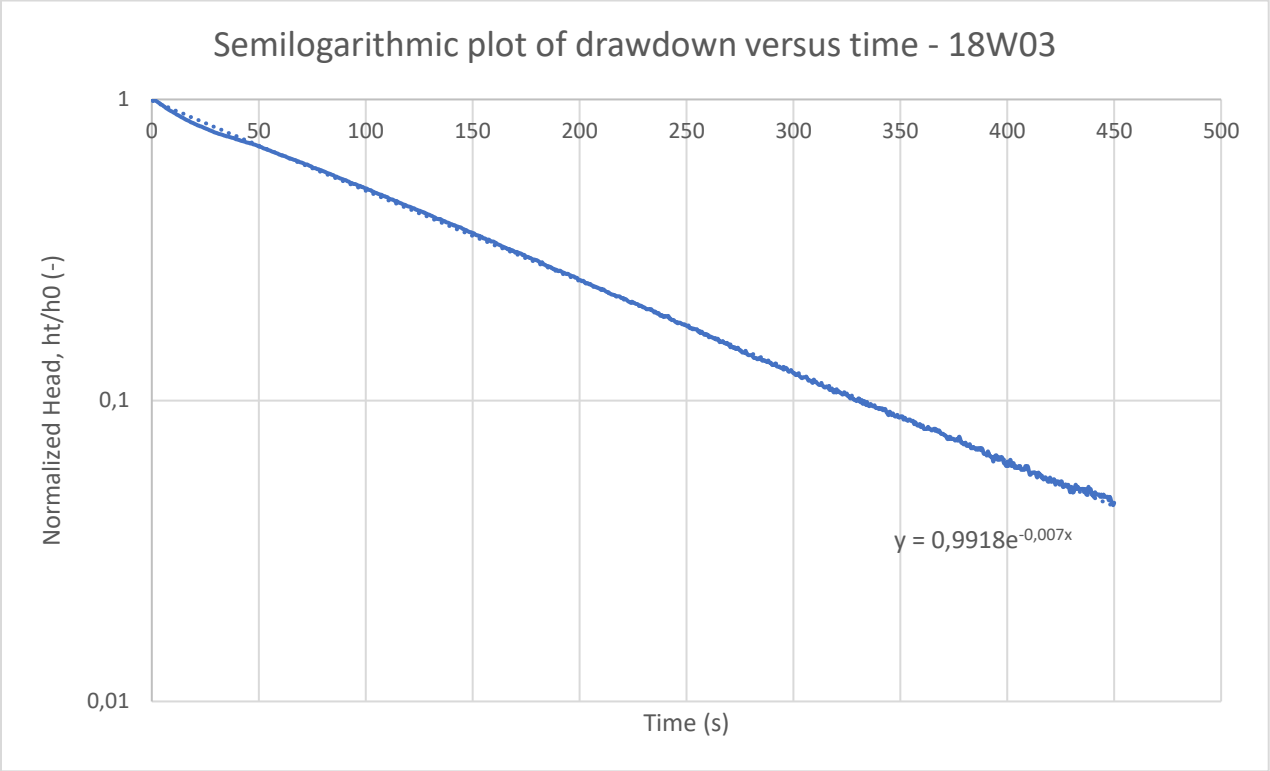


**Figure B3.** Semi-logarithmic plot and analysis performed manually in Excel for well 18W03.

## C. SOIL DEPTH

A compilation of soil depth data, which obtained from WSP's and SWECOS's geotechnical investigation is presented in Table C1. The locations are in coordinate system SWEREF 99 TM. The data for S1-S9 and 18W01was obtained from probing results. The rest of the data was obtained from WSP and SWECO.

**Table C1.** Soil depth data obtained from WSP and SWECO

| Name of location | X | Y | Soil depth [m] |
|---|---|---|---|
| S1 | 6597876 | 687161 | 4.9 |
| S2 | 6597869 | 687167 | 4.6 |
| S3 | 6597862 | 687174 | 4.8 |
| S4 | 6597855 | 687181 | 4.5 |

| Name of location | X | Y | Soil depth [m] |
|---|---|---|---|
| S5 | 6597848 | 687188 | 2.8 |
| S6 | 6597841 | 687194 | 2 |
| S7 | 6597841 | 687176 | 6.4 |
| S8 | 6597852 | 687168 | 5.8 |
| S9 | 6597860 | 687156 | 6.3 |
| 17W01 | 6597827 | 687191 | 2.5 |
| 17W02 | 6597821 | 687182 | 4.8 |
| 17W03 | 6597815 | 687175 | 5.7 |
| 17W04 | 6597820 | 687170 | 7 |
| 17W05 | 6597831 | 687175 | 6 |
| 17W06 | 6597838 | 687173 | 6.4 |
| 17W07 | 6597828 | 687167 | 5.6 |
| 17W08 | 6597840 | 687163 | 5.6 |
| 17W09 | 6597858 | 687170 | 5.2 |
| 17W10 | 6597830 | 687159 | 6.1 |
| 17W11 | 6597838 | 687154 | 5.4 |
| 18W01 | 6597850 | 687136 | 9.1 |
| 18W02 | 6597866 | 687152 | 6.8 |
| 18W03 | 6597881 | 687168 | 3.6 |
| 18S01 | 6597841 | 687142 | 6.2 |
| 18S03 | 6597836 | 687114 | 12.6 |
| 18S05 | 6597805 | 687158 | 3.8 |
| 91GB312 | 6598112 | 686485 | 15.2 |
| 08W104 | 6598076 | 686536 | 9.7 |
| 08W102 | 6598071 | 686586 | 10.5 |
| 91GB316 | 6598081 | 686604 | 11.6 |
| 91GB317 | 6598077 | 686641 | 14.9 |
| 91GB318 | 6598074 | 686662 | 7.5 |
| 09W020 | 6598048 | 686692 | 5.6 |
| 09W021 | 6598039 | 686738 | 6 |
| 14W011 | 6598064 | 686708 | 3.3 |
| 14W014 | 6598045 | 686794 | 8.1 |
| 14W013 | 6598046 | 686848 | 9.1 |
| 14W015 | 6598033 | 686850 | 12 |
| 14W016 | 6598001 | 686941 | 19.1 |
| 14W017 | 6597972 | 686987 | 15.2 |
| 06W158B | 6597905 | 687060 | 10.8 |
| 06W158A | 6597898 | 687066 | 11.2 |

The result of interpolated soil depth using the data in Table C1 can be seen in Figure C1. The area to the east of the former fire station does generally have quite low soil depth, which means

that the elevation of the bedrock is close to the ground level. This could be confirmed in the soil map (Figure 7). While deep soil could be observed in the areas to the west and northwest of the former fire station.

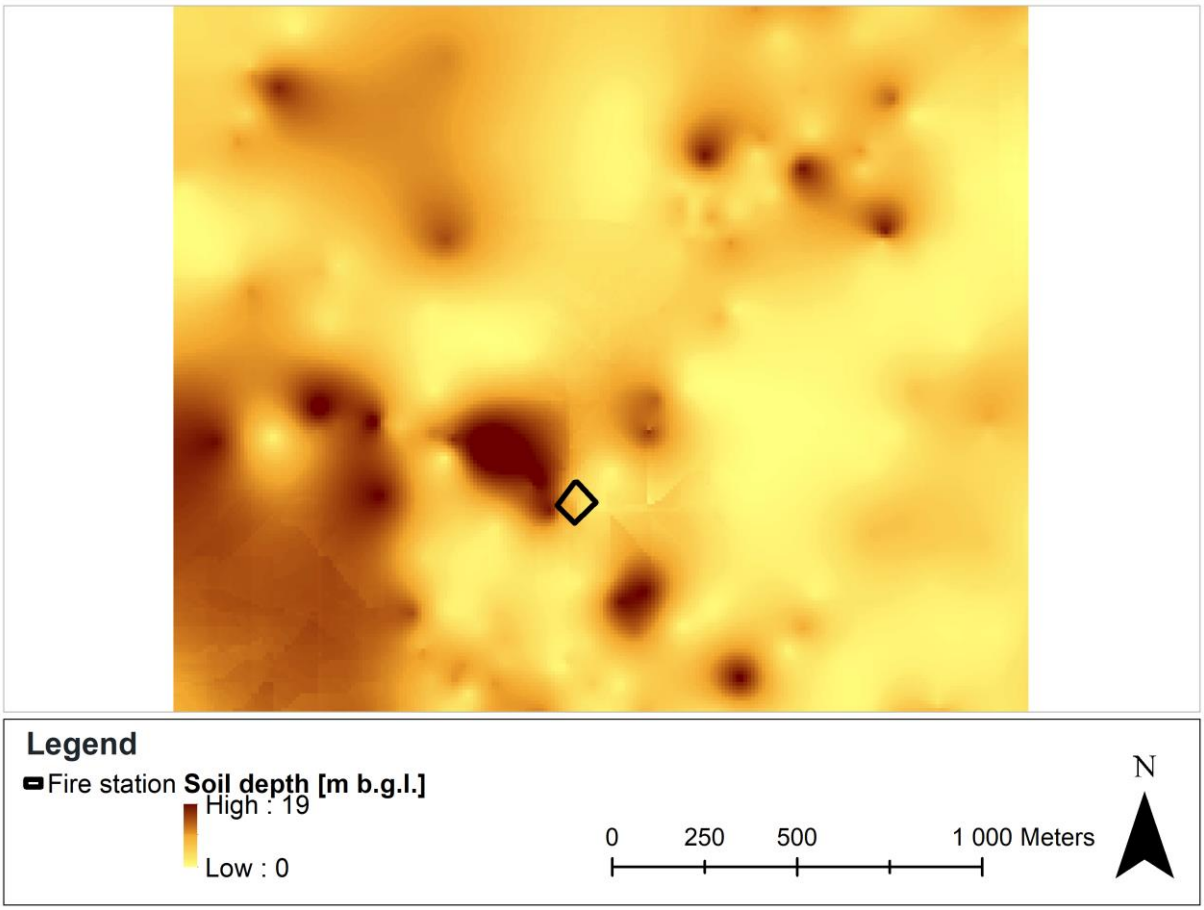


**Figure C1.** Interpolated soil depth over the area of the former fire station and its surroundings, where shallow soil depth is representing in yellow and deep soil depth in brown.